TKK Dissertations 95
Espoo 2007

MODELING AND DETECTION OF HIGH IMPEDANCE ARCING FAULT IN MEDIUM VOLTAGE NETWORKS

Doctoral Dissertation

Nagy Ibrahim Elkalashy

Helsinki University of Technology
Department of Electrical and Communications Engineering
Power Systems and High Voltage Engineering

TKK Dissertations 95
Espoo 2007

MODELING AND DETECTION OF HIGH IMPEDANCE ARCING FAULT IN MEDIUM VOLTAGE NETWORKS

Doctoral Dissertation

Nagy Ibrahim Elkalashy

Dissertation for the degree of Doctor of Science in Technology to be presented with due permission of the Department of Electrical and Communications Engineering for public examination and debate in Auditorium S4 at Helsinki University of Technology (Espoo, Finland) on the 26th of November, 2007, at 12 noon.

Helsinki University of Technology
Department of Electrical and Communications Engineering
Power Systems and High Voltage Engineering

Teknillinen korkeakoulu
Sähkö- ja tietoliikennetekniikan osasto
Sähköverkot ja suurjännitetekniikka

Distribution:
Helsinki University of Technology
Department of Electrical and Communications Engineering
Power Systems and High Voltage Engineering
P.O. Box 3000
FI - 02015 TKK
FINLAND
URL: http://powersystems.tkk.fi/eng/
Tel. +358-9-451 5049
Fax +358-9-451 5012
E-mail: nagy.elkalashy@tkk.fi

© 2007 Nagy Ibrahim Elkalashy

ISBN 978-951-22-9014-7
ISBN 978-951-22-9015-4 (PDF)
ISSN 1795-2239
ISSN 1795-4584 (PDF)
URL: http://lib.tkk.fi/Diss/2007/isbn9789512290154/

TKK-DISS-2363

Multiprint Oy
Espoo 2007

HELSINKI UNIVERSITY OF TECHNOLOGY
P. O. BOX 1000, FI-02015 TKK
http://www.tkk.fi

ABSTRACT OF DOCTORAL DISSERTATION

Author Nagy Ibrahim Elkalashy

Name of the dissertation

Modeling and Detection of High Impedance Arcing Fault in Medium Voltage Networks

Date of manuscript 18.09.2007 | Date of the dissertation 26.11.2007

☐ Monograph ☒ Article dissertation (summary + original articles)

Department: Electrical and Communications Engineering
Laboratory: Power Systems and High Voltage Engineering
Field of research: Electrical Power Systems
Opponents: Professor Mansour Abdel-Rahman, Dr. Seppo Hänninen
Supervisors: Professor Matti Lehtonen, Helsinki University of Technology, Finland; Professor Mohamed A. Izzularab, Minoufiya University, Egypt; Professor Abdel-Maksoud I. Taalab, Minoufiya University, Egypt; Ass. Professor Hatem A. Darwish, Minoufiya University, Egypt

Abstract:

In this dissertation, a universal arc representation using the Electromagnetic Transient Program (EMTP) is first developed. It is accomplished based on the bilateral interaction between EMTP network and Transient Analysis Control System (TACS) field. This arc modeling procedure is used as a useful guide to present a new model for high impedance arcing faults due to leaning trees. At the Power Systems and High Voltage Laboratory, Helsinki University of Technology (TKK), Finland, experiments have been performed to measure the fault characteristics due to leaning trees and therefore to verify the proposed model. Towards investigating detection facilities of this fault type, the fault model is incorporated at different locations in 20 kV Medium Voltage (MV) networks using the ATPdraw program, which is a graphical interface utilized to simplify the ATP/EMTP processing. Then, phase quantities and residual components are taken at different measuring nodes in the simulated networks. It is revealed that the main feature of this fault type that can enhance its detection is the periodicity of electromagnetic transients created by repetitions of the arc-reignition after each current zero-crossing. This feature is obtained considering different earthing concepts. Different detection techniques are proposed based on Discrete Wavelet Transform (DWT). The absolute sum of the wavelet coefficients in the respective frequency band is investigated for the detection purposes while several selectivity functions are proposed for the first time. The selectivity functions are presented using Logic Functions, fundamental current components and transient power directionalities. Test cases provide evidence of the efficacy of the proposed techniques.
This dissertation is written in a form of the article dissertation. Its core depends on both of a summary and six original publications.

Keywords: Arc Models, Earth Faults, High Impedance Arcing Faults and Fault Detection.

ISBN 978-951-22-9014-7 | ISSN 1795-2239
ISBN 978-951-22-9015-4 (PDF) | ISSN 1795-4584 (PDF)
ISBN (others) | Number of pages xiv + 160 p.

Publisher: Helsinki University of Technology, Power Systems and High Voltage Engineering

Print distribution: Power Systems and High Voltage Engineering

The dissertation can be read at http://lib.tkk.fi/Diss/isbn9789512290154

Acknowledgements

First of all, thanks should be forwarded to God, Most Gracious, Most Merciful, Who guides me in every step I take.

Great Teachers- I would like to take this opportunity to acknowledge Professor Matti Lehtonen, Helsinki University of Technology (TKK) for all his guidance and encouragement. Several ideas in this dissertation have been benefited from his insightful discussions during two years studying in Finland. I am also grateful to my former teachers at Minoufiya University Professor Hatem Darwish, Professor Abdel-Maksoud Taalab and Professor Mohamed Izzularab for their exemplary dedication for researching. What a pleasure to interact with them!

A great teacher who never die in my heart- I would like to acknowledge my teacher Professor Hatem Darwish who was supportive of my research and who, unfortunately, passed away. During cooperation with him on several challenging research works, he has been rewarding me a unique experience. May Allah bless him!

Research Support- I would like to express my appreciation for the support I got from Egyptian Educational Mission, Fortum säätiö and Helsinki University of Technology (TKK). Many thanks go to superiors and colleagues at Electrical Engineering Department, Minoufiya University and also at Power Systems and High Voltage Engineering, TKK for inspirational work environments at Egypt and Finland, respectively. A gratefully thank is to Mr. Hannu Kokkola and Mr. Veli-Matti Niiranen for the assistance with experimental measurements at Power Systems and High Voltage Laboratory, TKK, Finland. I also would like to thank Dr. Seppo Hänninen and the people who involved in the preparation of the staged faults. I would like to acknowledge Mr. Abdelsalam Elhaffar, Mr. Murtaza Hashmi and Mr. Abdulla Abouda for their faithful discussions. I also would like to acknowledge Dr. John Millar for checking the language of Publications [P.II], [P.V] and [P.VI]. I would like to thank Professor Liisa Haarla, Dr. Pirjo Heine and Mrs. Uupa Laakkonen for their help. I would like to express my appreciation to the pre-examiners Associate Professor Ülo Treufeldt and Dr. Seppo Hänninen for their honest and faithful comments.

Friends in need are friends indeed- I am very grateful to a lot of friends who answered my call for help in Finland. Also, I should mention my neighbor Abouda's sons Ahmed and Ali for their funnies.

Dearest Family- At the last, but not least, I cannot forget to express my warmest gratitude to my great mother, grandmother, uncles, brothers and sisters, mother and father-in-law, son Ibrahim and beloved wife for their patience and endless support.

TKK, 04.08.2007

Nagy I. Elkalashy

This work is dedicated to the soul of my father Ibrahim Abou-Elazm Elkalashy.

Dissertation's Publications and Author's Contribution

The core of this dissertation work is based on the following publications which are referred as Publication [P.I] – [P.VI]:

[P.I] H. A. Darwish and N. I. Elkalashy "Universal Arc Representation Using EMTP", *IEEE Transactions on Power Delivery*, vol. 2, no. 2, pp. 774-779, April 2005.

[P.II] N. I. Elkalashy, M. Lehtonen, H. A. Darwish, M. A. Izzularab and A-M. I. Taalab "Modeling and Experimental Verification of High Impedance Arcing Fault in Medium Voltage Networks" *IEEE Transactions on Dielectric and Electric Insulation*, vol. 14, no. 2, pp. 375- 383, April 2007.

[P.III] N. I. Elkalashy, M. Lehtonen, H. A. Darwish, M. A. Izzularab and A-M. I. Taalab "DWT-Based Investigation of Phase Currents for Detecting High Impedance Faults Due to Leaning Trees in Unearthed MV Networks" *IEEE/PES General Meeting*, Tampa, Florida, USA, June 24-28, 2007.

[P.IV] N. I. Elkalashy, M. Lehtonen, H. A. Darwish, A-M. I. Taalab and M. A. Izzularab "DWT-Based Extraction of Residual Currents throughout Unearthed MV Networks for Detecting High Impedance Faults due to leaning Trees" *European Transactions on Electrical Power*, ETEP, vol. 17, no. 6, pp. 597-614, November/December 2007.

[P.V] N. I. Elkalashy, M. Lehtonen, H. A. Darwish, A-M. I. Taalab and M. A. Izzularab "A Novel Selectivity Technique for High Impedance Arcing Fault Detection in Compensated MV Networks" *European Transactions on Electrical Power*, ETEP, published online on 23 April 2007, DOI: 10.1002/etep.179.

[P.VI] N. I. Elkalashy, M. Lehtonen, H. A. Darwish, A-M. I. Taalab and M. A. Izzularab "DWT-Based Detection and Transient Power Direction-Based Location of High Impedance Faults Due to Leaning Trees in Unearthed MV Networks" *The 7th International Conference on Power Systems Transients*, IPST2007, Lyon, France, June 4-7, 2007.

This work has been carried out under joint supervision between Minoufiya University, Egypt and Helsinki University of Technology (TKK), Finland. Professor Mohamed Izzularab, Professor Abdel-Maksoud Taalab and Professor Hatem Darwish participated from Minoufiya University and Professor Matti Lehtonen shared from TKK. The author of this dissertation has had the main responsibility of all Publications except [P.I]; its responsibility was divided between him and Professor Hatem Darwish. Professor Hatem Darwish has suggested to find how to implement the arc in EMTP and made this paper well-written. The candidate introduced the time domain model of the arc in EMTP and therefore he performed and evaluated the results and then he organized the paper sections. The coauthors of other Publications [P.II] – [P.VI] have recommended the research topic at the beginning stage of the study as they are the supervision committee. They also discussed

the results to improve the Publications. For Publication [P.II], Professor Matti Lehtonen promoted for modeling faults due to leaning trees. However, the experimental and simulation results were mainly carried out and introduced by the candidate. Laboratory setup was made with the assistance of Mr. Hannu Kokkola and Mr. Veli-Matti Niiranen. Publications [P.III] and [P.IV] were presented by the main author. For Publication [P.V] and [P.VI], Professor Matti Lehtonen suggested to check the directionality idea between the transient current and voltage as a detection selectivity function. The candidate introduced the methodology to extract this directionality using DWT and then he performed the result and wrote the paper. Finally, the developed detection algorithm and selectivity function were tested using staged faults accomplished in a MV network where these fault cases were obtained from Professor Matti Lehtonen and Dr. Seppo Hänninen.

Table of Contents

List of Symbols and Abbreviations

g	Time-varying arc conductance,
G	Stationary arc conductance,
τ	Arc time constant,
τ_o	Initial arc time constant,
τ_c	Cassie's time constant,
τ_m	Mayr's time constant,
A and B	Constants,
u	Instantaneous voltage,
u_a , u_b, u_c	Phase voltages,
u_r,	Residual voltage,
u_{st},	Stationary voltage of the arcing fault,
u_o,	constant voltage per arc length,
i	Instantaneous current,
$\|i\|$	Absolute value of the instantaneous current,
i_a, i_b , i_c	Phase currents,
i_r	Residual currents,
I_{real}	In-phase current component,
I_{imaj}	Quadrature-phase current component,
I_r	Residual current amplitude,
I_{peak}	Current peak value,
R_{tree}	Tree resistance,
U_o	Static characteristic of the breaker arc voltage,
P	Arc power losses,
P_1 *and* P_o	Constants of arc cooling power,
W	Arc input power,
Q	Arc energy content per unit volume,
μ	Arc resistivity per unit volume,
λ	Arc power losses per unit volume,
l	Arc length,
l_o	Initial arc length,
$\psi(.)$	Mother wavelet,
a_o^m	Dilation,
$nb_oa_o^m$	Translation,
a_o and b_o	Fixed values with a_o>1 and b_o>0.,
m and n	Integers,
d1, d2 and *d3*	DWT details levels 1, 2 and 3, respectively,
S_I	The detector in discrete samples using the current DWT detail coefficients,
S_U	The detector in discrete samples using the voltage DWT detail coefficients,

h	Counter for carrying out a sliding window covering 20 *ms*,
N	A number of samples per sliding window,
P_a	The discriminator computed by multiplying the DWT detail coefficients of the phase-a voltage and current and then averaging over two power cycles.
P_r	The discriminator computed by multiplying the DWT detail coefficients of the residual voltage and current and then averaging over two power cycles.
R	A ratio of the residual fundamental current component of each section with respect to the residual current amplitude of the parent section,
$I_{r(.)pre}$	Pre-fault residual current,
$I_{r(.)during}$	During-fault residual current,
Δt	sampling time step,
W_1	Sliding window of first level of DWT details,
W_2	Second level sliding window,
TKK	Helsinki University of Technology,
MV	Medium Voltage,
HVDC	High Voltage Direct Current,
EMTP	Electromagnetic Transient Program,
ATP	Alternative Transient Program,
TACS	Transient Analysis Control System,
TNA	Transient Network Analyzer,
FFT	Fast Fourier Transform,
DFT	Discrete Fourier Transform,
WT	Wavelet Transform,
CWT	Continuous Wavelet Transform,
DWT	Discrete Wavelet Transform,
db14	Daubechies wavelet 14,
DSP	Digital Signal Processing board,
MCU	Microcontroller Unit,
ADC	Analog-to-Digital Converter
CM	Combined Cassie-Mayr model,
CMC	Cassie-Mayr-Cassie model,
RRRV	Rate of Rise of Recovery Voltage,
SLF	Sort Line Fault circuit.

1- Introduction

Stresses exerted on the electrical equipment due to disturbances are appearing in the form of either overvoltages or overcurrents. The overvoltages behavior is an impulsive increase in the system voltage. Suppression devices are used to protect the electrical networks against these overvoltages. On the other hand, the overcurrents behavior is an unexpected increase in the current due faults when they are shunt faults. The protection against such faults is more challenging because it requires intelligent discriminators to isolate them quickly before catastrophic failures [1]-[2]. It is recommended to use and to enhance special protection systems that can be quite effective at times in preventing cascading outages [2].

Generally, if the faulty section is not isolated, property damage, legal liability or possible loss of life may result. Over the years, conventional protection schemes have been successfully used to detect and to protect against the low impedance faults where a small resistance only limits the fault current. However, when the resistance of the fault path is very high and therefore the fault current can not be easily recognized, it is called a high impedance fault. Such fault case can not be reliably detected, in particular in distribution systems, using the conventional relays because its current is very small [3]. One of the main features of this fault type is that it is associated with arcs. The main goal of this dissertation is to model the arc, to model the high impedance fault and then to detect this fault where a detection of the fault due to leaning trees in MV networks is studied.

1.1 Problem Description

Towards modeling and detecting of the high impedance arcing faults, the arc representation has to be studied and the fault characteristics have to be measured using experiments or to be captured from field tests. The fault model can be then represented using the well-known EMTP program and its detection can be investigated. Considering this research scope, the problem description and motivation are briefly described in this section.

1.1.1 Arc Model Representation

The arc is generally defined as a continuous luminous discharge of electricity across an insulating medium which is changed into a conducting medium due to a huge number of free electrons and ions. The arc was firstly studied concerning interruption capabilities of circuit breakers, in which arc models were initially introduced to enhance circuit breaker testing. Using these models, the capability of arc quenching can be predicted and design enhancements can be achieved with a lower number of experimental tests. Therefore, the time is reduced and the technical and economical problems of the experimental tests are overcome. The arc models have been recently modified to study the performance of arcing faults in different voltage levels and to test their detections and their discriminations.

There are several breaker arc cards built in the EMTP program [4], [5]. Unfortunately, the structure of these cards was inadequate to fulfill different applications. Recently, the shortcomings have been partially rectified with ver. 3.x of the EMTP [4]. Although models

of this version show an improved accuracy, flexibility to account for universal applications is missing. For example arcing fault, arc furnace, empirical forms, innovations in arc models … etc. can not be directly implemented. This can be remedied with the arc representation in [6]. Although this primary representation accounted for P-τ model only, additional efforts are directed for further enhancement towards universality in [P.I].

1.1.2 High Impedance Arcing Fault Characteristics and Detection Challenge

The high impedance fault detection is a long standing problem. The fault natures have been studied since the early 1970's with the hope of finding some characteristics in the waveforms for practical detections. The high impedance faults result when an unwanted electrical contact is made with a road surface, sidewalk, sod, tree limb, some other surface or object which restrict the flow of fault currents to a level below that reliably detectable by conventional protection devices. Such faults can be earth or phase faults [3].

The high impedance faults have two main characteristics: the low fault currents and arcing. The first characteristic is happened because these faults produce little or no fault current. Typical currents range is from 10 to 50 A [3], [7]. For 12.5 kV Feeder, typical results of staged faults are illustrated in Table 1. It can be seen that for object like tree, the fault current is less than 0.1 A for 20 kV level as experimentally measured in [P.II]. This fault current is furthermore reduced during the winter time in Nordic Countries and therefore the detection of faults due to trees is more challenging.

The second characteristic of high impedance faults is the presence of arcing phenomena as a result of air gaps due to the poor contact made with the earth or with an earthed object. These air gaps create a high potential over a short distance and arcing is produced when the air gap breaks down. However, the sustainable current level in the arc is not sufficient to be reliably detected. Part of this is due to the constantly changing conditions of the surface supporting the arc and maintaining high impedance. Therefore, a random electrical behavior is an associated feature with the high impedance faults. As the arcing often accompanies these faults, it further poses fire hazard and therefore the detection of such faults is critically important.

Detection of high impedance faults with high reliability is a challenge for protection engineers. The protection reliability is measured by dependability and security. A high level of dependability occurs when the faults are correctly recognized. On the other hand, a high level of security occurs when the faults are not falsely indicated. A high dependability forces a lower security level and vice versa. The dilemma is to find a sensitive high impedance detector with conserving on the protection security.

Table 1. Typical fault currents on various surfaces [7].

No.	Surface	Current (A)
1	Dry asphalt	0
2	Wet sand	15
3	Dry sod	20
4	Dry grass	25
5	Wet sod	40
6	Wet grass	50
7	Reinforced concrete	75

1.1.3 Blackouts due to Tree Faults

Recently, an interesting event was that three major blackouts were closely occurred in 2003, in which for two of them, the fault object was a tree. They were blackout on the 14th of August in North America [8]-[9], blackout on the 23rd of September in Southern Sweden and Eastern Denmark [10] and blackout on the 28th of September in Italy [11]-[13]. The tree flashovers have caused the tripping of a major tie-line between Italy and Switzerland in the 28th of September and then it extended to a blackout. Also, the tree contact was the reason of a heavy loaded line tripped out with the corresponding blackout on the 14th of August. The failure to adequately manage tree fault resulted in the line outages and therefore blackouts.

In Nordic Countries, fault categories in MV distribution networks are classified into snow burden 35%, fallen trees 27%, boughs on pole transformers 9%, diggers 6%, lightning impulses 6%, and the rest are probably caused by animals [14], [15]. Due to the large forest area in these countries, the electrical network is exposed to the faults due to leaning trees. This kind of faults is categorized as high impedance arcing faults due to high resistance of the tree and associated arcs. These faults due leaning trees are hazardous for both human beings and electrical equipments where a hazard of electric shock can occur and fires can be also initiated in the forest area in particular in the summer time.

1.1.4 Feature Extraction for Detecting Faults

Tracking harmonics is usually used for the fault detection. However, power systems have time-varying harmonics due to applications of power electronic devices, switching and fault events. Therefore, most efforts are introduced in order to develop accurate and efficient measurement schemes for estimating power system voltage and current phasors and their spectra. Phasor measurements and harmonic analysis have been carried out using Fast Fourier Transform (FFT). However, there are pitfalls such as aliasing, leakage and picket fence effects [16]-[18]. To alleviate the aliasing, the sampling frequency must be greater than twice the highest frequency in the signal to be analyzed. When the number of samples per cycle period of resolution frequency is an integer, the leakage effect is avoided. However, the picket fence effects are produced if the waveform has frequencies which are not integer multiples of the resolution frequency. The last condition to apply FFT algorithms is that waveforms must be stationary and periodic. However, the network waveforms are not stationary due to the disturbances.

To overcome such drawbacks, Wavelet Transform (WT) is recently introduced and it can analyze the signals in terms of their time-frequency localization [19]-[21]. Therefore, it is suitable for wide varieties of signals and problems in the power systems. The WT principle is that a set of basis functions is generated using dilating and translating a single prototype function called a mother wavelet. Its main advantage is the ability to focus on short-time interval for high-frequency components and long-time intervals for low-frequency components. This ability improves the analysis of signals with localized impulse and oscillation in particular in the presence of a fundamental and low-order harmonics. In a sense, wavelets have a window that is automatically adapted to give the appropriate resolution [20].

However, the wavelet execution time is one of the limitation issues restricting its practical implementation. This issue is in the phase of overcoming where discrete wavelet transforms (DWT) have been experimentally represented using Digital Signal Processing

(DSP) board with reducing its lengthy execution time as reported in [22]. This experimental implementation ensures the capability and encourages incorporating DWT in digital relays.

1.2 Arc Model Applications for Investigating the Network Transients

The arc models have been considered for more accurately representing the electrical networks either in normal operation or abnormal conditions. For example, the arc furnace is modeled to investigate the network during such complicated nonlinear load and therefore overcome the associated problems such as unbalance, harmonics, interharmonics and voltage flickers. During this load, the dynamic interaction of the arc melt process as a nonlinear load with the network is an essential study point of view. For a wide range of this load study, its interaction can be carried out using simulations. Therefore, an accurate arc model should be incorporated in the simulations, where the arc furnace load has been modeled as three parts: supply system, nonlinear load and controller models [23].

During the abnormal conditions of the network such as shunt or simultaneous faults, the fault may be permanent or transient. The permanent type is ultimately associated with arcs. In a typical scenario, a high impedance path to the earth may be established in a location with a degraded insulation. The fault may remain in the high impedance stage for indefinite period, or it may establish a low impedance path to ground, resulting in a high current earth fault. Such faults often exhibit arcing and therefore the arcing signature can enhance their detection [24]. In another typical fault scenario, an energized conductor comes in close proximity to an earthed object without making solid contact. Small air gap are presented between the conductor and the fault object. When the conductor voltage builds to a sufficient magnitude in each half-cycle, the air gaps will break down and arcing current will flow. Such arc behavior can be called arc reignition or arc restriking based on the breakdown instant through the half-cycle. The arc then extinguishes when the line voltage goes through zero and so on. The other fault scenario is a downed conductor which is also associated with arcs due to bad contacting with the earth surfaces. From these fault scenarios, it is revealed that the arc element should be considered to model and to represent the fault impact on the network and therefore to enhance the fault detection.

Furthermore, the transient faults are eventually arcing fault type where the arc interaction with the network can contribute to introduce an adaptive single-phase autoreclosure function. In this case, the fault has to be estimated either permanent or transient using protection techniques as reported in [25]. If this fault is transient, an adaptive reclosing instant is estimated based on the extinction instant of the arc where the arcing fault period is divided into primary and secondary periods. The primary period is from the fault instant up to the fault current interruption instant; however, the secondary period is from the end of the primary period until the arc media are fully de-ionized. Adaptive autoreclosures were introduced based on zero-sequence power or using artificial intelligent algorithms [26], [27]. Such algorithms were completely proposed using simulated arcing fault cases where the arc is the vital element in these simulations.

There is another point of view for the arc model applications. It is a test of the circuit breaker interruption capability. As it is well-known, a trip signal is sent to the circuit breaker to interrupt the current. However, the interruption is carried out when the breaker arc is extinguished. This arc extinction is accomplished at current zero-crossings because at these instants the input power to the arc element is the minimum. To confirm the breaker

interruption capability, it should be tested. However, realizing experimental direct test circuit is extremely difficult. Therefore, synthetic test circuits are considered. For a wide range of testing circuit breakers, the simulations are more helpful. Thus, the dynamic arc models are the core for testing and furthermore for designing circuit breakers.

Interrupting High Voltage Direct Currents (HVDC) is more challenge because there is no zero-crossing in the current waveform. However, the AC circuit breakers associated with three parallel branches are utilized for interrupting the HVDC currents [28]. These branches are commutation, Rate of Rise of Recovery Voltage (RRRV) and energy dissipation circuits as shown in Figure 1.1. The aim of commutation circuit is to create a zero-crossing by generating an oscillatory current superimposed to the HVDC current. The commutation circuit can be active or passive where there are more details addressed in [28]. The second branch which is the RRRV circuit is used to control transient recovery voltages appearing on the breaker terminals after its arc extinction. The third branch is used to dissipate a stored energy in the HVDC system. Designing the HVDC breakers can not be directly accomplished in the laboratory. However, there are simulation stages before the experimental tests. Furthermore, the simulations are then used for testing the HVDC circuit breakers in their applications as reported in [29]. In these simulations, the accuracy of such breakers design and their test is mainly depending on the dynamic arc models.

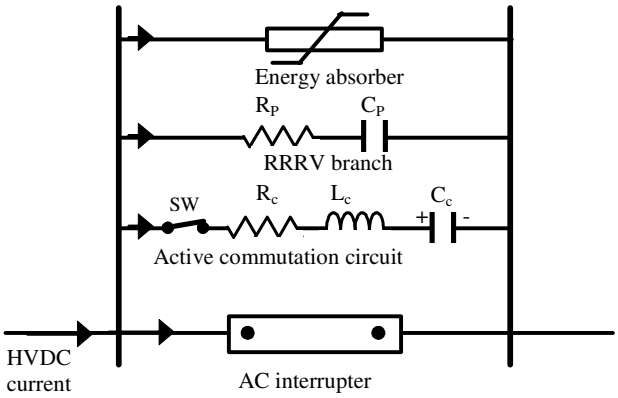

Figure 1.1 Basic circuit configuration of HVDC breaker module [28].

1.3 Directionality as a Protection support in Electrical Networks

According to the fault conditions in the network, electrical phase quantities (voltage, current and power) may change their directions. Therefore, a faulty zone can be distinguished from healthy zones or the fault point direction can be estimated. In other words, relays involving interaction between two electrical input quantities may have the differentiation ability or polarity marking which are necessary for the correct operations.

The differentiation ability is considered in different protection schemes such as differential current and differential power principles which contribute to a unit protection. The differential current performance result in the current directions and therefore it discriminates between internal and external faults. The sum of the current flowing in essentially is equal to the sum of the currents flowing out during normal operation or

external faults [30]. However, this rule is changed during internal faults. Therefore, the differential relay setting is adjusted considering the relation between average and difference currents of the protected unit terminals.

In [31], [32], the Wavelet Transform was applied on the currents at terminals of a protected transmission line. It was found that, the wavelet output spikes of the currents are in phase when the fault is external. However, they are out of phase when the fault is internal. Therefore this directionality of the wavelet output spikes were exploited to present a unit protection function. However, establishing a relay based on a spike is not a reliable protection scheme.

Recently, another differential relay depending on the power directionality is introduced [33], [34]. In the same manner of the current differential function, the differential power relay is stable during normal operation and external faults because the flow in and flow out powers are approximately equal. However, this protection scheme was introduced and tested with the transmission lines only and it is not yet generalized or applied on the other electrical equipment. Also, it is not examined on the networks with different earthing concepts.

The above mentioned protection schemes are applied in high and extra high voltage networks. In distribution networks, there is another practice for the directionality that relays sense the direction of current or power flow at a specific location and, thereby, indicate the fault point direction. A common practice is to use the output of the directional sensing unit to control the operation of the fault sensor which often is an instantaneous or an inverse-time overcurrent unit or both units together [30]. Thus if the current flow is the desired operating direction and its magnitude is greater than the fault sensor's pickup (minimum operating) current, the relay can operate. On the other hand, if the current flow is in the opposite direction, no trip can occur even though the current magnitude is higher than the pickup current. The fault direction is estimated from the phase angles of voltage and current phasors, where a polarizing quantity, normally the voltage, is used as a reference. In other concept, the difference in phase angle between the positive-sequence component of the current during fault and prefault conditions is used as an indicator to the fault point [35].

When the distribution networks are unearthed or compensated, the network overvoltages are used as a fault detection aid for earth faults. However, when the network energizes several feeders, the directionality between fundamental residual voltage and currents can discriminate between the faulty and healthy feeders [36]. Higher fault resistances limit the earth fault detection using such technique.

The protection schemes mentioned in this section are some principles of the network protection. However, they are not reliable to detect high impedance faults in particular when the fault resistance is very high like the tree resistance. A reliable detector of high impedance faults is still a challenging issue for protection engineers.

1.4 High Impedance fault Detection

As aforementioned, high impedance faults are defined as all low current faults which cannot be detected using conventional protections. Towards detecting the high impedance faults, most of the efforts have been directed to identify the fault features and therefore to clarify practical considerations for their detections [37]-[45]. The fault feature extraction is

carried out using different filters such as FFT, Kalman Filter, Fractal and Wavelet Transforms [3], [37]-[48]. Numerous detection algorithms have been motivated, depending on harmonic contents such as second order, third order, odd harmonics, even harmonics, nonharmonics, high frequency spectra and harmonic phase angle considerations [42]-[45]. However, such techniques are still limited by larger fault resistance, in particular resistances greater than 100 kΩ, such as the tree resistances.

In order to improve high impedance fault detection capability and also in order to provide a high degree of security, a sophisticated detection technique was discussed in [24]. This technique was depending on parallel algorithms such as energy, randomness, arcing phase signature and load analysis algorithms. The energy algorithm monitored the level of energy contained in a specific range of frequency components. It might be difficult to identify changes in these energies due to connected loads. However, the non-harmonic components gave a much more dramatic indicator of high impedance arcing faults. The randomness algorithm was depending on a variability of instantaneous fault current magnitudes due to changing of physical fault conditions at a particular time. The randomness algorithm also calculated the amount of randomness associated with a fault using the energy contained at a non-fundamental frequency as a monitoring quantity. The arcing phase signature algorithm was depending on the arc signature on the current at a specific phase angles of the applied voltage, specifically near the voltage peaks. This signature was particularly visible in the high frequency (above 2 kHz) components of current. The load analysis algorithm was added to enhance the security term of the detection reliability. This algorithm identified a number of normal events and the corresponding waveforms on the network. This sophisticated detection technique became more complicated when applying the algorithms, for example energy and randomness algorithms, on multiple frequencies on each phase, on neutral current and further on the summation of odd harmonics, even harmonics and nonharmonics as discussed in [37]. Given all these inputs and information, a decision about the presence of a fault is neither quickly nor easily made.

In the same manner, the random behavior of the high impedance fault current was used as a detector aid in [49]. In this detection technique, the positive and negative current peaks in one cycle to those in the next cycle were compared. Therefore, a current flicker was measured and the current asymmetry was calculated. Such detection method was suggested to detect the downed-wire faults, which is also known as high impedance faults. However, the fault current has extremely small changes when the fault object has an extremely high resistance such as the tree and therefore the current flicker or asymmetry can not detect this fault.

1.5 Earth Fault Detection in Unearthed and Compensated MV Networks

The transients produced in electrical networks due to faults often depend on the neutral point treatments. They can be completely isolated from the ground, earthed through impedance or solidly earthed at their neutral. In Nordic Countries, the neutral is commonly unearthed and compensated MV networks are increasingly being used [36], [46]. There is an important trait for the unearthed system. The directionality of the residual currents in the healthy and faulty branches with respect to the residual voltage is obvious during earth

faults [36]. This behavior is used for protection objectives. However, the fault resistances associated with leaning trees are very high limiting its detection using current magnitudes.

Compensated earthing has grown in interest and its practical applications have increased [36], [46]. In this case, the earth fault current is somewhat small when it is compared to its value in a corresponding unearthed system. This is due to the parallel resonance of the inductance connected to the neutral and network earth capacitances. Therefore, traditional detectors reacting at current thresholds are no longer practical. One of the protection methods for detecting earth faults in compensated networks was to short circuit the Petersen coil using a parallel resistance to enable their detection. However, the coil function was not fully gained in this case. Furthermore, a complicated mechanism is required to apply such techniques.

One of the main contributions of [46], [47] was based on analyzing the relative direction variations of transient residual voltages and currents which occur during earth faults. When a fault occurred, whatever the earthing system used, the transients of the residual current and voltage are in opposite directions in the defective section and in the same direction in the others. However, the sensitivity limit is reached for larger fault resistances. This sensitivity will be improved with the aid of the DWT as discussed in chapter 5 [P.V].

Other earth fault detection issue was discussed in [48], where a comparison of the residual current with each phase current was used to distinguish the faulty feeder. The scalar product is used as the means of comparison. The other detection technique was introduced based on analyzing the variation of the system parameters with respect to their steady state values [50]. However, the detection based on the system parameters identifications is still unreliable with the high impedance faults.

1.6 Wavelet Transform (WT)

As aforementioned, the network waveforms are not stationary due to disturbances. Therefore, FFT is not suitable for well-timed tracking and it is important to use an appropriate signal processing technique such as WT. Recently, wavelet analysis has been used in several applications in the power systems. For example in a power quality research area, it is applied for monitoring and for analyzing power system disturbances [51]-[56]. For partial discharge applications, it is considered for de-noising the measure signals and therefore enhancing the partial discharge monitoring task [56]-[61]. In digital protection area, the discrimination between transformer inrush currents and internal faults has been carried out using WT [62]-[66]. Also, fault detection and classification considering high impedance types have been enhanced when the wavelet analysis is considered [32], [40]-[42], [67]-[77].

Wavelets are families of functions generated from one single function, called the mother wavelet, by means of scaling and translating operations. They are oscillatory, decaying quickly to zero either side of its central path, and integrating to zero. The scaling operation is used to dilate and compress the mother wavelet in order to obtain the respective high and low frequency information of the function to be analyzed. Then the translation is used to obtain the time information. In this way a family of scaled (dilated)

and translated (shifted) wavelets are created and serve as the base for representing the function to be analyzed [19]-[21].

Mathematically, the Continuous Wavelet Transform (CWT) of an input signal $x(t)$ with respect to a mother wavelet $\psi(t)$ is generally defined as:

$$\mathrm{CWT}_{\psi} f(a,b) = \frac{1}{\sqrt{a}} \int_{-\infty}^{\infty} x(t)\psi^{*}(\frac{t-b}{a})dt \tag{1.1}$$

where $\psi^{*}(.)$ is a complex conjugate of the mother wavelet $\psi(.)$, a is the dilation or scale factor and b is the translation factor. It is apparent from the above equation that the original one-dimensional time domain signal $x(t)$ is mapped to a new two-dimensional function space across scale a and translation b. In other words, a WT coefficient $\mathrm{CWT}_{\psi}(a,b)$ at a particular scale and translation represents how well the original signal $x(t)$ and scaled/translated mother wavelet match. These coefficients are thus a wavelet representation of the original signal with respect to the mother wavelet.

CWT has a digitally implementable counterpart called Discrete Wavelet Transform (DWT), which it is in the form:

$$\mathrm{DWT}_{\psi} f(m,k) = \frac{1}{\sqrt{a_o^m}} \sum_{n} x(n)\psi(\frac{k - nb_o a_o^m}{a_o^m}) \tag{1.2}$$

where the mother wavelet $\psi(.)$ is discretely dilated by the scale parameter $a_o{}^m$ and translated using the translation parameter $nb_o a_o{}^m$, where a_o and b_o are fixed values with $a_o>1$ and $b_o>0$. m and n are integers. In the case of the dyadic transform, which can be viewed as a special kind of DWT spectral analyzer, $a_o=2$ and $b_o=1$. DWT is implemented using a multistage filter with down sampling of the low-pass filter output.

To overcome the complexity encountered in DWT real time implementations, a novel DWT computational procedure has been introduced and experimentally verified in [22]. As shown in Figure 1.4, the real-time implementation of the dyadic DWT is depicted. The inner product of the updated sliding window vector of the sampled signal [W_1] and the DWT filter coefficients (high and low-pass filter coefficients C_f) is convoluted with the processed frame. This process is repeated every two real-time shifts [$2\Delta t$], to insure the down-sampling process, in the first level of calculation to obtain the approximation a_1 and detail d_1. From the first stage, the second one can be calculated by performing the inner product of a_1 and DWT filter coefficients along the calculated frame every 4 real-time shifts [$4\Delta t$]. Similarly, level three is executed every [$8\Delta t$], level four every [$16\Delta t$] … and so on. In other words, a separate sliding window for each level with N element is only used, where N equals to the number of DWT digital filter coefficients interpreting the used mother wavelet. The first level-sliding window [W_1] updates its real-time data from the samples of the analyzed discrete input signal. However, the second level-sliding window [W_2] is updated from the first level output a_1 and the third level from a_2 and so on. This represents a distinguished computation procedure with limited burden compared with the conventional computation methods.

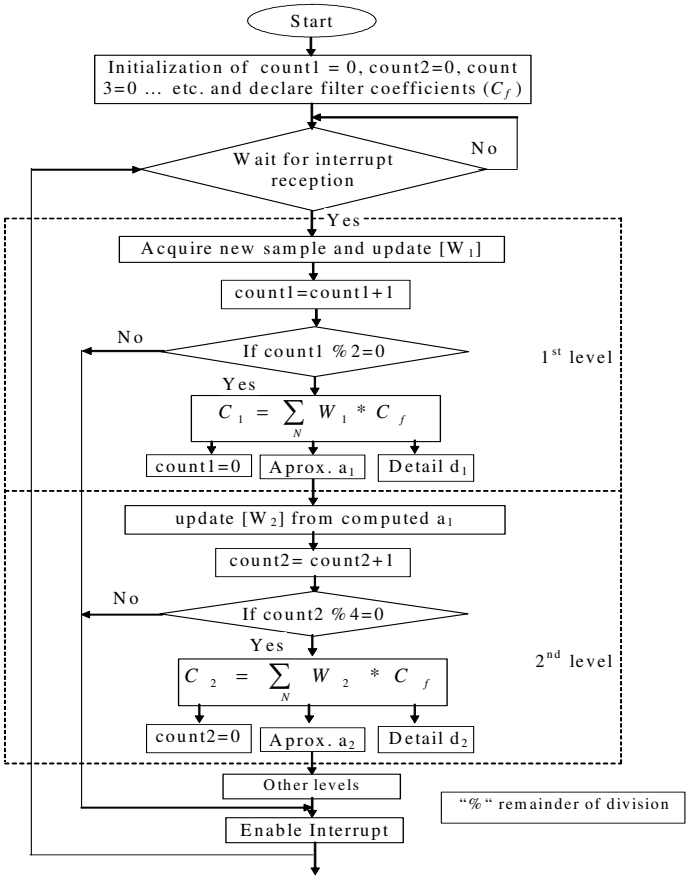

Figure 1.4 Flow chart of implemented DWT in real-time [22].

1.7 Electromagnetic Transient Program (EMTP)

EMTP is a computer program for simulating electromagnetic, electromechanical, and control system transients on multiphase electric power systems. It is used in this dissertation to simulate the arc and fault models and to represent their interactions with the networks. It was first developed as a digital computer counterpart to the analog Transient Network Analyzer (TNA). Many other capabilities have been added to EMTP over the years and it has become a standard program. One of the EMTP's major advantages is its flexibility for accurate modeling; an experienced user can apply the program to a wide variety of studies. The cost and space considerations of analog simulation give preference to the EMTP program. For example, it is not possible with scaled down analog models to simulate distributed natures of transmission line parameters [78]-[80].

Alternative Transient Program (ATP) was started as a new program from a copy of EMTP however with different commercialization. Therefore, the ATP manual is just a complete set of rules for EMTP input and output. However, there are slight differences such as circuit breaker models embedded in EMTP but they are not set in ATP. To overcome this drawback, ATP includes TACS controlled resistance that can provide breaker arc interaction. For more flexibility of a programming language, MODELS is recently introduced to interact with the source code of ATP.

ATPDraw is a graphical and mouse-driven preprocessor to the ATP version of the EMTP program on the MS-Windows platform [81] where the user can construct an electrical circuit using the mouse and selecting components from menus. Then, ATP input file is generated according to its codes. Most of the standard components of ATP, as well as TACS and MODELS are supported in ATPDraw. Line/Cable modeling is also included where the user specifies the geometry and material data and he has an option to view the cross section graphically and to verify the model in the frequency domain.

1.8 Work Contribution

The arc model representations in EMTP are divided into three different types. These three representations of arc models are: Avdonin, Urbanek, and Kopplin model as reported in the EMTP rulebook [4]. They are internally built-in and just require parameter identification. Therefore, the system investigation is limited to a bounded area declared by the model card parameters. In this dissertation, a universal breaker arc representation in the form of controlled voltage source in the EMTP program is presented as reported in [P.I]. The arc voltage and current signals are measured and transported from the EMTP power network into the TACS filed where they are used as inputs to the dynamic arc equation. Parameters of this equation are computed exploiting the FORTRAN facilities. The dynamic arc equation which is a first order differential equation is solved using a controlled integrator. Then, the obtained arc resistance value is multiplied by the arc current to compute the arc voltage which is fed back to the power network in the next step and so on. Therefore, the arc interaction with the power network is carried out. A comparison of this proposed representation with the EMTP built-in Avdonin model is performed. Thermal limiting curve derivation and breaker performance evaluation in a direct test circuit, Short Line Fault (SLF) circuit, and transmission system are carried out. Possibility of implementing different arc models using the novel representation is also explored. The universality is verified by implementing several examples of practical arc models such as improved Mayr, series arc and arcing fault models.

When high impedance fault detection techniques were directly introduced using either staged filed data or experimental results, the better performance of such techniques is restricted to the fault cases used in the proposing stages of these techniques. This limitation is due to sophistications of the experiments and staged fault cases. However, if the fault element is accurately modeled and easily represented at different locations in electrical networks, the evaluation of the fault detection techniques will be more reasonable. Therefore, an experimental setup accomplished at Helsinki University of Technology (TKK), Finland is used to establish a high impedance fault of a leaning tree type as presented in [P.II]. The test results are used to model the fault. The model parameters are determined. The experimental work is implemented using the ATP/EMTP package. The tree impedance is represented using a resistance and the arc element is modeled by a thermal model, which realized using universal arc representation in the ATP code. The simulation results are compared with the experimental results to examine the fault model validity. The comparison is carried out between the experimental and simulated fault features extracted using DWT.

The detection of faults due to leaning trees in MV networks is discussed for the first time in this dissertation. As aforementioned, this fault current is less than 0.1 A in a 20 kV voltage level and therefore its detection is extremely difficult. Towards introducing a

detection technique, the fault due to leaning trees occurring at different locations in 20 kV networks is simulated by ATP/EMTP. The impact of the arc reignition periodicity on the network currents is used to detect this difficult fault. In the vicinity of the current zero-crossing, the initial transients lead to fingerprints boosting secure fault detections [P.II]. These transients are localized based on the DWT detail coefficient of the feeder currents to reliably detect the fault. The absolute sum over a period of one power cycle is computed and used as a detection flag or as a detector [P.III]. This detector is high not only at the fault beginning but also during the fault period. Also, this detector performance is attained with all phases at any measuring node fixed at the beginning of feeders. However, the faulty phase detector is the highest when the phase detectors are compared and the faulty feeder detector is the highest one when the feeder flags are evaluated. Therefore, Logic Functions are introduced to determine the faulty phase and also the faulty feeder as discussed in [P.III]. When wireless sensors are used for enhancing the fault detection and location processes, the detection technique is evaluated at different measuring nodes but another selectivity function is introduced as following [P.IV]. A ratio of the residual fundamental current of each section with respect to the parent section in the corresponding feeder is estimated for locating the faulty section. It is found that this ratio is close to one at all measuring nodes starting from the main transformer until the fault point. On the other hand, this ratio is close to zero at the other measuring nodes. This feature is correct only when the network is balance. Then, this selectivity function is modified to overcome this point of shortcoming.

Also by exploiting the transients repeated for each half cycle due to the arc reignitions after each current zero-crossing, another detection procedure is introduced in [P.V] and [P.VI]. The fault localization is carried out by investigating the DWT detail coefficient of the measured voltages. The absolute sum over one power cycle is computed for the setting aim. The fault section is estimated using a novel selectivity protection function as following. The DWT detail coefficients of the currents and voltages are multiplied together. Then, a summation is computed over a period of two power cycles to estimate its polarity. This polarity is used as the directionality condition, in which, it is negative when the fault is behind this measuring node and it is positive when the fault is not behind. Therefore, this feature can discriminate between the healthy and faulty sections or feeders. This technique is applied on three-phase quantities and also on residual components. Furthermore, this technique is evaluated using field data. Test cases provide evidence of the efficacy of the proposed technique.

1.9 Dissertation Outline

Briefly, the dissertation consists of this summary and Publications [P.I] – [P.VI]. The dissertation presentation is as following.

- The universal arc representation using EMTP is introduced in chapter 2.
- Modeling of high impedance arcing fault due to leaning trees is presented and experimentally verified in chapter 3.
- The fault detection and different selectivity techniques are proposed in chapters 4 and 5.
- Conclusions and future considerations are summarized in chapter 6.
- Finally, Publications [P.I] – [P.VI] are enclosed.

2- Evolution and Representation of Arc Models

Efficient arc models combine simplified model forms in addition to a little sophistication in their programming. The arc models developed hitherto can be classified into two categories. The first category is based on dielectric recovery [81]-[84] and the other one is concerned with arc thermal characteristics [85], [86]. For miscellaneous applications, the thermal models were widely used as they give a better interpretation of the arc behavior than that is given by the dielectric recovery. Therefore, most of the efforts have been directed to develop new thermal models or to improve the existing ones. The validity of thermal arc models either for testing the circuit breaker interruptions or for representing arcing faults is achieved based on conformities between the measured and computed performances. The thermal models are intensively discussed in this chapter.

Thermal models have the longest history of the dynamic arc models since Cassie 1939 [87] and Mayr 1943 [88] introduced the first description of arc conductivity in a form of first order differential equation. Thermal arc models are usually classified into two forms. In the first one, the physical phenomenon of the arc is considered to explore the effect of circuit breaker design parameters on the interruption performance such nozzle size, speed of the flow, types of heat transfer ... etc. [86], [89], [90]. In the second form, the arc is modeled considering its external characteristic only such as Cassie, Mayr, combined Cassie-Mayr, modified Mayr, Improved Mayr models, … etc [85], [87], [89], [91]-[97]. Based on the second type of thermal models, characteristics of the breaker arc in the form of arc voltage, current, and rate of change of current are measured on the vicinity of current zero. These measurements should be recorded with highest possible time resolution to extract the model coefficients. This type of models is usually utilized when the arc is investigated as a part of the power system, which is satisfactory for modeling breaker arcs, long arcs and high impedance arcing faults and therefore for the dissertation subject.

2.1 Mathematical Derivation of Thermal Arc Models

The mathematical analysis of dynamical breaker arc extinction is very difficult due to the rapid change of the conductivity in a few microseconds around the current zero point. Therefore, most of the efforts have been directed to find a comparatively simple mathematical description in the form of integral modeling and without involving the physical processes. These models were proposed to represent actual circuit breaker arcs near by the current zero. They were concerned with the variation of arc resistance, arc current, arc power losses of arc space under certain simplifying assumptions with time span few hundreds of microseconds around current zero. In which, the arc conductivity was calculated based on the energy balance theory. Cassie followed by Mayr started these concepts of arc modeling for the description of arc behavior. The mathematical bases of these models established the preliminary rules of dynamic arc behavior description. The simplified integral equation(s) parameters of these models were expressed in terms of arc time constant, arc power losses … etc. in the vicinity of the current zero.

The energy balance states that the arc conductivity is a function of the arc power input, arc power losses, and time [85]. It is given in the form:

$$g = \frac{i}{u} = F(W, P, t) \tag{2.1}$$

where i is the instantaneous arc current, u is the instantaneous arc voltage gradient, g is the instantaneous arc conductivity per unit length, W is the power input to the arc per unit length, P is the power loss from the arc per unit length and t is the time.

The equation can be investigated and expressed as:

$$g = F(Q) = F(\int (W - P)dt) \tag{2.2}$$

where Q is the energy content per unit length of the arc associated with its temperature and state of ionization. Accordingly, the general form of the arc model can be obtained as follow:

$$\frac{1}{g}\frac{dg}{dt} = \frac{F'(Q)}{F(Q)}\frac{dQ}{dt} = \frac{F'(Q)}{F(Q)}(W - P) \tag{2.3}$$

Under particular forms selected for $F(Q)$ and P, the equation of Cassie and Mayr can be deduced.

Cassie assumes constant resistivity (μ), constant power loss (λ), and constant energy content (c) where they are constant per-unit-volume. Accordingly, the assumed constant cross-section area (A), which is dependent on the current and time, requires that the current density and voltage gradient are also constant in the steady state case. This gives a static characteristic (U_o) as in:

$$U_o = \sqrt{\mu\,\lambda} \tag{2.4}$$

Thus, the aforementioned assumptions lead to:

$$g = F(Q) = \frac{A}{\mu} = \frac{Q}{\mu c} \quad \text{and} \quad P = A\lambda = \frac{Q\lambda}{c}, \text{ where } A = \frac{Q}{c} \tag{2.5}$$

Then the differential equation, which Cassie was obtained, is in the from:

$$\frac{1}{g}\frac{dg}{dt} = \frac{1}{\tau}\left(\frac{u^2}{U_o^2} - 1\right) \tag{2.6}$$

where $\tau = c/\lambda$ is the arc time constant.

On the other hand, Mayr assumptions are that thermal ionization is according to Saha equation and heat losses are due to thermal conductance only [85]. This leads to:

$$g = F(Q) = Ke^{\left(\frac{Q}{Q_o}\right)} \tag{2.7}$$

By substituting in the general form of heat balance equation (4), Mayr differential equation is in the form:

$$\frac{1}{g}\frac{dg}{dt}=\frac{1}{\tau}\left(\frac{u\,i}{P}-1\right) \tag{2.8}$$

where, $\tau=Q_o/P$ is the arc time constant.

The experimental results have shown that Cassie's dynamic arc equation is recommended for modeling the arc in pre-current zero regime while the Mayr's equation is suitable for post-current zero one. On other words, the evaluation of using only one dynamic equation of Cassie or Mayr is not sufficient for quantitative calculation over pre and post current-zero crossing.

2.2 Extended Study of Thermal Models

Extensive studies were conducted to improve these models. In [90], a formulation of the Combined Cassie-Mayr (CM) model was introduced. The CM model employs each equation of the two forms in its appropriate arc representation period. Cassie's equation before current zero and Mayr's equation after current zero where the transition from Cassie's to Mayr's equation at current zero is applicable due to the two equations are identical at zero power input. Similarly, Cassie-Mayr-Cassie (CMC) model was introduced [95]. In this extended model, Cassie represents the arc in pre-zero interval and Mayr, which is used in post-zero, is taken from the solution of Cassie at the zero-crossing point. After current zero, if the arc resistance is increased the successful interruption is occurred. However in case of the failure interruption, the modified Cassie differential equation is then utilized but with new parameters. The defect of considering these models is that different assumptions between the pre and post current-zero crossing produces unrealistic change in the conductivity time response at the transition instant.

A parallel arrangement of Cassie and Mayr arc representation was introduced in [93], [96]. In this case, both model equations are solved simultaneously and arc resistance is obtained by summing up the resultant resistance of each equation. The arc behavior of a circuit breaker is described using four constant parameters model as given below:

Cassie: $$\frac{1}{g_C}\frac{dg_C}{dt}=\frac{1}{\tau_C}\left(\frac{i^2}{U_O^2\,g_C^2}-1\right) \tag{2.9}$$

Mayr: $$\frac{1}{g_M}\frac{dg_M}{dt}=\frac{1}{\tau_M}\left(\frac{i^2}{P\,g_M}-1\right) \tag{2.10}$$

Then: $$\frac{1}{g}=\frac{1}{g_C}+\frac{1}{g_M} \tag{2.11}$$

where g_C and g_M are the conductivity of the Cassie and Mayr parts of the arc, respectively. Both equations have two constant parameters: U_o is the constant part of the arc voltage, τ_C is Cassie's time constant, P is the steady state power loss, and τ_M is Mayr's time constant. From the evaluation of this model, it was found that in the vicinity of current zero, the contribution of the Mayr equation is increased while the Cassie portion goes to zero. For this model, four parameters must be determined. Therefore, solving two differential

equations and determination of arc parameters of a certain circuit breaker would be troublesome.

The Modified Mayr model has been considered one of the important contributions in the area of dynamic arc modeling [97]. The parameters used for arc behavior estimation are: arc time constant $\tau(g)$ and arc power losses $P(g)$. Both parameters are usually expressed in terms of the arc conductivity and they are specified for each circuit breaker. Therefore, Mayr differential equation is altered to the following form:

$$\frac{1}{g}\frac{dg}{dt} = \frac{1}{\tau(g)}\left(\frac{u\ i}{P(g)} - 1\right) \tag{2.12}$$

$$\tau(g) = \tau_o\ g^{\alpha} \quad \text{and} \quad P(g) = P_o\ g^{\beta} \tag{2.13}$$

If $\tau(g)$ and $P(g)$ are constants, the equation is identical to the form of Mayr's model. However, if $\tau(g)$ is constant and $P(g)=U_o^2\ g$, where U_o=constant, it becomes identical for the Cassie's equation model as illustrated by Moller in [92]. Generally, the model simplicity and its parameter plausibility are the major advantages for its wide range of applications. However, the arc model has power functions of arc conductivity in the denominators. After current zero, this conductance becomes very small in case of successful interruption. Therefore, numerical errors may occur, which would be tolerated using very small time step of calculation.

One of the innovations in arc models is the Improved Mayr model, which is recently introduced by KEMA, High Power Laboratory Group [94]. This adaptive arc model is given by:

$$\frac{1}{g}\frac{dg}{dt} = \frac{1}{\tau}\left(\frac{u\ i}{\max(U_o|i|,\ P_o + P_1\ u\ i)} - 1\right) \tag{2.14}$$

where P_1 and P_o are constants of cooling power and U_o is the constant arc voltage in the high current area. Equation (2.14) is used to represent the dynamic arc equation during pre-zero current period, in which model conformity with Cassie in high current area is fulfilled. However, Improved KEMA model has constant cooling power, which is dominant near current zero area. This is fulfilled by the ***max*** statement of (2.14). After the current zero crossing, the equation is reduced to the Mayr arc model as follows:

$$\frac{1}{g}\frac{dg}{dt} = \frac{1}{\tau}\left(\frac{u\ i}{P_o} - 1\right) \tag{2.15}$$

This is exactly the Mayr arc model with two parameters as in (2.8), while the KEMA arc model generally has three free parameters as in (2.14).

2.3 Arcing Fault Models

Transmission line arcing faults are widely experienced in power systems and they are usually categorized as transient faults. Their identifications would involve some difficulties compared with other types of transient faults. Therefore, efficient long arc models are highly demanded to represent the bilateral interaction between the system and the arc

element [98]-[103]. Furthermore, classifying these types of faults would enhance the operation of extra high voltage autoreclosures. The dynamic behaviors of arcing fault are described either by normalizing the volt-ampere characteristics or by considering the power balance of arc column with estimating the model parameters by variant methods. Alternatively, the arcing faults have been represented by approximating the arc interaction as a square wave voltage locked with the arcing current and accompanied by additional harmonics. This wave voltage amplitude is estimated depending on the arc length, arc constant voltage per unit length … etc. The model is modified to include a current dependant voltage source with a distorted rectangular waveform [102].

There are two arcing fault models that have been recently introduced using the dynamic equations. The first one is the Kizilcay model [99], [100]. The second one is the Johns model [101]. Kizilcay model is a well-trusted as its effectiveness was experimentally verified in [104]. Considering the Kizilcay model, a synthetic test circuit is developed to obtain the parameters of primary and secondary phases of the arc along a 380 kV insulation string [102]. The arcing fault equation of the Kizilcay model is given as:

$$\frac{dg}{dt} = \frac{1}{\tau}(G - g) \tag{2.16}$$

$$G = \frac{|i|}{u_{st}} \quad \text{and} \quad u_{st} = (u_o + r|i|)l \tag{2.17}$$

where G is the stationary arc conductance, r is the resistive component per arc length, u_o is constant voltage per arc length, and l is the time dependent arc length.

When the Johns model [101] is considered, the stationary arc conductance G can be evaluated as following:

$$G = \frac{|i|}{u_o l} \tag{2.18}$$

While the arc time constant τ was empirically derived for the arc current as:

$$\tau = \frac{\alpha I}{l} \tag{2.19}$$

where I is the peak value of the fault current when it is considered a bolted one and the coefficient α is about 2.85×10^{-5}. It was empirically obtained by fitting the dynamic arc equation time response to match the experimental cyclograms of the arc currents ranging from 1.4kA to 24kA.

The parameters formulas of the previous two models have been introduced to fulfill arcing fault characteristics in the transmission line systems. Kizilcay model parameters described in (2.17) are modified to represent the arcing faults in MV networks as reported in [105]. The modification is that u_o and r are not considered constant; however, they are dependent on the arc length as in the form:

$$u_o = 900 + \frac{400}{l} \quad \text{and} \quad r = 0.040 + \frac{0.008}{l} \tag{2.20}$$

Regarding the time constant τ, it is also modified as following:

$$\tau = \tau_o (\frac{l}{l_o})^{\alpha} \qquad (2.21)$$

where τ_o is the initial arc time constant, l_o is the initial arc length, α is a coefficient of negative value. Since the arc length variation is highly dependent on external factors like wind, conventions of the plasma and surrounding air, it is difficult to consider these random effects accurately in the arc model.

2.4 Universal Arc Representation [P.I]

The arc simulations are strictly carried out using the EMTP program, in which, a valid arc implementation is accomplished in [P.I]. This representation facilitates establishing the time domain model of any dynamic arc equation by exploiting the bilateral interaction between the EMTP power networks and TACS field. In this section a brief declaration of the proposed arc representation and its evaluation are summarized.

2.4.1 The Proposed Arc Representation

The proposed representation of the arc model can be explained with the help of Figure 2.1. The generator is used to provide the breaker with the short circuit current level and the R_c-C_c branch is used to control the Rate of Rise of Recovery Voltage (RRRV). The breaker arc is represented by TACS controlled voltage source type 60. The value of the voltage is computed in the TACS field by multiplying the computed arc resistance by the arc current measured by sensor 91. This resistance is derived from the dynamic arc equation(s) exploiting the TACS tools. At the next step, the corresponding arc voltage is fed back into the power network via controlled voltage source type 60. In this manner, arc interaction with the power system elements is fully considered. It should be noted that during pre-zero current periods, the controlled voltage source is connected to the system, as the switch SW is normally closed until current zero crossing. While for testing the breaker RRRV withstanding during post current-zero interval, the switch is opened and the breaker voltage is transported into TACS field by sensors 90. Then, the RRRV against the zero current conductivity states interruption/reignition conditions according to post zero dynamic arc equation(s). In order to distinguish between the pre and post zero current periods, control signals are generated. Implementation details of the modified Mayr model (2.12) and (2.13) using the proposed arc representation is preliminarily given in [6] and also summarized in the Appendix of [P.I]. However in [P.I], the arc representation universality is achieved and approved considering a wide range of arc models.

2.4.2 Evaluation of the Proposed Arc Representation

An SF6 breaker rated at 123 kV and 40 kA breaking current is used as a test sample [97]. In which, the characteristic arc time constant $\tau(g)$ and power loss $P(g)$ functions were obtained experimentally via series of short circuit tests as given by Figure 2.2. It is obvious from Figure 2.2 that $P(g)$ and $\tau(g)$ functions are divided into three functions considering the magnitude of the conductivity (g). This would represent an obstacle to EMTP Avdonin model as this model only accounts for a single function of $P(g)$ and $\tau(g)$.

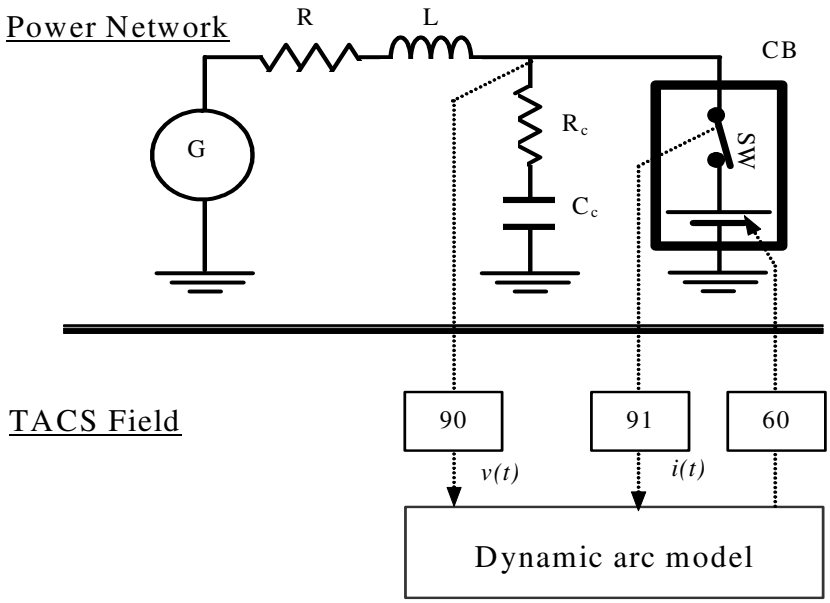

Figure 2.1 EMTP network of synthesizer generator and breaker.

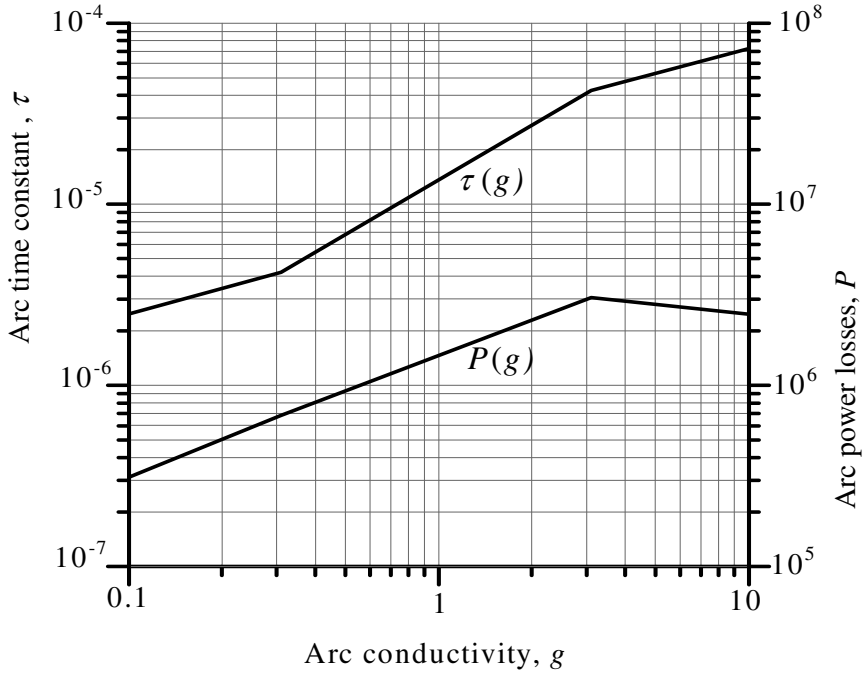

Figure 2.2 Reported P-τ functions of the circuit breaker [97].

Figure 2.3 illustrates a comparison of the computed limiting curves when they are estimated using the universal arc representation and when considering EMTP Avdonin model cards. When the limiting curve is computed using the universal arc representation, the $P(g)$ and $\tau(g)$ functions which are divided into three functions of g are computed exploiting the flexibility of Fortran expressions in the TACS field. The corresponding thermal limiting curve is shown in Figure 2.3 as a solid line. On the other hand, declaring these three functions of $P(g)$ and $\tau(g)$ is impossible using EMTP Avidonin model cards. In order to sort out this issue, two solutions can be considered. The first one is to select the $P(g)$ and $\tau(g)$ function corresponding to the lowest value of g and use them in the declaration of the arc parameters. The other solution is to do some regression forms in order to reduce the three functions into a single function. After testing these two solutions, it is found that the first one is the appropriate and the corresponding limiting curve is shown in Figure 2.3 as a dot line.

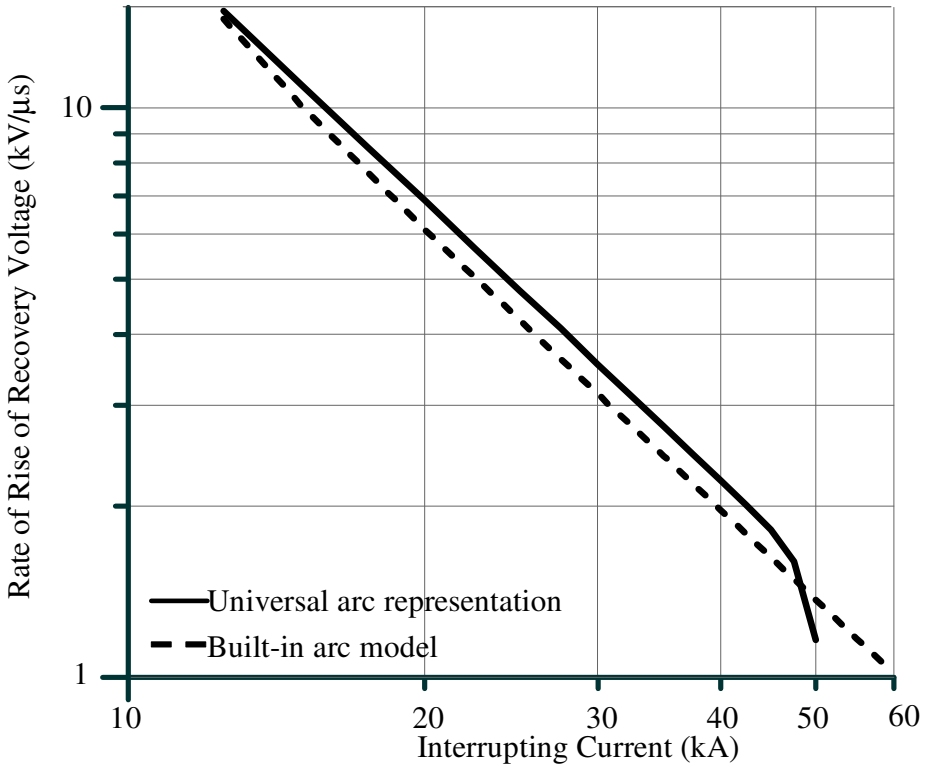

Figure 2.3 Comparison of the computed limiting curves.

When these curves, which are computed by the proposed representation and by EMTP built-in model, are compared with the experimentally reported curves shown in Figure 2.4, there is a good matching between the derived curves using the proposed representation and the reported curves traced for zero time delay of voltage application on the arc channel post current zero. There are different delay times accounting for a free interval of conductivity decaying before the application of RRRV as reported in [97]. The reason of this matching is that the three $P(g)$ and $\tau(g)$ functions of Figure 2.2 are realized in the EMTP considering the flexibility of TACS FORTRAN expressions as mentioned before. However, these three functions of $P(g)$ and $\tau(g)$ can not be realized in EMTP Avidonin built-in model cards as the arc parameter card is declared by $P(g)$ and $\tau(g)$ corresponding to the lowest part of g curves.

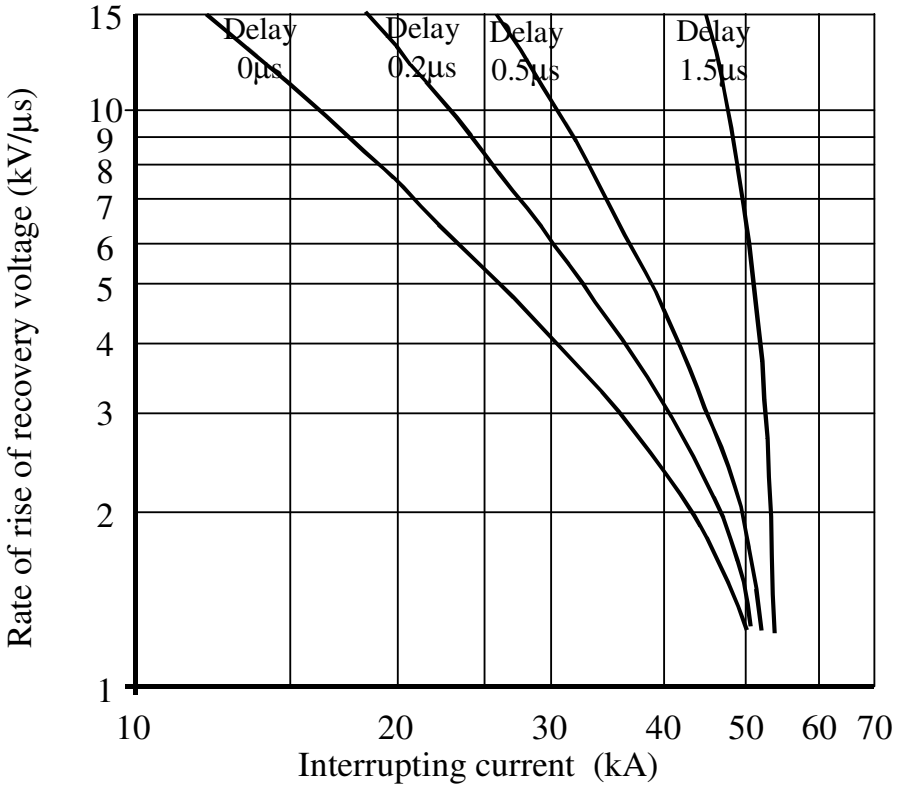

Figure 2.4 Reported thermal limiting curves [97].

In order to confirm the accuracy of the proposed arc representation, a single function of $P(g)$ and $\tau(g)$ is considered for the proposed representation and Avdonin built-in models. Then, the thermal limiting curves are computed and the results of both models are fairly close as shown in Figure 2.5. This reveals that the proposed representation has the same accuracy of the built-in models as far as single function for $P(g)$ and $\tau(g)$ is considered. However, the proposed representation has the advantage of flexible consideration of multi functions defining $P(g)$ and $\tau(g)$. It should be also noted that the curve of zero time delay is only considered in the comparison. Other curves with different time delays cannot be considered as the built-in model format does not fulfill such conditions. More comparisons, to confirm the accuracy, are discussed in [P.I] such as the breaker performance in the time domain using a direct test circuit and power transmission system.

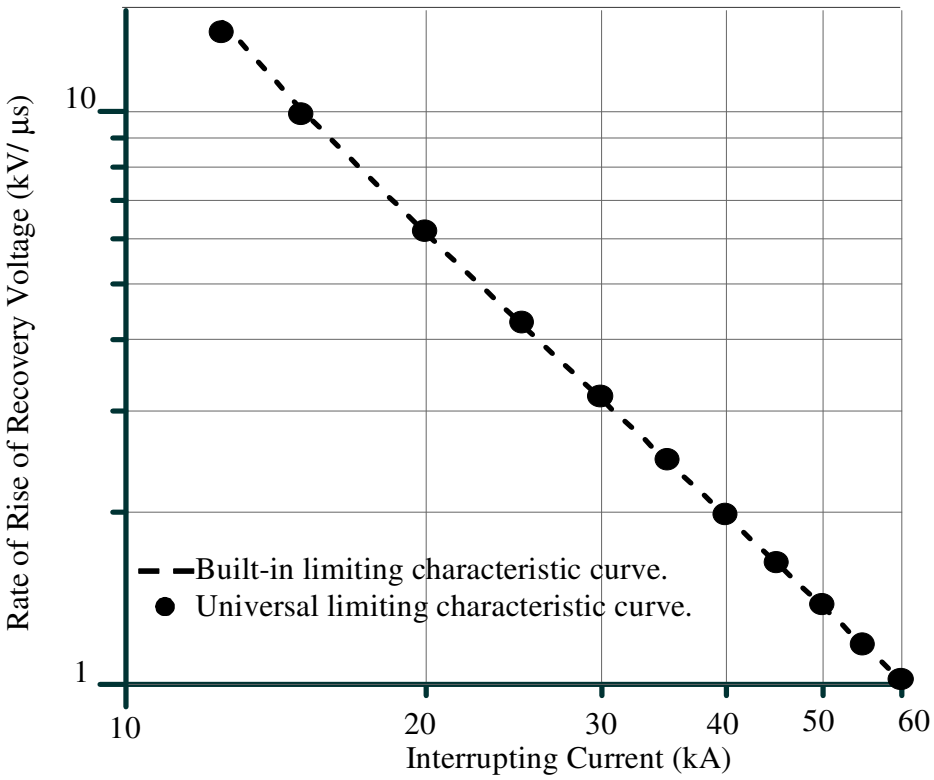

Figure 2.5 Thermal limiting curves of the two models for the same arc parameters.

2.4.3 Improved Mayr Model Representation

The improved Mayr model has been discussed in section 2.2. The dynamic equations (2.14) and (2.15) are used to represent the arc during pre and post-zero current periods, respectively. Although, this model cannot be realized considering built-in models, it can be easily implemented using the proposed representation. The arc representation is adopted to account for KEMA model by solving (2.14) and (2.15) in the TACS field. These modifications are only incorporated without altering the representation concept.

Two SF6 breakers rated at 245 kV / 50 kA / 50 Hz are used as a test example. The parameters of the first one are: τ = 0.27 µs, P_o = 15917, P_1 = 0.9943, and U_o = 100 V while for the second breaker: τ = 0.57 µs, P_o = 24281, P_1 = 0.9942, and U_o = 1135 V. These values have been obtained from the least square fit of KEMA experimental results as reported in [94].

The proposed arc representation can be validated by recognizing the computed waveforms of arc voltage and current in vicinity of current zero when the breaker is tested through Short Line Fault (SLF) test circuit. The aforementioned circuit breakers are tested in practical test circuits used by KEMA (90% SLF test). When the two breakers are tested using the universal arc representation, the first one has successful interruption while the second has reignition state and their voltage and current waveforms in the vicinity of zero-current are depicted in Figure 2.6. These waveforms present perfect match to the measured waveforms reported in [94]. This efficiently ensures the proposed arc representation.

2.4.4 Arcing Fault Representation

For representation of the fault arcs using the universal representation, the breaker arc equations are replaced by Kizilcay model (2.16) and (2.17). Primary arc parameters are: l = 350 cm, τ = 1.3 ms, u_o = 12 V/cm, and r = 1.3 mΩ/cm. The secondary arc parameters are considered as given in [99]. The obtained currents and voltage of primary and secondary fault arc are depicted in Figure 2.7. The computed results are identical to that ones obtained by the experimental setup and the consecutive ATP simulation reported in [99]. There is an offset in the voltage waveform shown in Figure 2.7.c. that is due to the capacitor residual charges. When the arc is extinguished, the residual charges voltage on the capacitor at this instant lead to this offset. The value of dc offset is dependent on extinction instant.

From the aforementioned investigation and comparisons, it is evident that the proposed representation has shown the flexibility to accommodate different arc models. Also, the arc elements are connected or altered over the power system arrangement in a straightforward methodology.

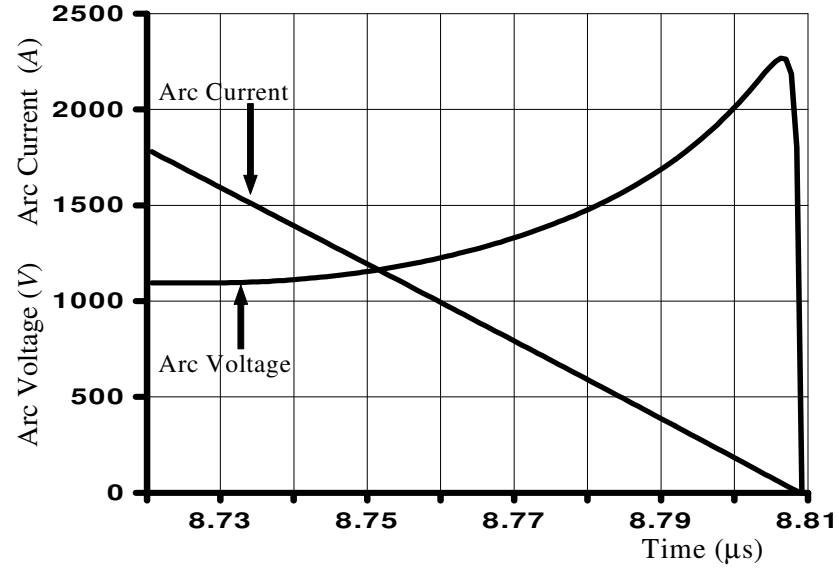

a. Successful interruption case

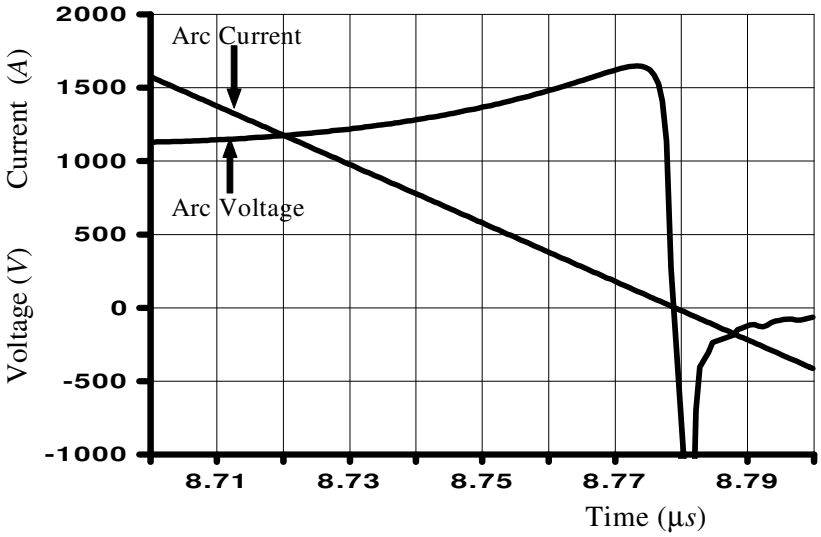

b. Reignition case

Figure 2.6 Arc current and voltage traces using the SLF test circuit

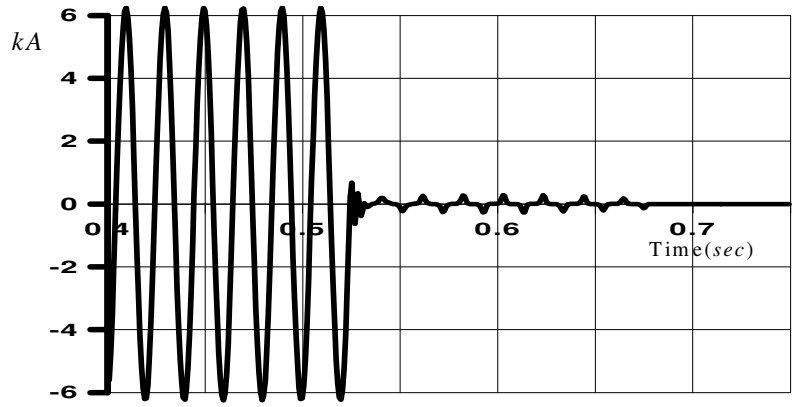

a. Arcing fault current.

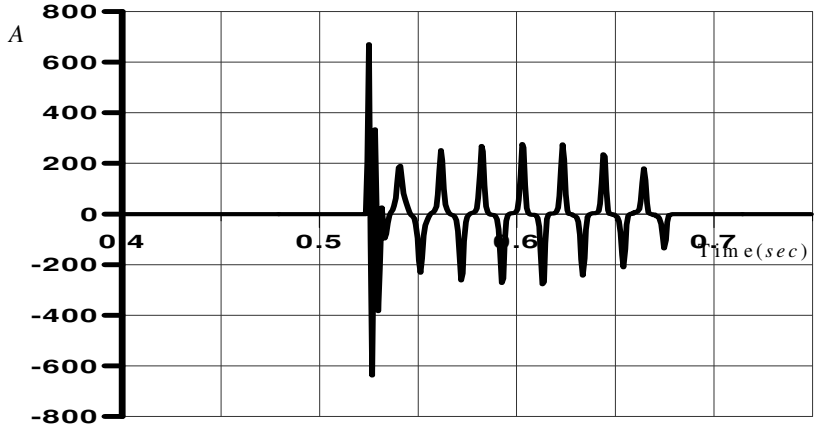

b. Secondary arc current.

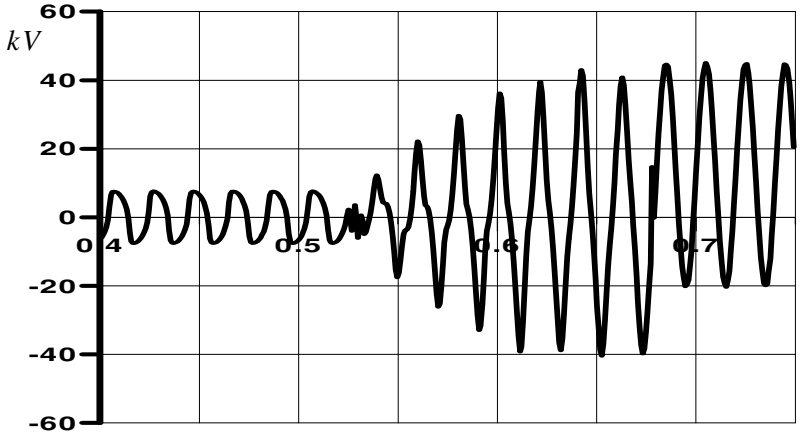

c. Arc voltage.

Figure 2.7 Currents and voltage for primary and secondary periods of the arcing fault.

3- Experimental Verification of High Impedance Arcing Fault Model in MV Networks [P.II]

In order to overcome the complications of obtaining staged fault data or of studying difficult abnormal conditions in the electrical networks, accurate fault model incorporated in the networks at different locations reproduces the well-known fault circumstances. Fault modeling requires experimental data to fulfill its equations and their parameters. Therefore in this chapter, an experimental setup is used to establish a high impedance fault of a leaning tree type. The test results are used to model the fault. The model parameters are determined. The experimental work is implemented using the ATP/EMTP package. The tree impedance is represented using a resistance and the arc element is modeled by a thermal model and realized using the universal arc representation in ATPDraw.

3.1 Experimental Results

An experiment was performed to measure the characteristics of a high impedance fault occurring in a 20 kV distribution network. The experiment was carried out at the Power Systems and High Voltage Laboratory, Helsinki University of Technology (TKK), Finland. Figure 3.1 shows the experimental setup. When the conductor is energized at 11.5 kV and the tree bends close, an arc is created as shown in Figure 3.2. More details about the experiment scenario are described in [P.II].

Towards accurate measuring, the experimental errors should be reduced. There are several sources for these errors: errors due to transducers such as current and voltage transformers and errors due to the reading/recording instruments such as Oscilloscopes and recorders. Regarding the experimental work, it is carried out at High Voltage Laboratory, TKK and the transducers in this laboratory are frequently calibrated as it can be revealed from the appendix of Publication [P.II]. There is another issue carefully considered to reduce the experimental error. This issue is the arrangement of these transducers (Current and Voltage), in which the calibrated resistance is directly connected with the fault element to accurately measure the fault current and therefore to avoid the error due to the current injected in the voltage transducer. Then, the voltage transducer is connected across both of the fault element and current transducer. The other point which can produce errors is the saturation of these transducers, however, the discussed fault is a very high impedance fault type and its disturbance is extremely small and such fault can not lead to saturation in the utilized transducers. So during this fault, the transducers operate in the linear portions of their characteristics.

Figure 3.3 illustrates the fault voltage and current waveforms when it is associated with arcs at different locations over the tree. It reveals that the distortions in voltage and current waveforms are influenced by the arc behavior. Non-steady state periods with spikes in the voltage and current waveforms are evident at reigniting instants. This is clearly depicted in the enlarged figures at the vicinity of the zero-crossings as shown in Figure 3.3.a. Identification of these features can enhance this fault detection. On the other hand, the arc

voltage or current waveform pattern can be approximately continuous as shown in Figures 3.3.b and 3.3.c.

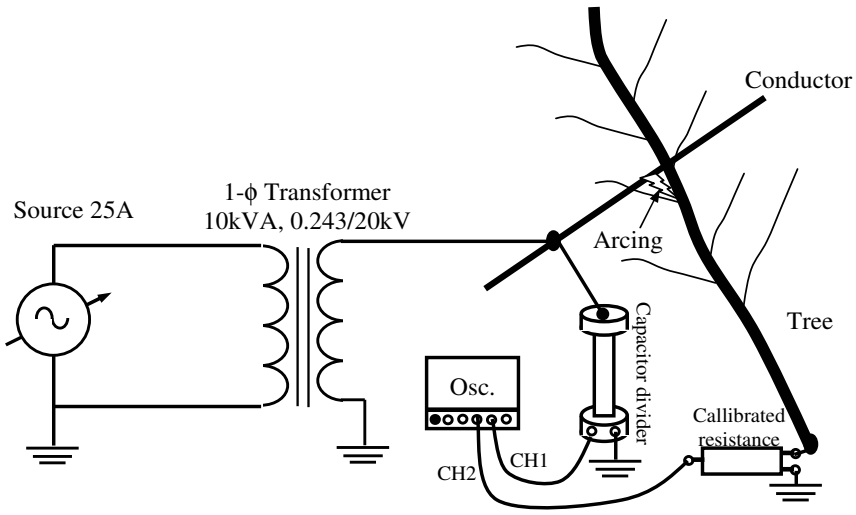

Figure 3.1 Experimental configuration.

Figure 3.2 Arc-associated tree bending over the conductor.

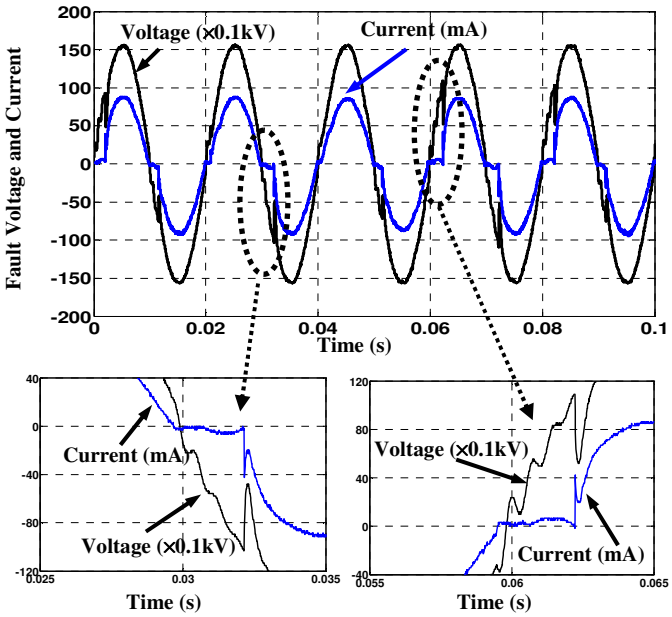

a. Enlarged view of waveforms and zero-crossings when the fault is in the foliage.

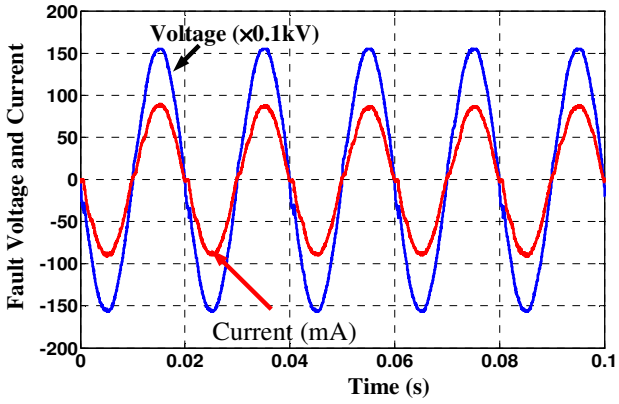

b. The waveforms when the fault is at the branch.

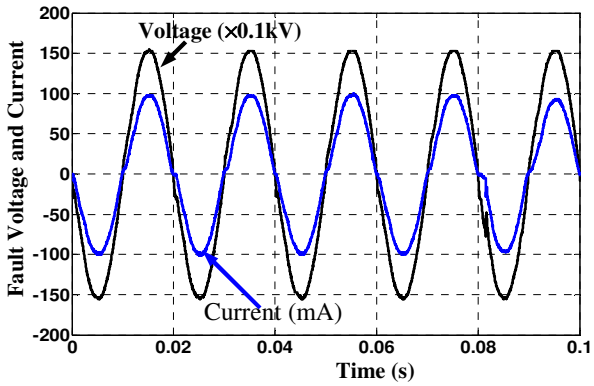

c. The waveforms when the fault is at the trunk.

Figure 3.3 Experimental waveforms at different fault locations over the tree.

3.2 Modeling of the Associated Arc

To enable measuring of the arc characteristics, the arc position is experimentally moved to a new point between the tree and the calibrated series resistance. The capacitor divider can then be connected across the arc element to only measure the arc voltage. The arc behavior changes from one half-cycle (power frequency) to the other as revealed by the experimental arc characteristics shown in Figure 3.4. This constitutes one cycle specific to an arc and it is characterized by unsymmetrical half-cycles. Therefore, the arc model parameters extracted using the positive half-cycle are inappropriate for the other.

This arc element can be modeled using the dynamic arc equation (2.16) of long arcs. However, the equation parameters such as the stationary arc voltage u_{st} and arc time constant τ are determined so as to match the experimental results. The experimental characteristics shown in Figure 3.4 are used to determine the arc model parameters. It is found that u_{st} can be a fixed value while the time constant is suggested to be described as [P.II]:

$$\tau = Ae^{Bg} \tag{3.1}$$

where A and B are constants. Therefore, there are three constants to model the arc performance. These parameters can be interpreted as which u_{st} describes the arc voltage clipping level. It can be determined as the arc voltage value when dg/dt=0 and it is synchronized with the instant of maximum current occurrence. The arc hysteresis in the simulation phase is sensitive to τ. The behavior of τ at the instant of reignition and during the half cycle is dominated by the constant A and B, respectively. The appropriate parameters for the positive half cycle shown in Figure 3.4 are u_{st} = 2520 V, A = 6.6E-5 and B = 41977 while for the negative half cycle they are u_{st} = 2100 V, A = 2.0E-5, and B = 85970.3. The corresponding simulated arc characteristics are illustrated in the comparison of Figure 3.5. These comparisons confirm the model accuracy.

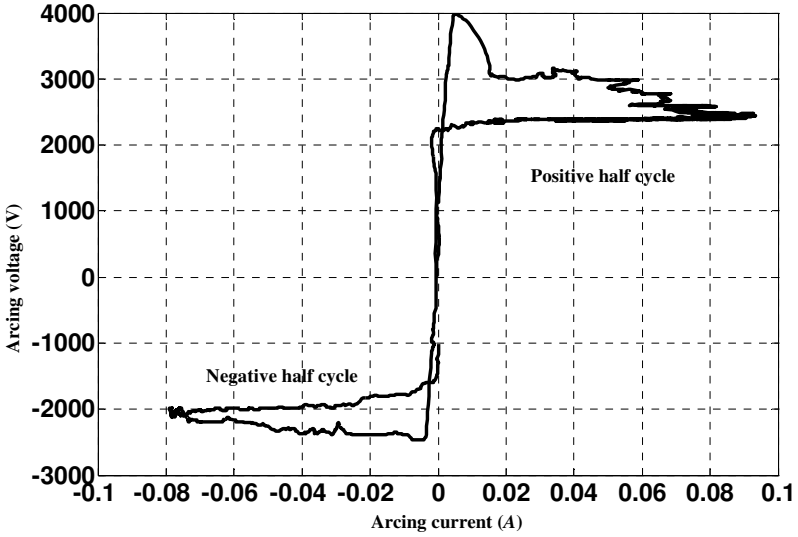

Figure 3.4 Experimental arc characteristics.

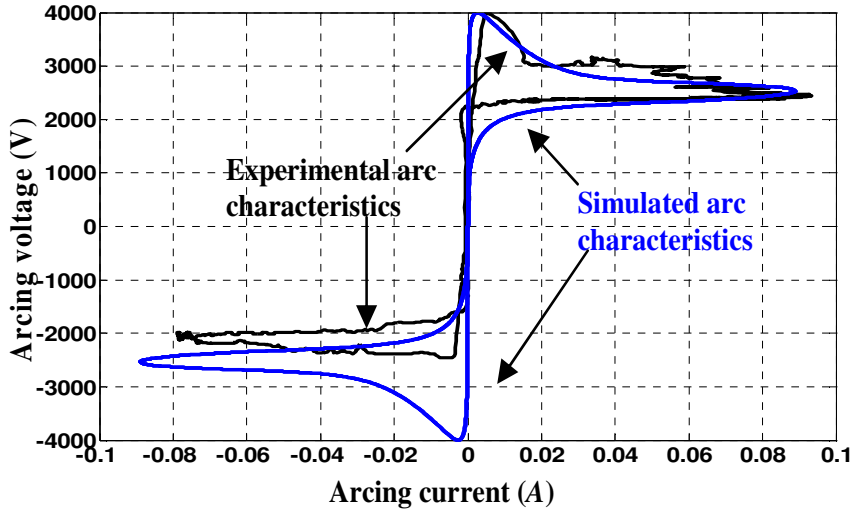

a. Fitting for the positive half cycle data.

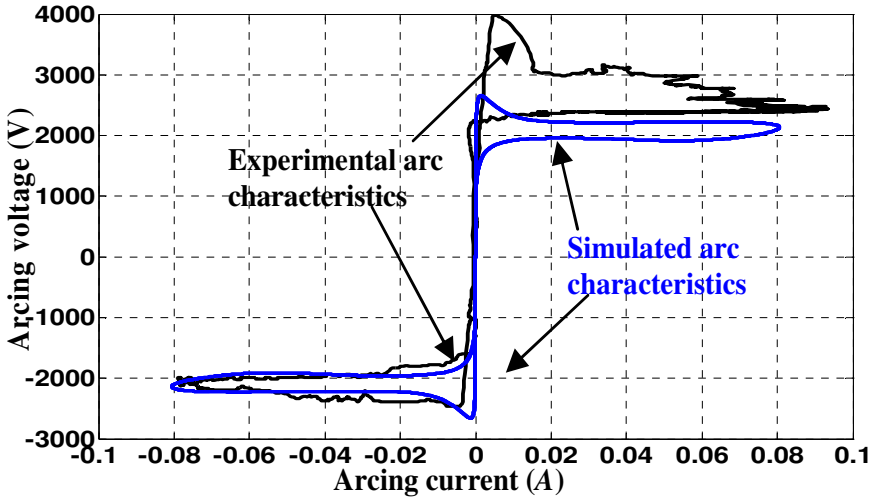

b. Fitting for the negative half cycle data.

Figure 3.5 Comparison of simulated with experimental arc characteristics

3.3 Simulation Results

The experimental system shown in Figure 3.1 was implemented using the ATP/EMTP program where the circuit was realized using ATPDraw. Figure 3.6 shows the corresponding ATPDraw network where it is divided into the power network to represent the experimental setup and the TACS field to solve the dynamic arc equation. The arc model was realized using the universal arc representation as described in [P.II]. The control signal required for the controlled integrator and acquired from the case depicted in Figure 3.3.a is shown in Figure 3.7.a. Considering the conductance at the zero-crossing, the dielectric of the arc medium until the instant of reignition is represented by a variable resistance as a ramp function of 0.5 MΩ/*ms* for a period of 1 *ms* after each zero-crossing and then 4 MΩ/*ms* until the reignition instant. These variables are used for matching the experimental current and voltage waveforms until the reignition instants. They are compromise ramp values obtained with the aid of fitting the resistance curves computed from the experimental voltage and current during such periods. The corresponding simulated fault waveforms are illustrated in Figure 3.7.b. In the same manner, the test case shown in Figure 3.3.c has been simulated as shown in Figure 3.7.c. The utilized fault parameters have been selected to be suitable for each case where the parameters R_{tree}, u_{st}, A and B are found to be 140.5 kΩ, 2520 V, 5.6E-7 and 395917 for the first simulated case, and 130.0 kΩ, 2050 V, 8.5E-5 and 99987 for the other, respectively. In the two simulated fault cases, the parameters A and B are compromised values for the positive and negative half cycles. In these cases, there are differences in the arc behavior and therefore the arc model parameters of each case are not the same. By comparing the simulated and experimental waveforms, it appears that the fault modeling due to a leaning tree is accurately represented.

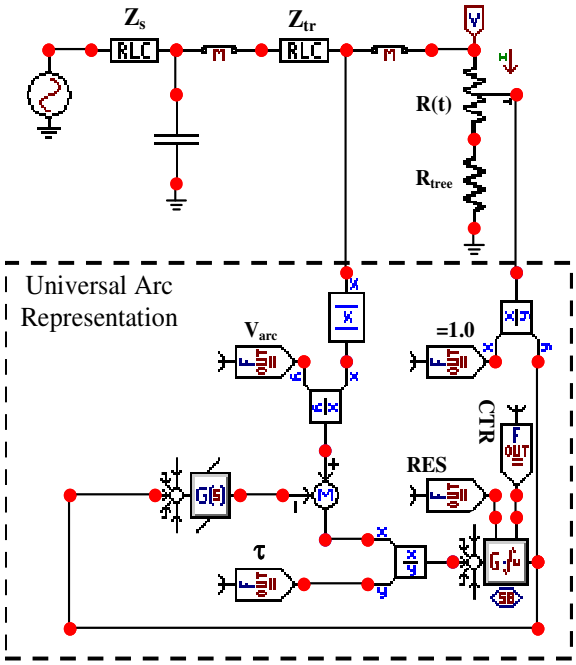

Figure 3.6 The ATPDraw network of the experimental setup

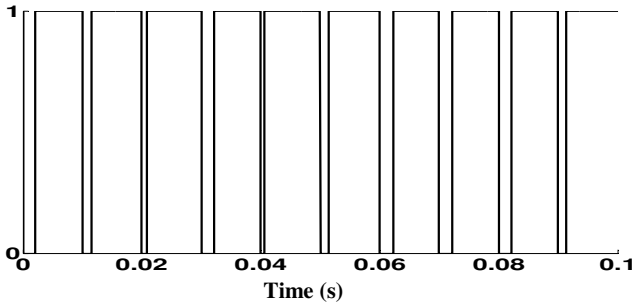

a. Control signal to distinguish dielectric and arcing periods.

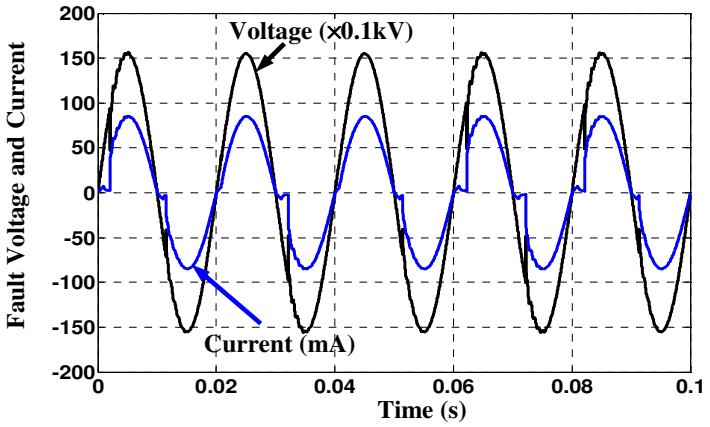

b. The case shown in Figure 3.3.a.

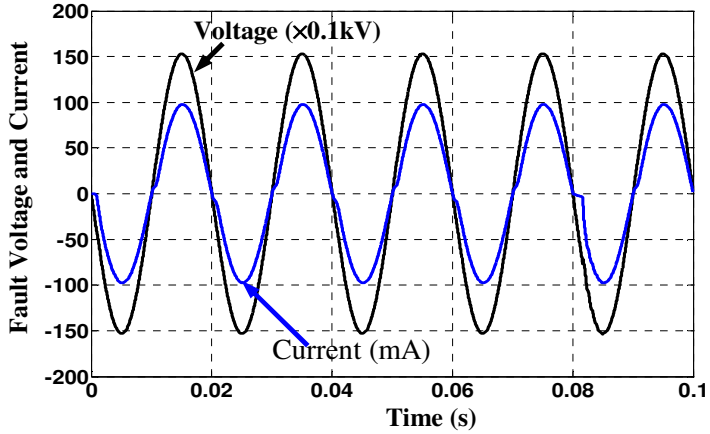

c. The case shown in Figure 3.3.c.

Figure 3.7 Simulation results.

3.4 Network Performance during the Fault

In MV networks, initial transients are generated when the networks are exposed to disturbances such as faults. These transients are ultimately controlled by the energy conservation theory. They are investigated to detect earth faults in unearthed and compensated MV networks [35], [36], [45], [46]. The initial transients are in the form of charge and discharge transient components. The discharge transient components are happened on the faulty phase when an earth fault occurs suddenly. This gives rise to the discharge transient component and therefore a voltage rise in the sound phases that is accompanied by the other created components called charge transient. These initial transients are depending on the network equivalent parameters, fault location, fault instant, and fault impedance [35], [46]. Because the compensation coil impedance is relatively high at the high frequencies, these transients are about similar in unearthed and compensated networks [35].

As aforementioned, an accurate simulation of the electrical networks associated with high impedance arcing faults is quite important to evaluate the possibility of a detection of these faults. Using the ATP/EMTP program, the simulated system can be divided into two main parts: the power network model and the representation of high impedance arcing fault described in the previous section.

Figure 3.8 illustrates a single line diagram of a 20 kV, MV network. The transmission line dependent frequency model of the EMTP program is intentionally selected to account for the unsymmetrical faults. The feeder lines are represented using the frequency dependent JMarti model. The neutral of the main transformer is singularly treated to manage different earthing methods.

The residual voltage and current waveforms can be analyzed for the fault detection purposes. They are computed as:

$$u_r = u_a + u_b + u_c \tag{3.2}$$

$$i_r = i_a + i_b + i_c \tag{3.3}$$

where i_r and u_r are the residual current and voltage, respectively. i_a , i_b and i_c are the phase currents. u_a , u_b and u_c are the phase voltages. In order to investigate these residual waveforms during the discussed fault, the equations (3.2) and (3.3) are implemented in the TACS field.

Figure 3.9 illustrates the ATPDraw network of the simulated system. It contains the MV network described in Figure 3.8, the universal arc representation of the associated arc with the tree resistance and the residual voltage and current (u_r and i_r) equations (3.2) and (3.3), respectively.

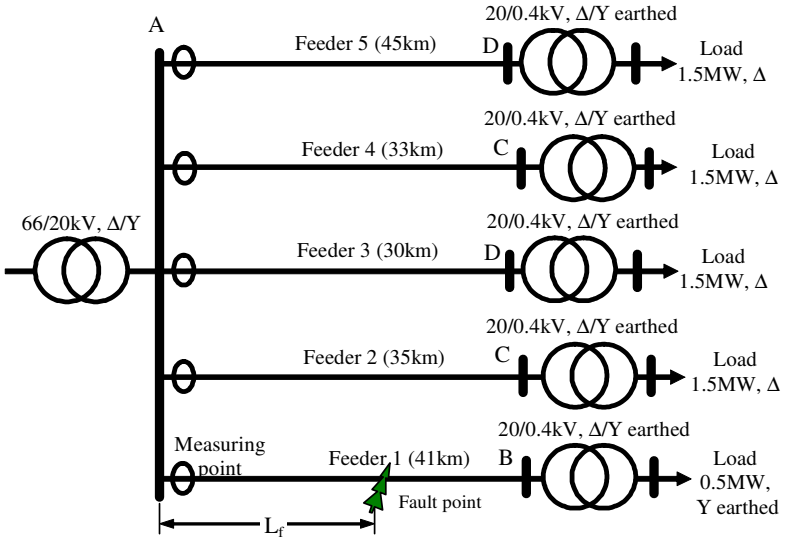

Figure 3.8 Simulated system for a substation energized 251 km distribution network.

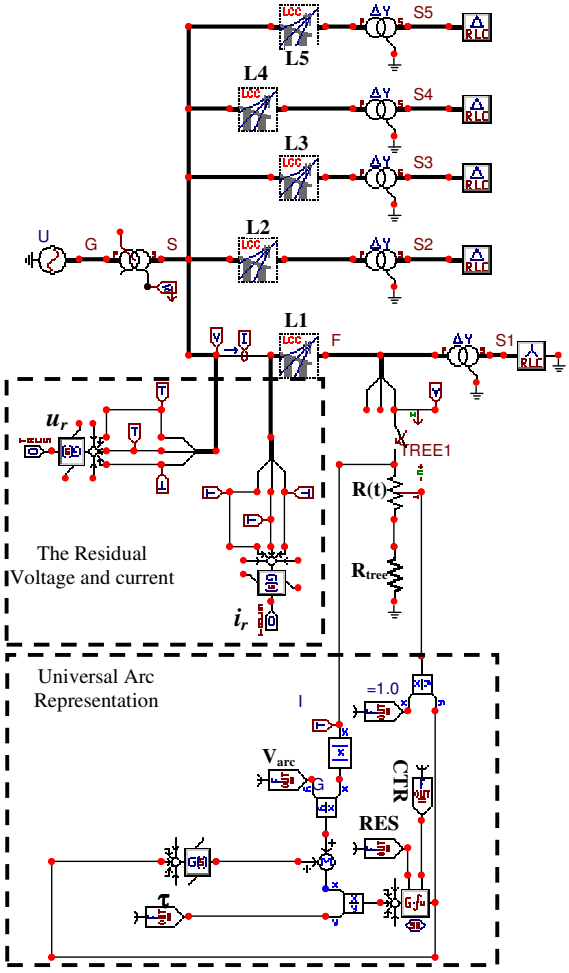

Figure 3.9. The ATPDraw network of the simulated system.

3.4.1 Unearthed Network

Although the unearthed network is not intentionally connected to the earth, it is naturally earthed by the phase to ground capacitances. Therefore, the phase fault current is very low and allow to a high continuity of service [30]. The main disadvantage of unearthed network is that it is subjected to transient overvoltages.

For a fault case due to a leaning tree occurred at 27 *ms* at the end of Feeder 1 in an unearthed 20 kV network depicted in Figure 3.8, the corresponding waveforms are shown in Figure 3.10. The residual and neutral voltages are shown in Figure 3.10.a where they ultimately depend on the fault impedance. The fault and residual currents are depicted in Figures 3.10.b and 3.10.c, respectively. The corresponding residual current is very small and the impact of the initial transients due to the arc reignitions is obvious after each zero-crossing via approximately one-quarter of the power cycles as illustrated in the enlarged view of the residual current shown in Figure 3.10.c. Therefore, it is appropriate to use a discrete signal processing technique such as DWT to extract these transients and therefore to localize the arc reignition instants.

3.4.2 Compensated Network

When the resonant earthing network is used, the earth fault current is correspondingly decreased because the network earth capacitance is in a parallel resonance with the inductance connected to the neutral. Because the neutral voltages of such networks are substantially higher than the isolated systems, a higher sensitive relay protection for high resistance faults can be gained [30], [35]. However, the tuning of the compensation coil is never precise where the switching can cause major changes in the network connections. In Nordic Countries, the compensated MV networks have increasingly been used [35].

Towards modeling the compensated network, the transmission line capacitance is compensated by an earthed inductance of 2.85 H where it is connected at the neutral point of main transformer in the network shown in Figure 3.8. The neutral and residual voltages during the tree leaning fault are illustrated in Figure 3.11.a where the fault occurrence is at the end of Feeder 1. The fault and residual currents are shown in Figure 3.11.b. The performance of this fault is changed with different earthing although the fault impedance is very high. However, the arc reignition fingerprints are still observed in the measured voltage and current waveforms. The same manner is also measured when the fault location and incipient instants are changed; however, the initial transients are affected.

Due to the fact that the impedance of the compensation coil is relatively high at high frequencies, these transients are about similar in the unearthed and compensated networks [35]. Regarding the high impedance arcing fault tree leaning type, these initial transients are repeated with each arcing reignition after each current zero-crossing via approximately one-quarter of power cycles as depicted in the residual waveforms.

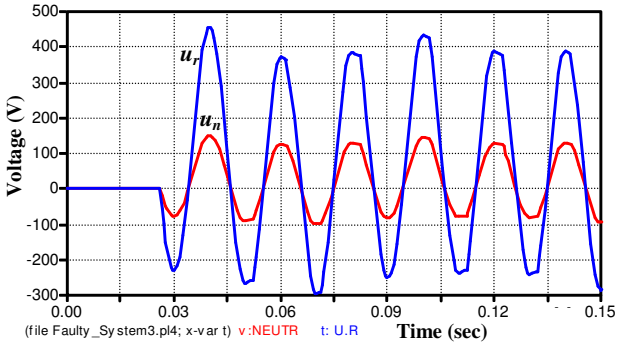

a. Measured neutral voltage (u_n) and residual voltage (u_r).

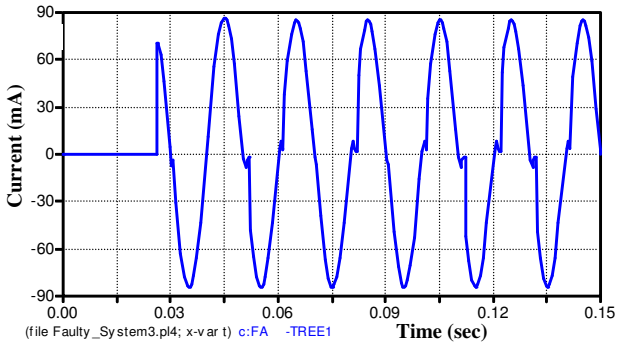

b. Fault current (i_f)

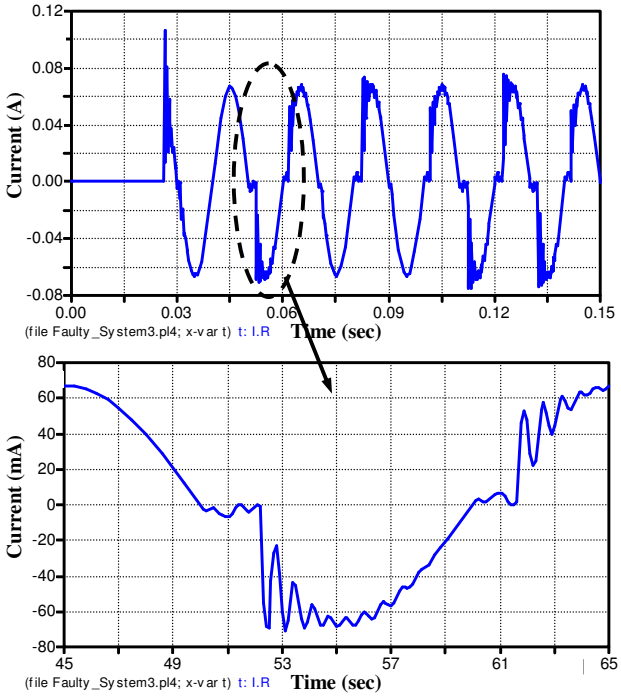

c. Enlarged view of residual current waveforms (i_r)

Figure 3.10 The transient waveforms when the network is unearthed.

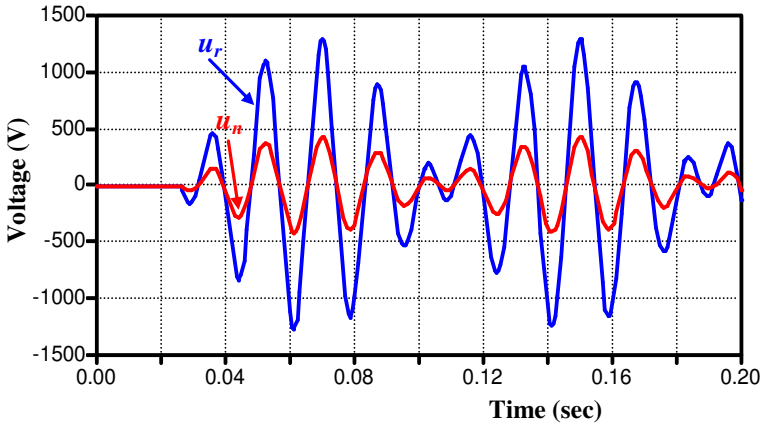

a. Neutral and residual voltages (u_n and u_r, respectively).

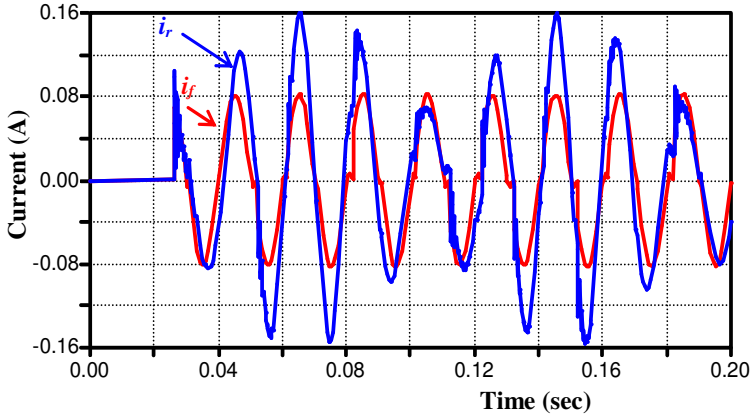

b. Fault and residual currents (i_f and i_r, respectively).

Figure 3.11 The waveforms when the fault occurs at the end of Feeder 1 on the compensated earth network.

4- DWT-Based Investigation of Network Currents for Detecting High Impedance Arcing Fault [P.III], [P.IV]

In this chapter, the impact of the arc reignition periodicity on the network currents is utilized to detect the faults due to leaning trees. In the vicinity of the current zero-crossing, the initial transients lead to fingerprints boosting secure fault detections. These transients are localized based on the DWT detail coefficient of the feeder currents to detect the fault. The fault detector is based on the absolute sum of the DWT detail coefficient over one power cycle. The selectivity function to estimate the faulty feeder or the faulty phase is based on Logic Functions where their inputs are the absolute sum of the DWT detail coefficients as reported in [P.III]. However, when the currents are measured not only at the main busbar but also at different measuring nodes throughout the network, another selectivity function is introduced based on the residual current ratio as addressed in [P.IV]. The ratio of the residual fundamental current of each section with respect to the fundamental current of parent section in the feeder is used as a discriminator to estimate the faulty section.

4.1 Feature Extraction and Fault Detection Algorithm using DWT [P.III]

The scenario of the fault detection and the faulty feeder estimation is illustrated in Figure 4.1. At the measuring node of each feeder, phase currents are measured and the fault features are extracted using DWT. The absolute sum of the detail d3 coefficient corresponding to the frequency band 12.5-6.25 kHz is computed over one cycle period of the power frequency for the fault detection purpose. The sampling frequency is 100 kHz. A timer is used to determine the fault period and it can be implemented using a samples counter. In order to find out the faulty phase, the absolute sum over one power cycle of the detail d3 of each phase is evaluated using a Logic Function, in which, the absolute sum of the faulty phase is the highest one when it is compared with the absolute sum of other phases. A similar feature is found when a comparison between the absolute sums of the feeders for the same phase current where the absolute sum of the faulty feeder is the highest one. Therefore, another Logic Function is designed to determine the faulty feeder. The selectivity of the faulty phase and feeder is taken into consideration after the fault detection is achieved. More details about the algorithm can be found in [P.III].

Several wavelet families have been tested to extract the fault features using the Wavelet toolbox incorporated into the MATLAB program [106]. It is found that Daubechies wavelet 14 (db14) is appropriate to localize this fault, in which characteristics of Daubechies wavelets (dbN) are arbitrary regular, compactly supported orthogonal and asymmetry. When the sampling frequency is equal to 100 kHz, the corresponding frequency distribution for each detail level is shown in Figure 4.2. The Detail d3 including the frequency band 12.5-6.25 kHz is investigated. The sampling rate can be reduced to 50

or 25 kHz but the used coefficients will be details d2 or d1, respectively. More reduction in the sampling frequency can be considered, however, the absolute sum detector has less gain.

For the tree leaning fault case occurred at the end of Feeder 1 of the network shown in Figure 3.8, extracted features from the phase current waveforms measured for different feeders using DWT are shown in Figure 4.3. This fault case started at 26 *ms*. The initial transients due to arc reignitions are frequently localized throughout the network feeders.

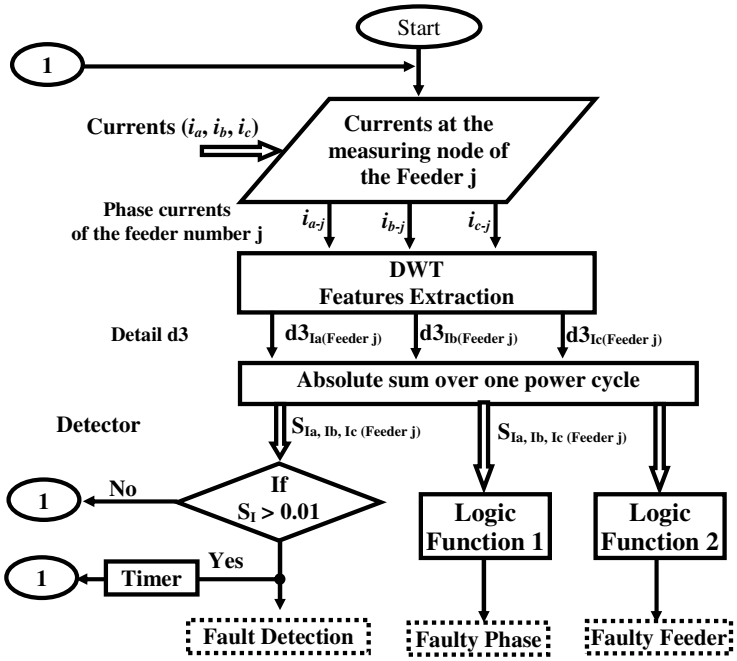

Figure 4.1 The proposed detection technique.

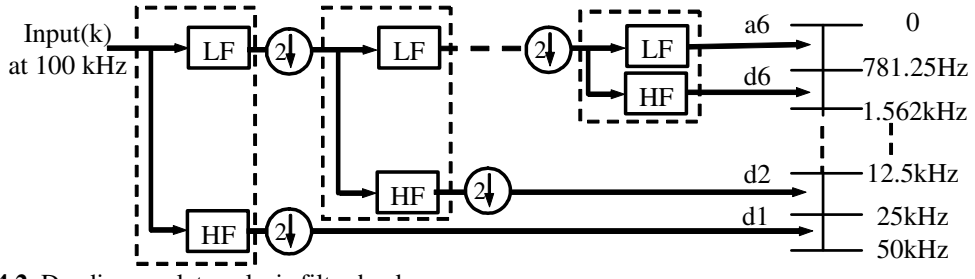

Figure 4.2 Dyadic wavelet analysis filter bank.

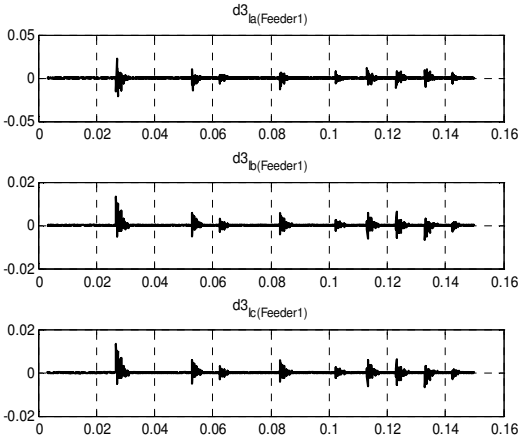

a. Details d3 of phase currents of Feeder 1.

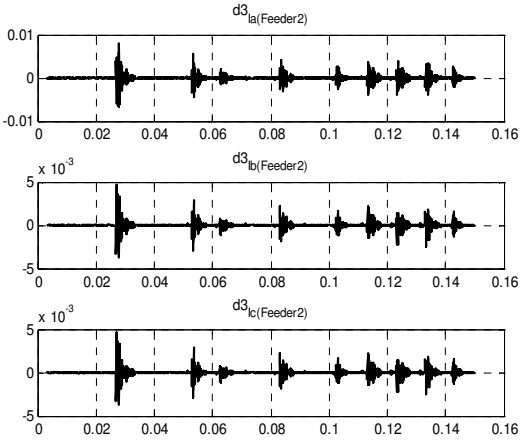

b. Details d3 of phase currents of Feeder 2.

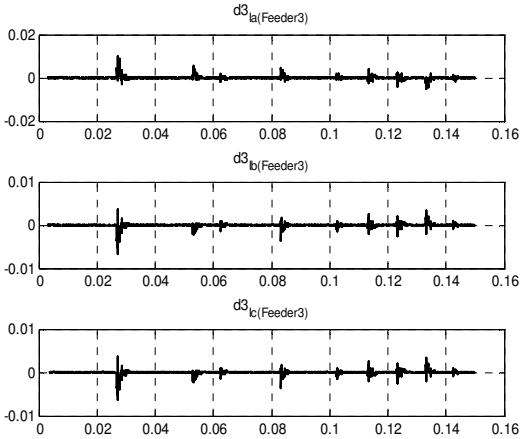

c. Details d3 of phase currents of Feeder 3.

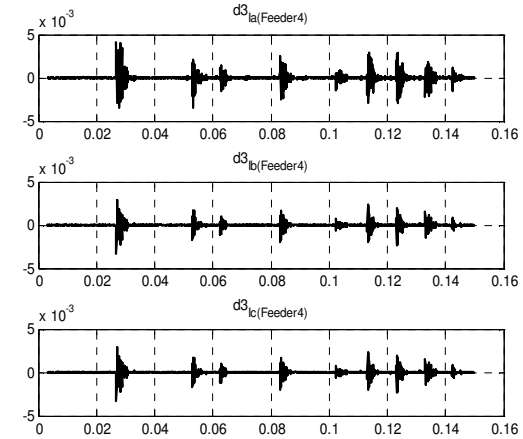

d. Details d3 of phase currents of Feeder 4.

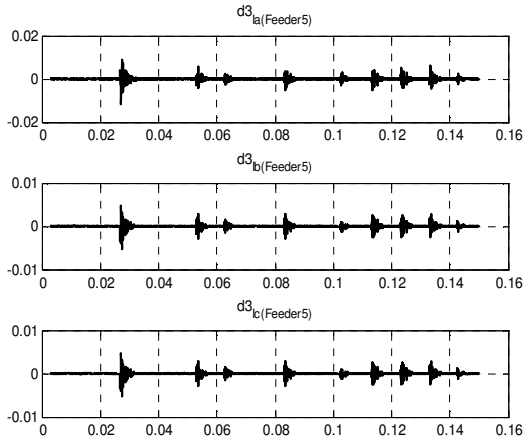

e. Details d3 of phase currents of Feeder 5.

Figure 4.3 Details d3 of phase currents at a beginning of the network feeders.

To find flags used as a fault detector, the absolute sum value of the detail d3 over one power cycle is computed in a discrete form at each measuring node. This absolute sum is in the form [41]-[107]:

$$S_I(k) = \sum_{h=k-N+1}^{k} \left| d3_I(h) \right| \tag{4.1}$$

where h is used for carrying out a sliding window covering 20 *ms* and N is a number of window samples. $d3_I(.)$ is the DWT detail level 3. For example, the detail $d3_{Ia(\text{Feeder1})}(.)$ is for phase-a and Feeder 1 and the corresponding detector S_I will be $S_{Ia(\text{Feeder1})}$. The performance of the detectors S_I for different phases and feeders is shown in Figure 4.4, in which the detectors all over the measured currents respond to the fault disturbance. This confirms the fault detection. Moreover, the considered detectors are high not only at the starting instant of the fault events but also during the fault period that improves the protection security. It should be notified that such detectors can localize the fault event; however, it is essential to determine the faulty phase and also the faulty feeder. Regarding the faulty phase determination it can be noticed with the aid of Figure 4.4 that the detector S_I of the faulty phase is the highest one. Similarly, the detector S_I of the faulty feeder is the highest when a comparison is carried out between the feeders at a certain phase as shown in Figure 4.5. More fault cases, which confirm this obtained feature, can be found in [P.III]. These cases are carried out by varying fault locations, fault instants and load conditions.

Figure 4.6.a illustrates the proposed technique that can be used for estimating the faulty phase where the inputs of the Logic Functions are the differences of the absolute sum S_I of each phase at a certain feeder. When the difference D (for example $D_{ab}=S_{Ia}-S_{Ib}$ for each feeder) is positive, it will be considered 1 and when it is zero or negative value, it is considered zero. When the fault is phase-a to ground, D_{ab} is positive while D_{ca} is negative disregarding the status of D_{bc}. In this case, the output Phase_a is high and other outputs are low whatever the status of D_{bc}. In the same manner, the discriminator output Phase_b or Phase_c is high when phase-b or phase-c to ground fault occurs, respectively. Such Logic Functions are possible to be implemented in the digital relays. A similar discriminator can be designed to estimate the faulty feeder where the corresponding Logic Functions is shown in Figure 4.6.b. More discussion is reported in [P.III].

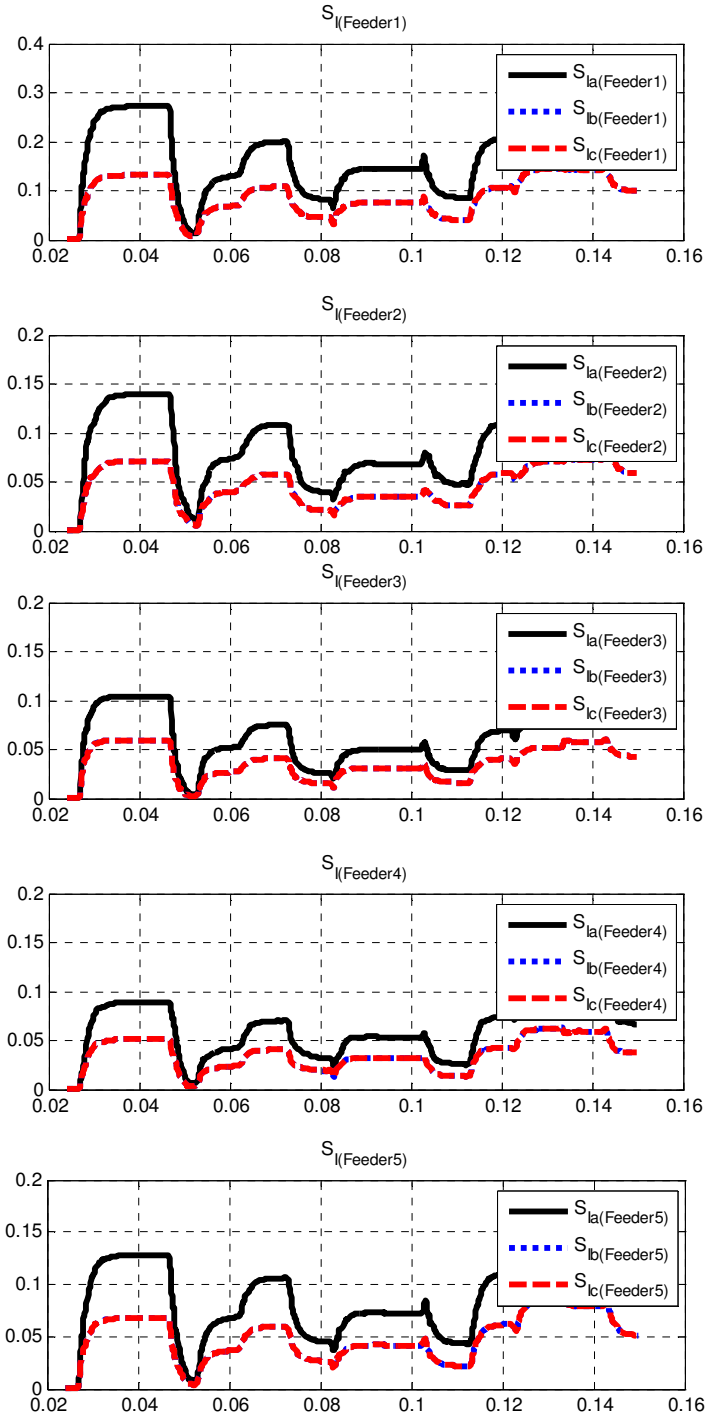

Figure 4.4 The detector S_I of different phases (S_{Ia}, S_{Ib} and S_{Ic}) at the beginning of certain feeder.

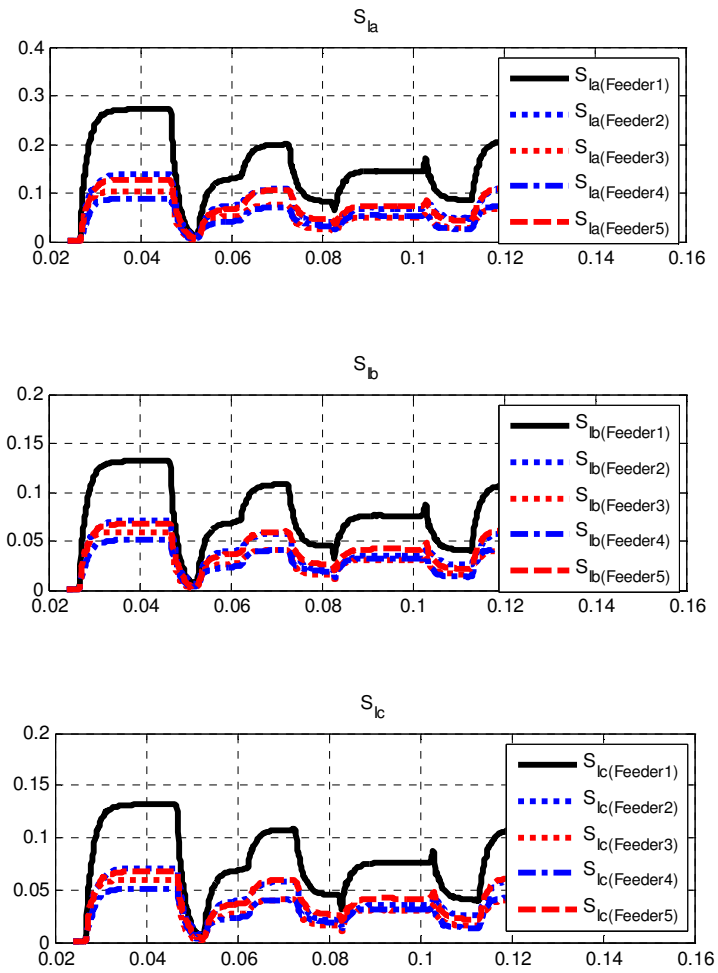

Figure 4.5 Comparison between the detector S_I of different feeders at a certain phase.

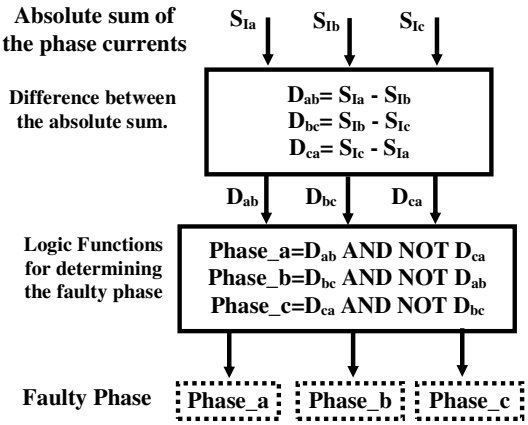

a. Faulty phase Discriminator.

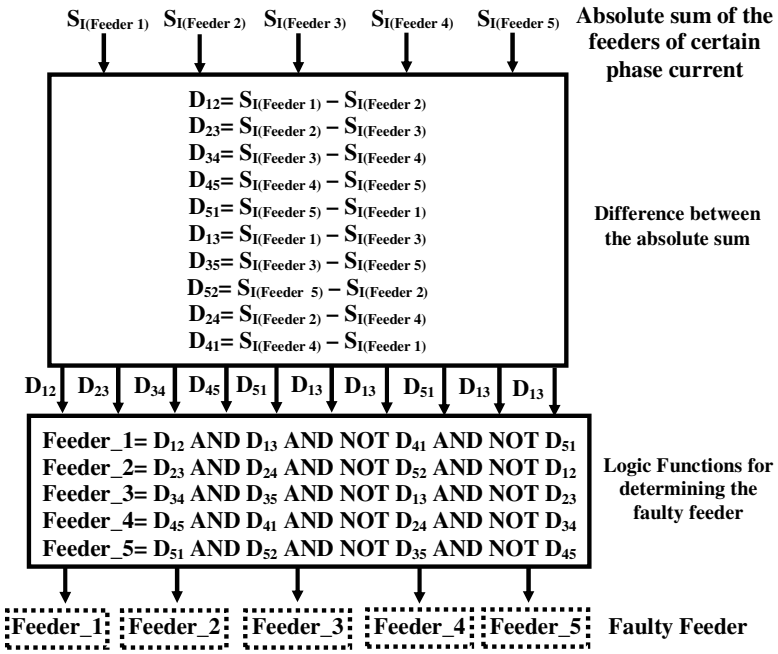

b. Faulty feeder discriminator.

Figure 4.6 The proposed Selectivity Function.

4.2 Wide Area Feature Extraction Using Wireless Sensor Concept [P.IV]

The wireless sensor concept is a modern insight used for various objects with saving time and expenses. The wireless sensor networks include compact microsensors and wireless communication capability. They are distributed in the network and electrical quantities are then frequently transmitted from different measuring points and investigated for several purposes such as load monitoring, fault detection and location, … etc. [108]-[111].

Towards increasing the wide area measurement systems, the wireless sensor networks are recently constructed. The availability of sensing devices, embedded processors, communication kits and power equipment enables the design of wireless sensor as depicted from the illustrated four major blocks in Figure 4.7 [111]. The supply is used to power the node. The communication block consists of a wireless communication channel which can be short range radio, fiber optic, or infrared. The processing unit is composed of memory to store data and applications programs, a microcontroller (MCU) and an Analog-to-Digital Converter (ADC) to receive signal from the sensing devise. The sensing block links the sensor node to the physical conditions. In our application, the sensing devise is used to measure the feeder line currents as discussed in [108]-[111].

In this section, the wireless sensor concept can be considered for enhancing the fault detection and location processes. In this case, the fault detection is carried out by testing the DWT performance on a wide area of the network. However, the contribution of this dissertation is produced from the standpoint of protection issue disregarding the investigation of wireless sensor performance or challenges. A fault case due to leaning tree is considered at the end of section EF in the complicated MV network shown in Figure 4.8. The corresponding ATPDraw network is depicted in Figure 4.9. The residual current waveform measured at the beginning of each section during this fault case is depicted in Figure 4.10. From the enlarged view of Figure 4.10, it can be seen that the initial transients at each zero-crossing are obvious at all measuring nodes (healthy and faulty sections).

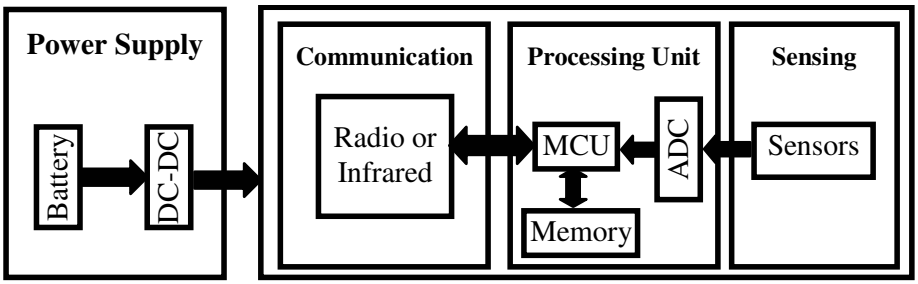

Figure 4.7 Architecture of the sensor node system [111].

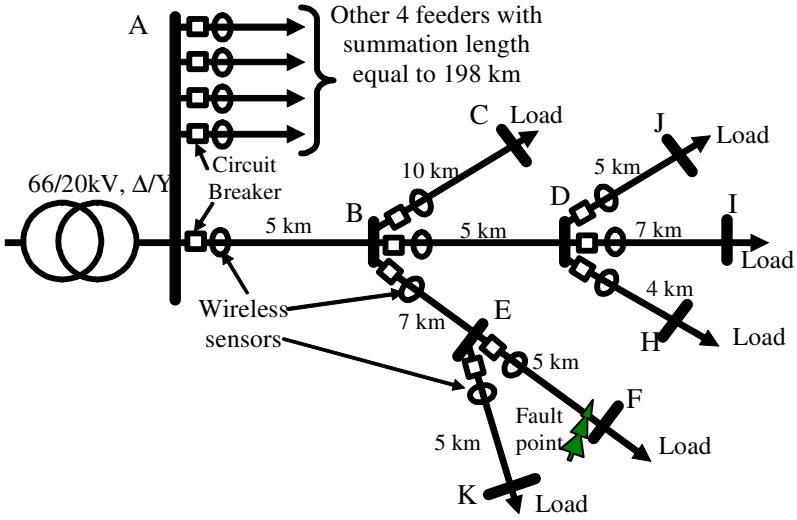

Figure 4.8 Simulated system for a substation energized 251 km distribution network.

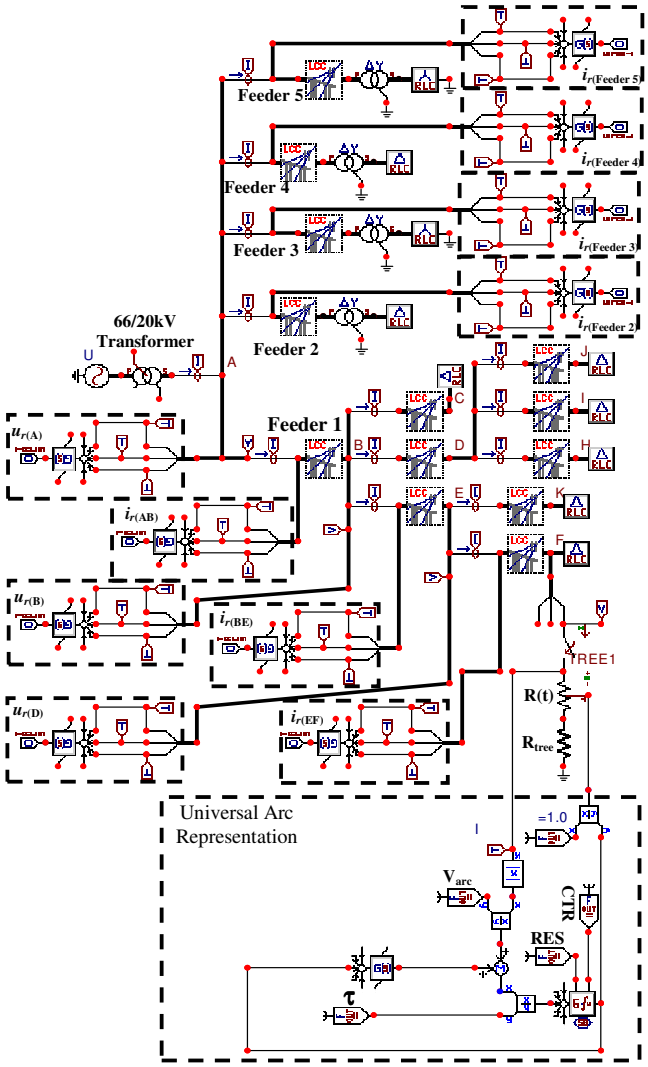

Figure 4.9 The ATPDraw network

Features of the residual currents shown in Figure 4.10 are extracted using DWT. In the same manner, the sampling frequency is 100 kHz and the mother wavelet is Daubechies wavelet 14 (db14). Figure 4.11 illustrates the corresponding detail levels d3, d4 and d5. The detectors S_{Ir} performance is evaluated and shown in Figure 4.12, in which, the fault is detected based on DWT. Furthermore, the detectors are high not only at the fault starting instant but also during the fault period which enhances the fault detection security. As aforementioned, such performance is due the arc reignitions after each fault current zero-crossing. Towards decreasing the sampling frequency at which the DWT is processed, when the detectors S_{Ir} of the DWT detail d4, which is indicated $S_{Ir(d4)}$, is considered a detector, the sampling frequency can be reduced to 50, 25 or 12.5 kHz; however, the used coefficient will be detail d3, d2, or d1, respectively. However, the faulty section cannot be discriminated using the detectors S_{Ir}.

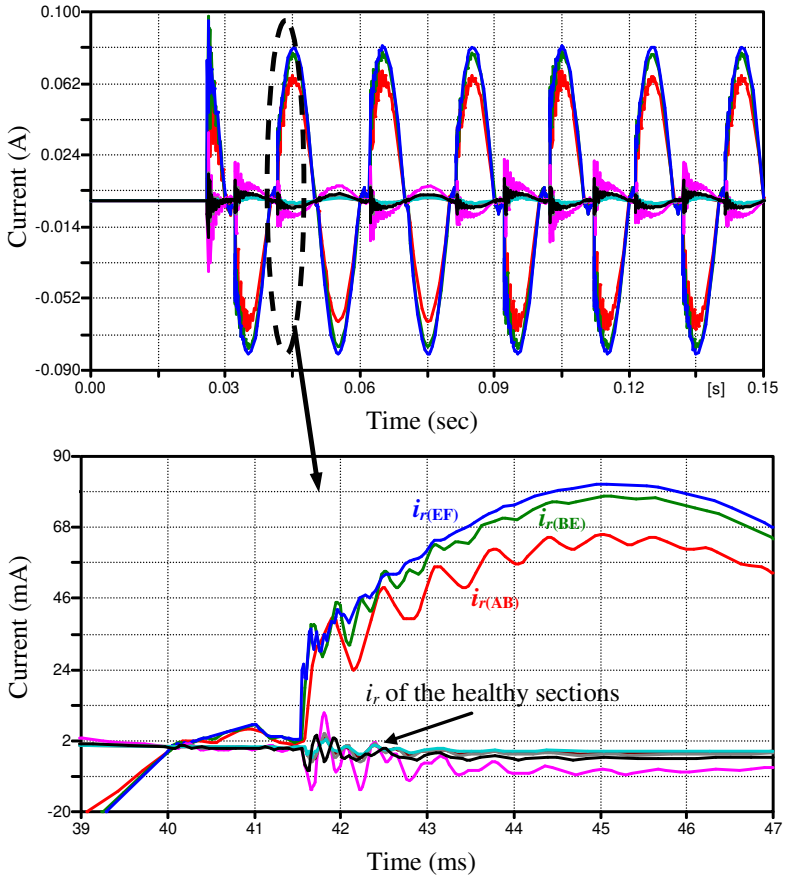

Figure 4.10 Enlarged view of residual current waveforms (i_r) when the fault occurred in section EF.

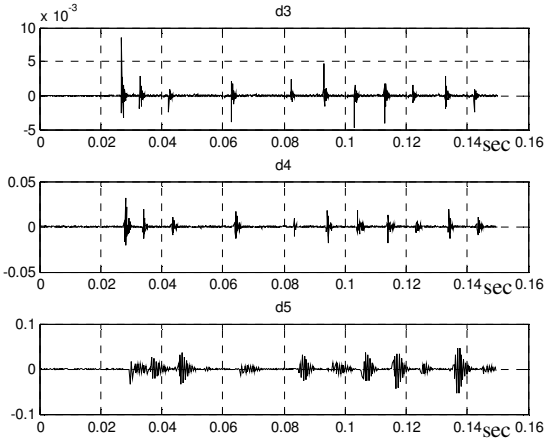

a. Details of the residual current in section AB ($i_{r(AB)}$)

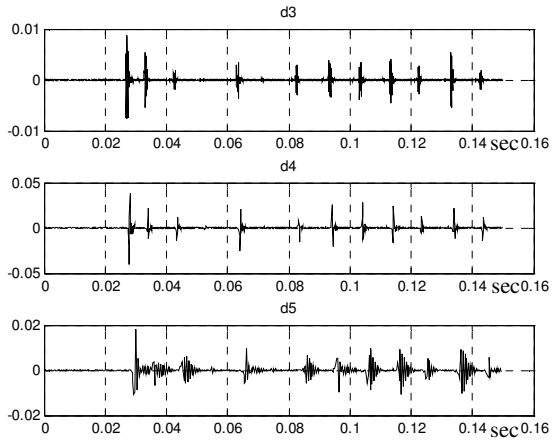

b. Details of the residual current in section BC ($i_{r(BC)}$)

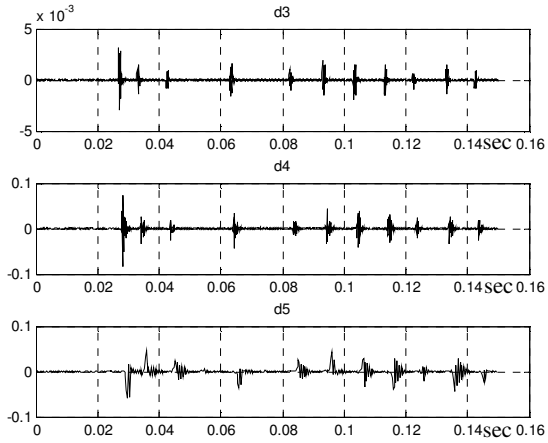

c. Details of the residual current in section BD ($i_{r(BD)}$)

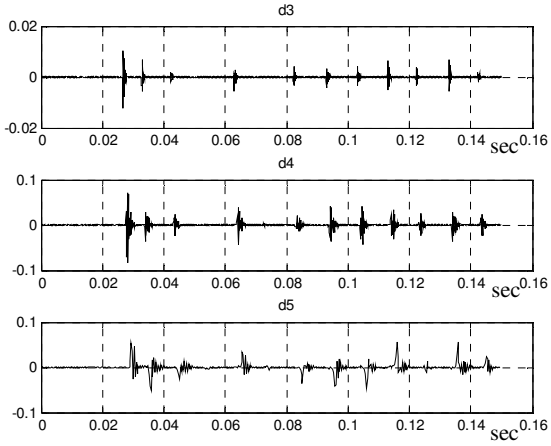

d. Details of the residual current in section BE ($i_{r(BE)}$)

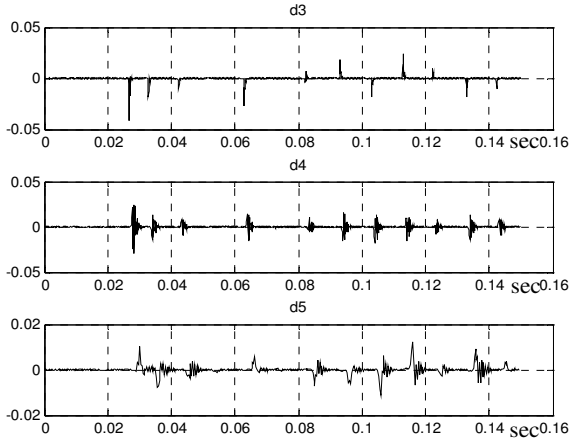

e. Details of the residual current in section EK ($i_{r(EK)}$)

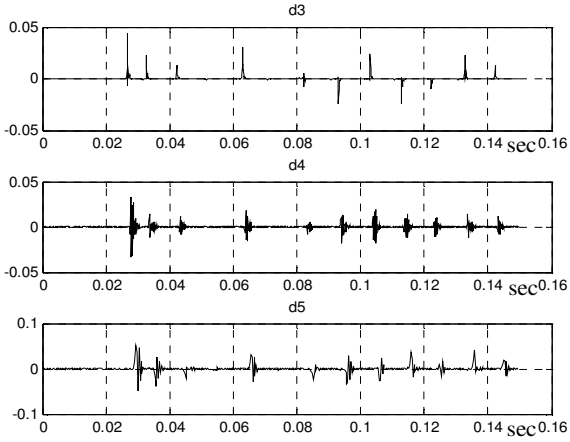

f. Details of the residual current in section EF ($i_{r(EF)}$)

Figure 4.11 Details of residual waveforms shown in Figure 4.10.

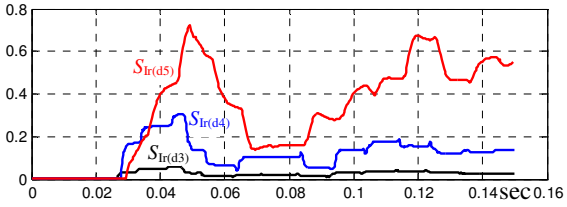

a. S_{Ir} of the residual current details in section AB ($i_{r(AB)}$)

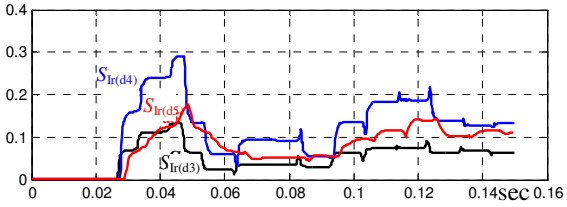

b. S_{Ir} of the residual current details in section BC ($i_{r(BC)}$)

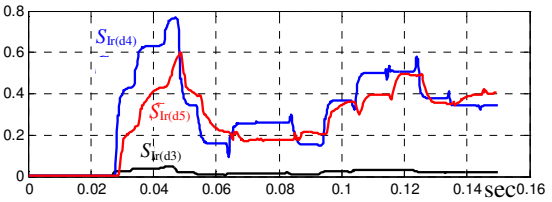

c. S_{Ir} of the residual current details in section BD ($i_{r(BD)}$)

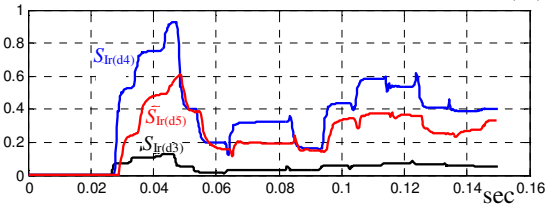

d. S_{Ir} of the residual current details in section BE ($i_{r(BE)}$)

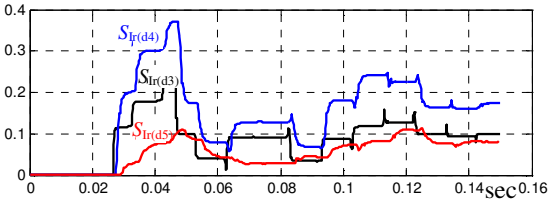

e. S_{Ir} of the residual current details in section EK ($i_{r(EK)}$)

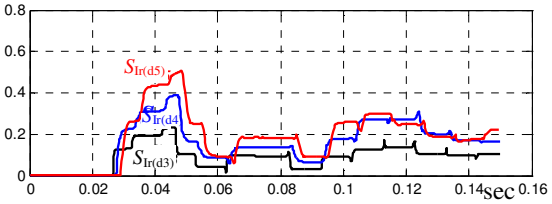

f. S_{Ir} of the residual current details in section EF ($i_{r(EF)}$)

Figure 4.12 The detector S_{Ir} of the details shown in Figure 4.11.

There is an observation obtained from Figure 4.10 is that the highest residual current amplitude is the measured one in the faulty section and in the upstream sections BE and AB. Therefore, this observation is exploited to introduce another selectivity function because it is difficult to design Logic Functions with a high number of measuring nodes. The proposed selectivity function depends on the ratio of the fundamental component of each section with respect to the parent section AB. Therefore, the fundamental component has to be tracked using a signal processing technique such Discrete Fourier Transform (DFT). The recursive DFT is in the form:

$$I_{real}(k) = I_{real}(k-1) + \frac{2}{N}(i_r(k) - i_r(k-N))\cos(k\theta) \tag{8}$$

$$I_{imaj}(k) = I_{imaj}(k-1) + \frac{2}{N}(i_r(k) - i_r(k-N))\sin(k\theta) \tag{9}$$

$$I_r(k) = \sqrt{I_{real}^2(k) + I_{imaj}^2(k)} \tag{10}$$

where $\theta = 2\pi/N$, $i_r(.)$ is the discrete input samples of the residual current. $I_{real}(.)$, $I_{imaj}(.)$ and $I_r(.)$ are the in-phase, quadrature-phase and residual current amplitude, respectively. The corresponding fundamental amplitudes of the residual current waveforms of different sections are shown in Figure 4.13. It illustrates that the residual current amplitudes of sections AB, BE and EF are higher than the others. Accordingly, the ratio of the residual fundamental current component of each section with respect to the residual current amplitude of the parent section AB is computed to estimate the fault path. For example, the ratio regarding section EK is:

$$R_{\mathrm{EK}} = \frac{I_{r(\mathrm{EK})}}{I_{r(\mathrm{AB})}} \tag{4.4}$$

where $I_{r(\mathrm{EK})}$ and $I_{r(\mathrm{AB})}$ are the fundamental residual current components of sections EK and AB, respectively. Similarly, the ratios regarding other sections are computed and their performance is shown in Figure 4.14. Because the fault is in section EF, the ratios R_{BE} and R_{EF} are the highest and they are approximately close to one during the fault. Before the fault, the ratios are not stable because the value of residual current of section AB is approximately zero. However, they are only considered when the fault existed where the fault existence can be ascertained using the detector S_{Ir}.

Towards increasing the fault location security, the aforementioned ratio is computed for the change of residual current amplitudes. This change is the difference between the residual current magnitude during and pre-fault measuring. However, such selectivity function needs to discriminate between pre and during-fault periods where this task can be carried out using the detector S_{Ir}. Furthermore, synchronization between the measured currents should be attained. This synchronization can also be achieved by evaluating the detector S_{Ir} performance throughout the network where the DWT details are responded to the fault event simultaneously at different measuring nodes.

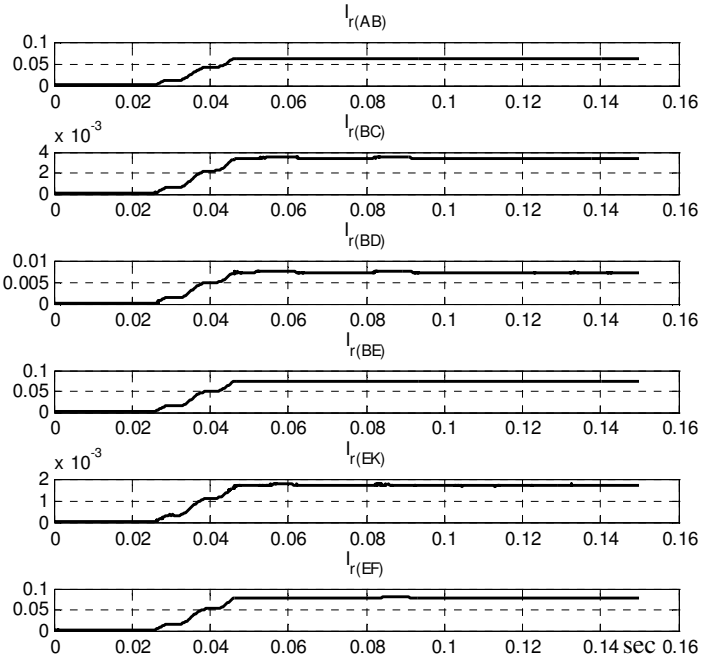

Figure 4.13 Fundamental components of the residual currents during the fault case shown in Figure 4.10.

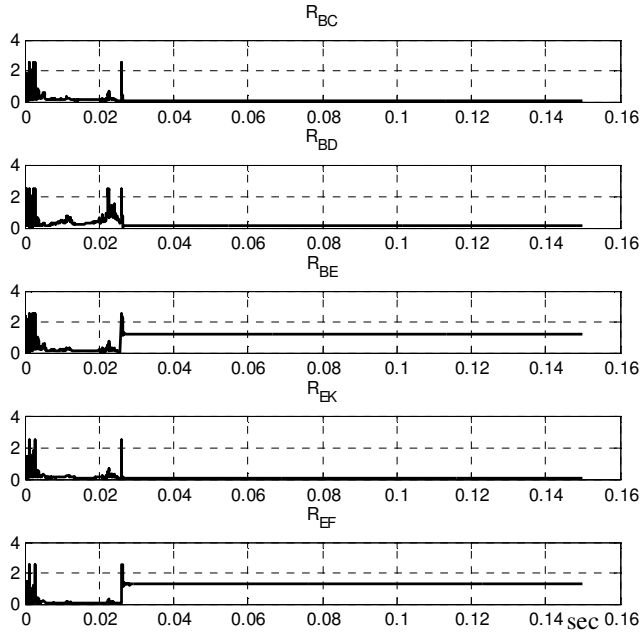

Figure 4.14 Discriminators R when the fault occurred in section EF.

5- DWT-Based Power Direction Selectivity of High Impedance Arcing Fault Detection [P.V], [P.VI]

Figure 5.1 shows another detection procedure proposed in this dissertation where it is also depending on DWT. However in this case, the network voltages and currents are taken at each measuring node. The fault features are extracted using DWT. The absolute sum, however, of the phase voltage detail d3 coefficient over one cycle period of the power frequency is estimated for fault detection purposes. A threshold value of 1.0 is suggested to discriminate the fault features from measurement noise, as described in [P.V]. This threshold value is better than the previous one suggested when the current waveforms were considered as in [P.III], [P.IV]. In order to determine the faulty feeder, the detail d3 of the voltage and current of each connected feeder are together multiplied to compute the power. Using the sum over a period of two power cycles, the power direction in the form of its polarity is utilized to identify the faulty feeder. When this power is negative, the fault occurrence is in the corresponding feeder; however, when it is positive the feeder is healthy. In a general form, when the fault features appear on the voltage details, the fault tracking process is considered. From the practical point of view, there is more challenge for detecting the faults due to leaning trees in MV networks. This challenge is due to the network noise. The main point to verify the detection possibility is applying the proposed technique on staged fault cases as evaluated in this chapter.

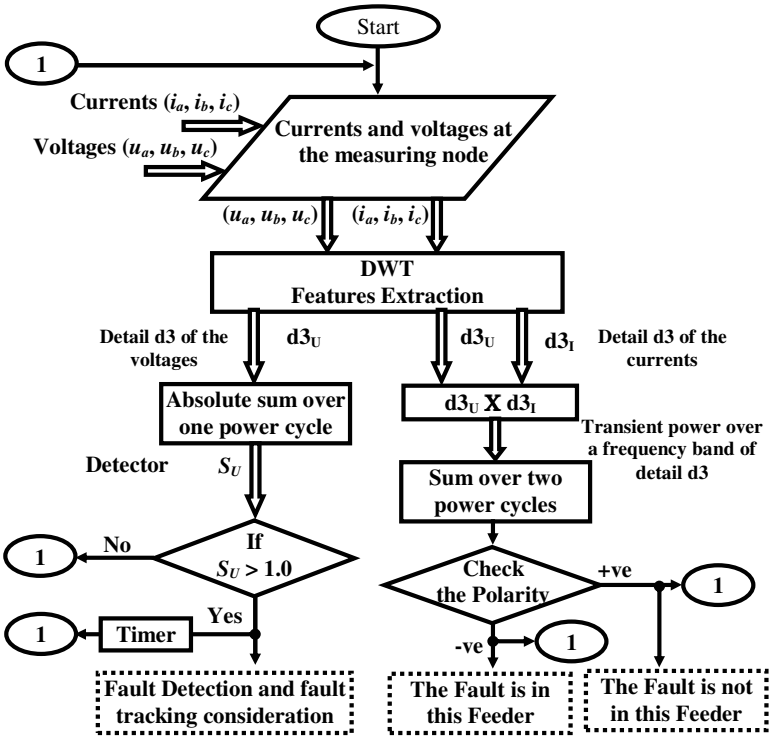

Figure 5.1 The flowchart for the detection technique implementation.

5.1 Feature Extraction from Phase Quantities [P.V]

Daubechies mother wavelet 14 (db14) and the details d3 are also used in this section for localizing the fault with a sampling frequency of 100 kHz. For the fault case occurred at the end of Feeder 1 in the network shown in Figure 3.8, the fault features are extracted from the phase voltages as shown in Figure 5.2. Also, the initial transients due to arc reignitions are frequently localized in the healthy and faulty phase voltage details. Using the voltage details in preference to current details, a performance of the detector S_{U}, which is the absolute sum value of the phase voltages, is shown in Figure 5.3. The performance of S_{U} ensures the fault detection.

A performance of the proposed discriminator method to estimate the faulty feeder can be ensured by Figure 5.4. The details d3 of the voltage and currents of the healthy feeders are in-phase. However, the detail of the faulty feeder current is out of phase. Such shifting can be tracked by multiplying the details of the voltage ($d3_U$) and current ($d3_I$) for each phase of each feeder. It can be considered as the harmonic-band power over the frequency range 12.5-6.25 kHz. The power polarity is estimated using summation over a period of two cycles. As an example, this power for phase-a and for Feeder j is:

$$P_{a(Feeder\ j)}(k) = \sum_{h=k-2N+1}^{k} \left(d3_{Ua}(h)\ d3_{Ia(Feeder\ j)}(h) \right) \tag{5.1}$$

where $P_{a(Feeder\ j)}(.)$ is used as a discriminator where its polarity is used to point out the fault point. The discriminator performance is shown in Figure 5.5. The discriminator polarity is positive for healthy feeders and negative for faulty Feeder 1 as confirmed for each phase. However, the faulty phase is not determined. Therefore, the proposed technique can be used considering the residual components (voltage and currents) as described in the following section.

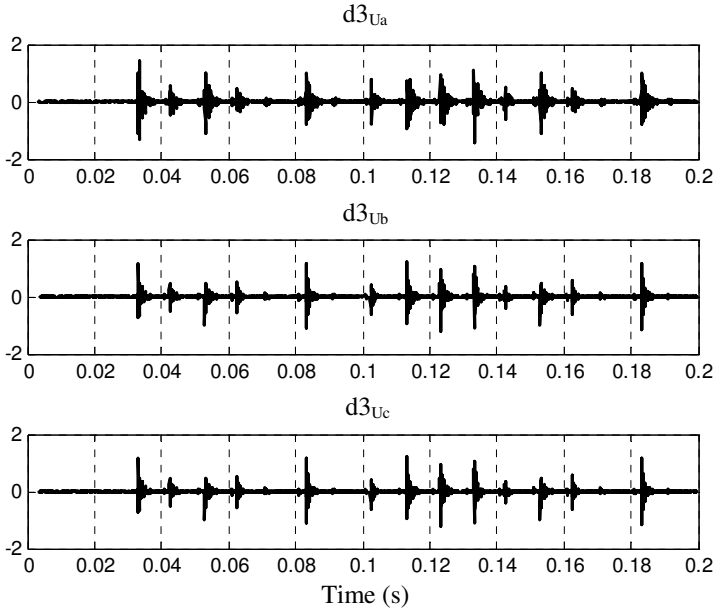

Figure 5.2 Details d3 of the phase voltages.

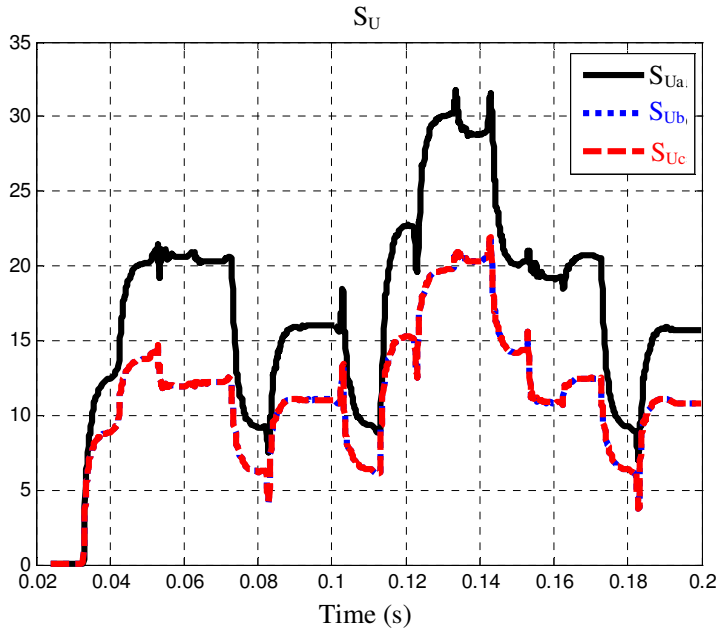

Figure 5.3 The detector S_U performance using the phase voltage details.

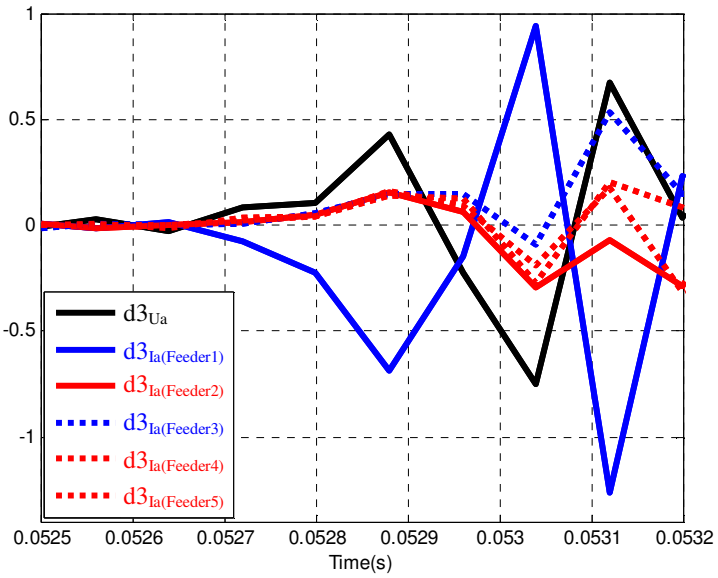

Figure 5.4 Enlarged view of phase-a voltage and feeder current details.

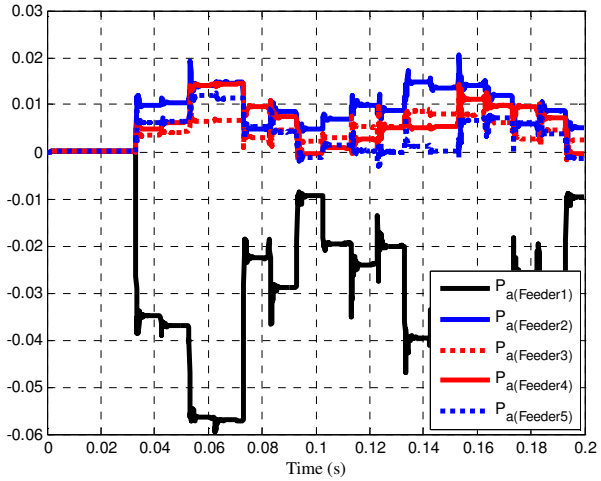

a. Comparison for phase-a.

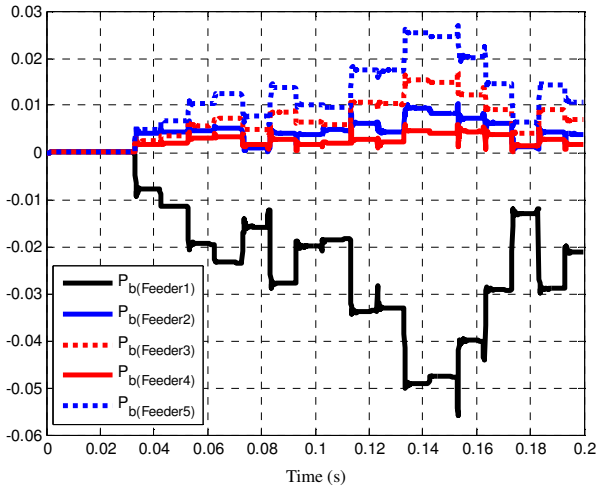

b. Comparison for phase-b.

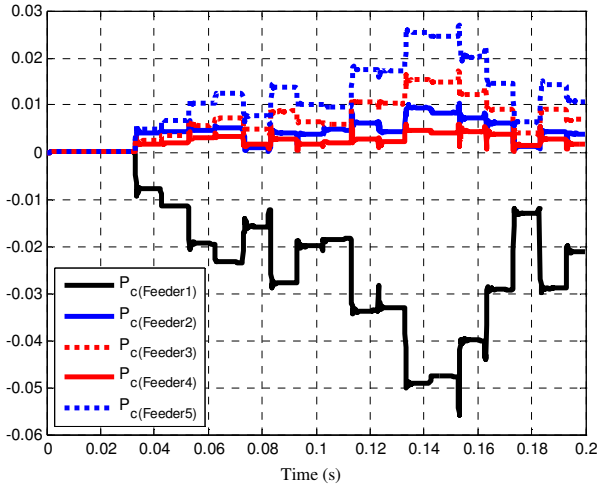

c. Comparison for phase-c.

Figure 5.5 Comparison between the discriminator P_a, P_b, and P_c of the different feeders.

5.2 Feature Extraction from Residual Waveforms [P.V]

Considering the same fault test case highlighted in the previous section, the fault features are extracted from the residual components [P.V]. The absolute sum value of the residual voltage details is recalculated and the results are depicted in Figure 5.6.a. It is evident that the fault is detected with a better detector gain when it is compared by Figure 5.3. The transient power directionality is tested using a similar formula in the form of (5.1) but the details of the phase quantities are replaced by the details of the residual waveforms. The corresponding performance of the discriminator P_r points out the faulty feeder as depicted in Figure 5.6.b, where its polarity is positive for healthy feeders and negative for the faulty Feeder 1. This proposed detection and selectivity technique is further evaluated at different fault conditions in [P.V].

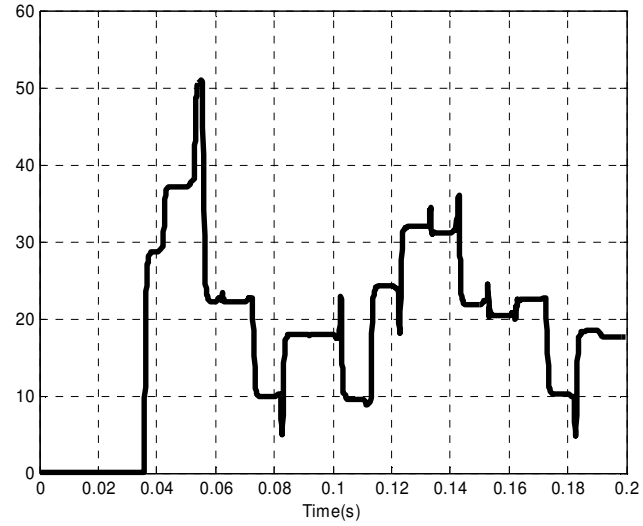

a. The detector S_{Ur}

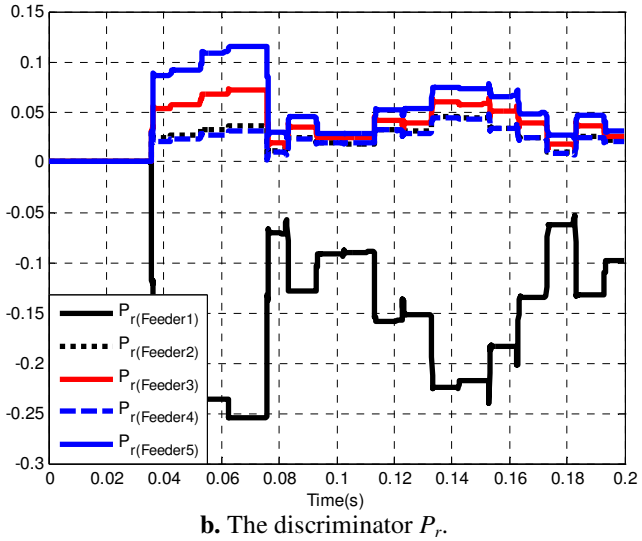

b. The discriminator P_r.

Figure 5.6 The performance when the second fault case conditions are considered.

5.3 Field Data Verification

When the fault object has a high resistance such as tree, the fault detection possibility is reduced because its impact on the network waveforms can not be easily recognized. In such fault cases, the fault features are very small and the network noise can also contribute to loss of the fault detection (or loss of dependability of the fault detection). The only method which can confirm the high impedance fault detection is to evaluate the detection techniques using field data either using actual fault cases or considering staged faults. In this section, the proposed technique introduced at the beginning of this chapter is examined using staged fault cases.

In November 1995, staged earth faults were accomplished in a 20 kV network using known fault resistances and also using natural trees. The network was only two feeders. However, these fault cases were not associated with arcs. Figure 5.7 shows a wire connection between the network conductor and the fault object which was a tree where it was connected to the faulty feeder before its energizing. Then, the breaker was switched onto the fault. Similarly, the fault object was replaced by a known resistance which is shown in Figure 5.8. The fault resistance values were in the range 23.2 to 236.4 kΩ. Although these fault cases were not actual fault scenarios, they can be used as an evaluation guide for the detection possibilities.

These fault cases are not associated with arcs. Therefore, the transients are only generated at the starting fault instant without repetition because the arc reignition impact on the network does not exist. The transient features are only localized at the fault occurrence instant when these staged fault cases are examined using the absolute sum of DWT residual voltage detail coefficient for the detection purposes and polarity of the transient powers as a selectivity function.

This technique is applied on 17 staged fault cases, in which, the sampling frequency is 10 kHz. Figure 5.9 illustrates the performance of detector S_{Ur} and discriminator P_{r} when the fault resistance is 236.4 kΩ. Although the effect of noises is obvious on the results, the proposed technique detects the fault and discriminates the faulty feeder which has a negative P_{r}. Towards improving the performance, the captured signals are de-noised. The de-noising procedure is carried out in the MATLAB environment. The strategy to de-noise signals is based on the one-dimensional stationary wavelet analysis using the graphical interface tools. The corresponding performance is shown in Figure 5.10. However, the detector gain is slightly reduced after the de-noising process.

Figures 5.11 to 5.13 confirm the performance for different fault resistances such as 162.8, 81.7 and 64 kΩ, respectively. Figures 5.14 to 5.16 illustrate the performance when the fault object is tree. However, the detector responded to the transients at the instant of the fault beginning because there are not associated arcs. From these Figures, the fault is detected and the faulty feeder is determined. The detector performance is summarized for extra ten cases in Table 5.1. Such staged fault cases practically confirm the efficiency of the proposed technique.

Figure 5.7 The tree as a fault object wired by the network conductor.

Figure 5.8 The resistance used as a fault object.

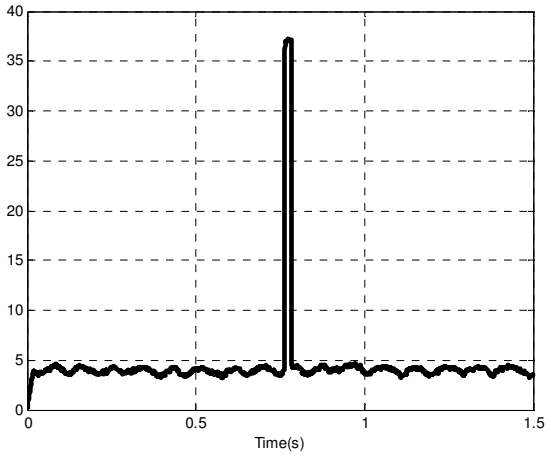

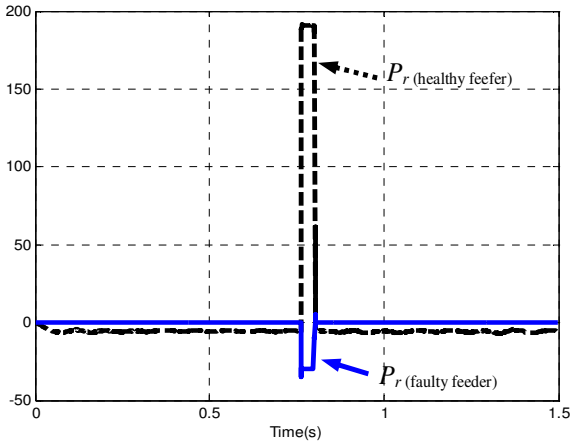

a. The detector S_{Ur} considering details d1 **b.** The discriminator P_r considering details d1

Figure 5.9 The performance when the fault resistance is 236.4 kΩ.

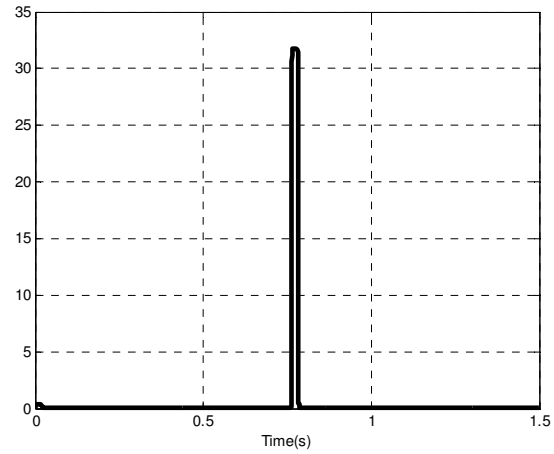

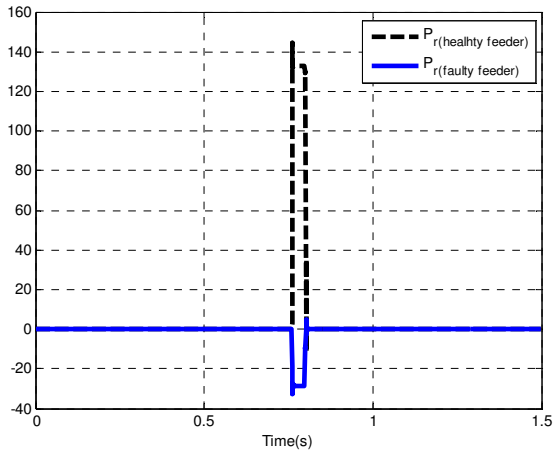

a. The detector S_{Ur} **b.** The discriminator P_r

Figure 5.10 The performance when measured signals of the staged fault are de-noised.

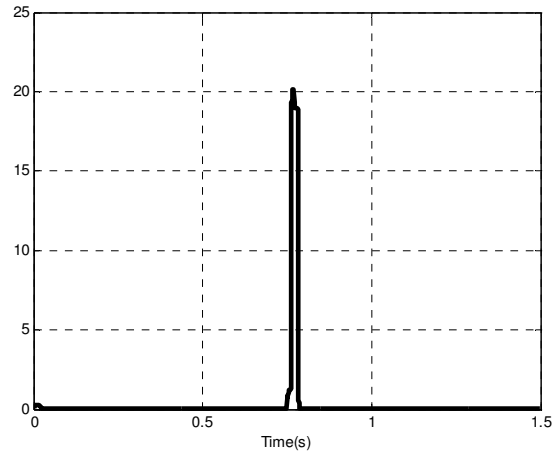

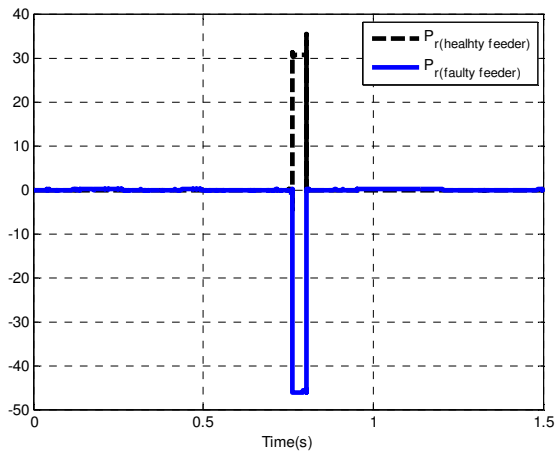

a. The detector S_{Ur} **b.** The discriminator P_r

Figure 5.11 The performance when the fault resistance is 162.8 kΩ.

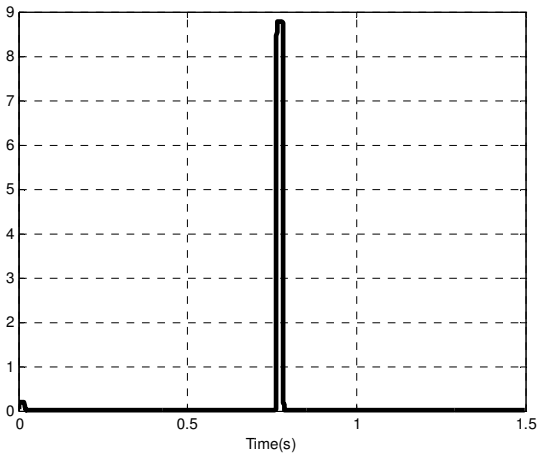

a. The detector S_{Ur}

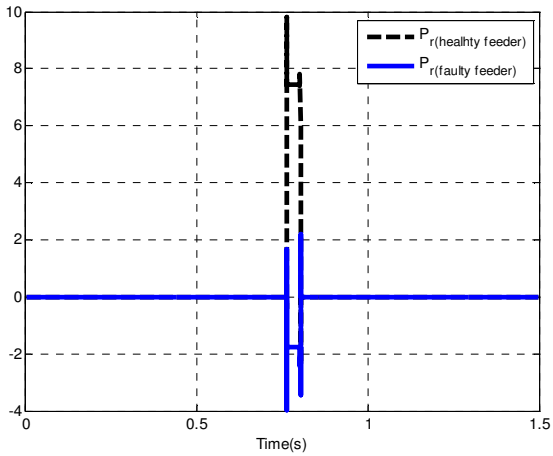

b. The discriminator P_r

Figure 5.12 The performance when the fault resistance is 81.7 kΩ.

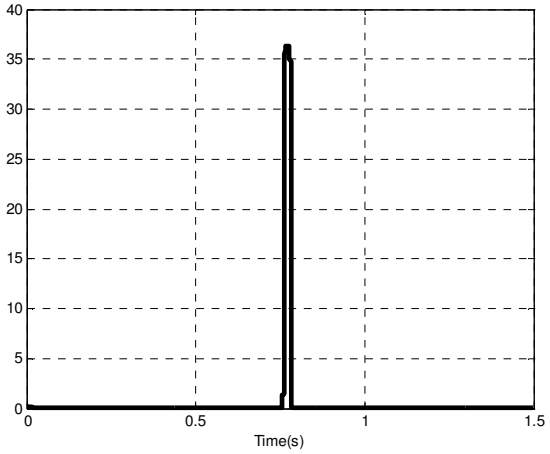

a. The detector S_{Ur}

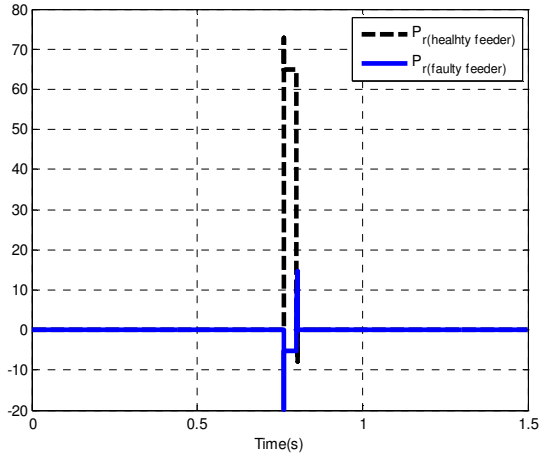

b. The discriminator P_r

Figure 5.13 The performance when the fault resistance is 64 kΩ.

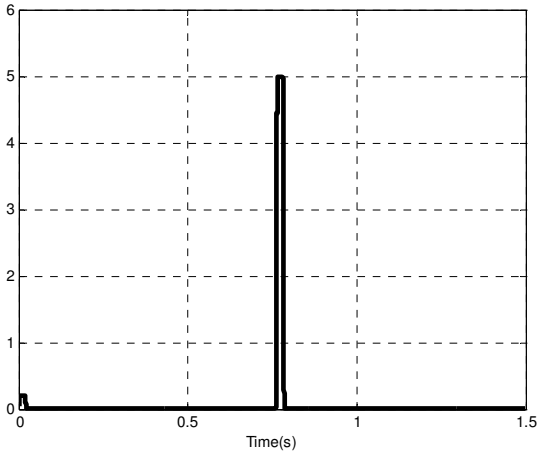

a. The detector S_{Ur}

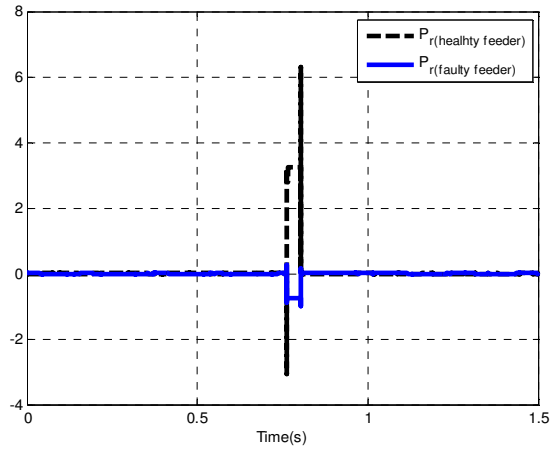

b. The discriminator P_r

Figure 5.14 The performance for a staged fault connected through a tree.

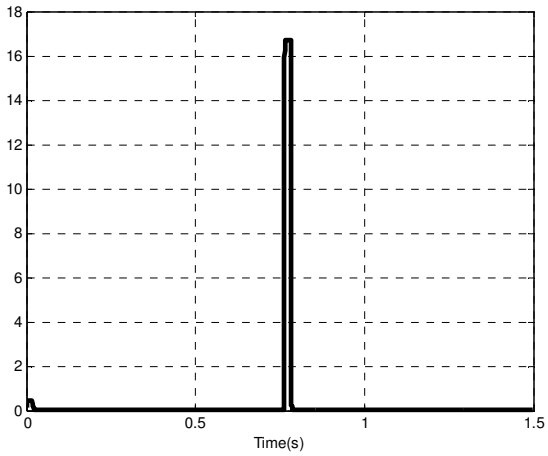

a. The detector S_{Ur}

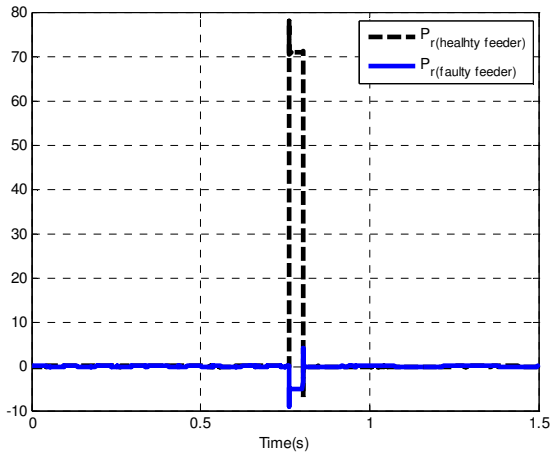

b. The discriminator P_r

Figure 5.15 The performance for a staged fault connected through a second tree.

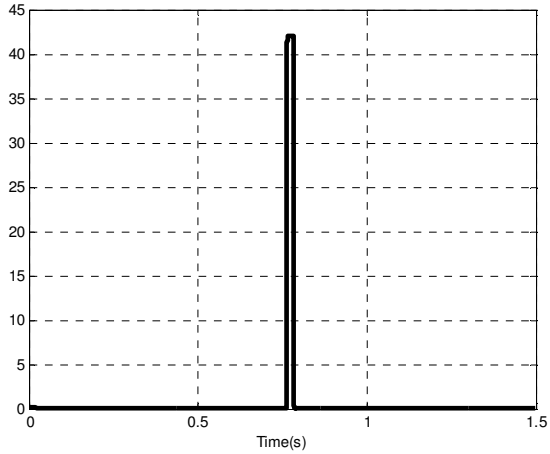

a. The detector S_{Ur}

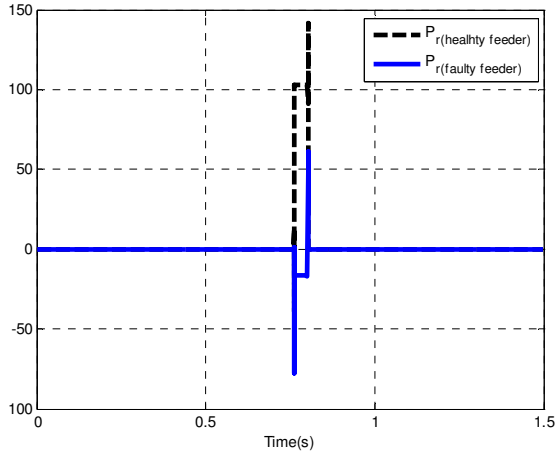

b. The discriminator P_r

Figure 5.16 The performance for a staged fault connected through a third tree.

Table 5.1 The detector S performance for the other staged fault cases.

No.	Fault Resistance	The detector S_{Ur}	No.	Fault Resistance	The detector S_{Ur}
1	23.2 kΩ	6.47	6	104.8 kΩ	10.0
2	23.2 kΩ	13.4	7	186.0 kΩ	20.0
3	40.8 kΩ	61.0	8	Tree	45.5
4	40.8 kΩ	6.37	9	Tree	11.1
5	64.0 kΩ	8.59	10	Tree	2.86

5.4 Testing the Proposed Detection Technique throughout the Network [P.VI]

In this section, the proposed detection technique is more tested throughout the network shown in Figure 4.8. Considering a fault test case occurring at the end of section BD, the detectors S_{Ur} performance for different residual voltages is shown in Figure 5.17. The detectors respond to the fault disturbance all over the network, which confirms the decision.

The discriminator P_r performance is depicted in Figure 5.18 at the measuring nodes A and B. At node A, the discriminator polarity is positive for healthy feeders and negative for the faulty Feeder 1 as shown in Figure 5.18.a. At node B, the discriminator P_r polarity is positive for the healthy sections BC and BE but it is negative for the faulty section BD shown in Figure 5.18.b. When the discriminator polarities are checked at the measuring nodes D and E, they are found positive, ensuring the sections behind are healthy. From the performance of the discriminator P_r, it can be indicated that the fault is in section BD. The other fault case occurred at the end of section EF is discussed in [P.VI].

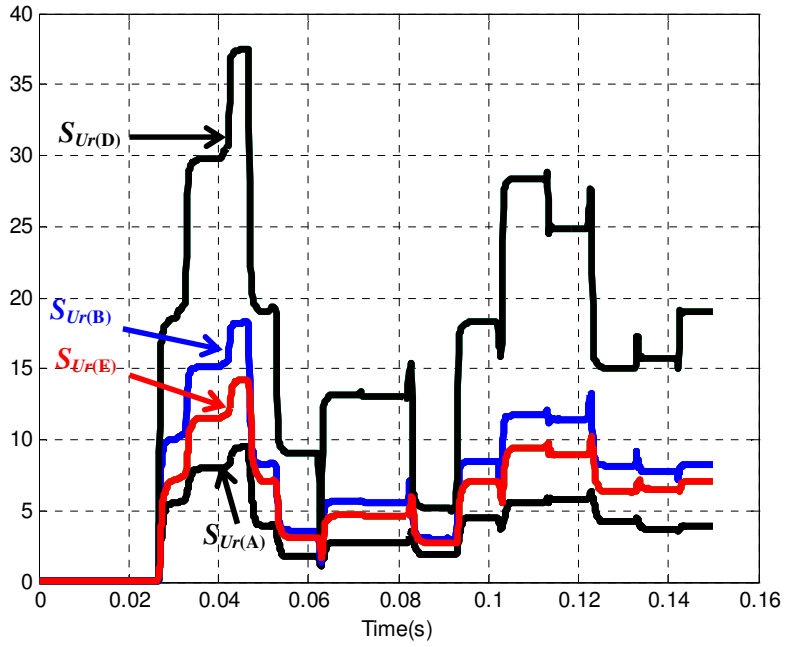

Figure 5.17 The detector S_{Ur} using the voltage details when the fault occurred in section BD.

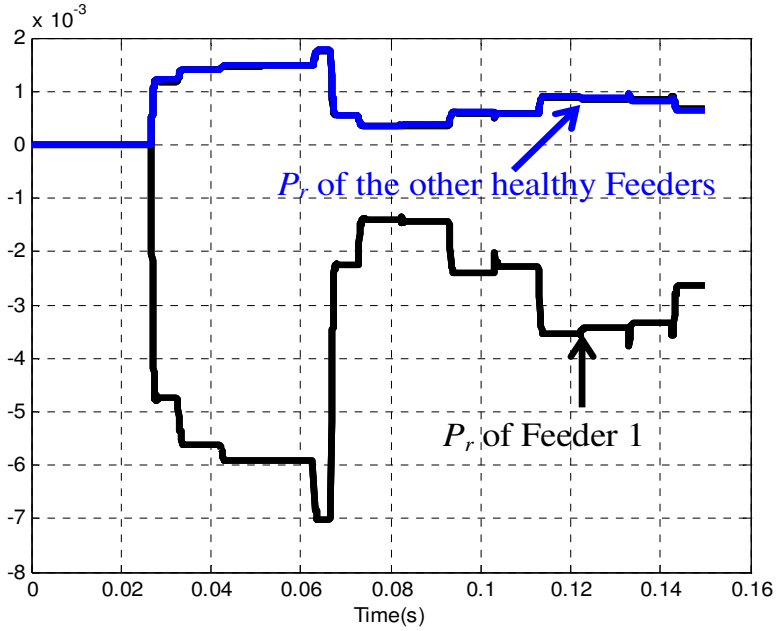

a. The discriminator P_r at node A.

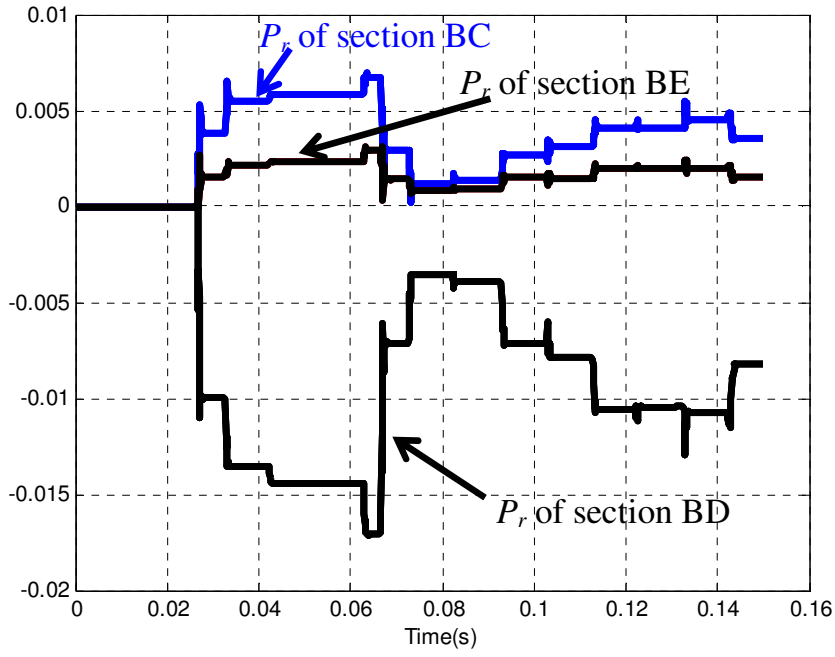

b. The discriminator P_r at node B.

Figure 5.18 The discriminator P_r when the fault occurred in section BD.

A simultaneous fault case is considered to evaluate the performance of the proposed detection technique. The fault scenario is as following. During a fault occurring in section EF at 26 *ms* another fault also caused by a leaning tree occurred in Feeder 5 at 90 *ms*. Figure 5.19 illustrates the detector S_{Ur} performance which ensures the fault detection. In Figure 5.20.a the discriminator P_r of Feeder 1 is negative from the fault instant at 26 *ms* and P_r Feeder 5 is changed from positive to negative polarity at 90 *ms* while the other healthy feeders are remaining positive during the faults. Such performance confirms that there is a fault in Feeder 1 and another fault in Feeder 5. Figure 5.20.b illustrates that the fault in Feeder 1 is in or behind section BE. It can be concluded from Figure 5.20.c that there is a fault in section EF.

Under certain circumstances controlled by the fault instant (or fault inception angle) of the second associated fault in Feeder 5, the effect of the initial transients from the second fault at its starting instant is sometimes more dominant than the initial transients created by the arc reignitions of the first fault in Feeder 1. Therefore, the discriminator P_r of Feeder 1 can be affected for a transition period of two cycles from the instant of the second fault. This period can be reduced by summing the band-power over one cycle. However, considering two cycles gives more stability for the power polarity response.

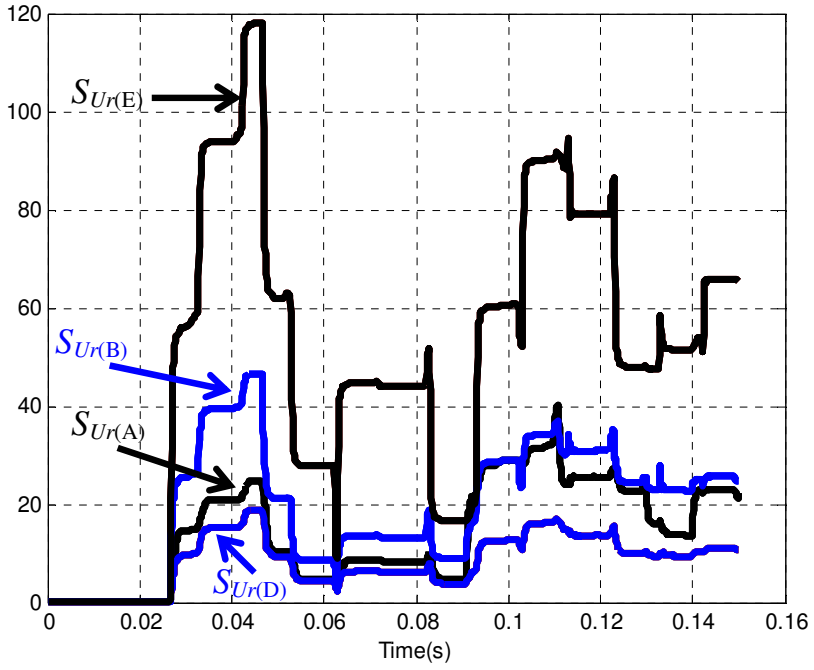

Figure 5.19 The detector S_{Ur} of the voltage details for a simultaneous fault case.

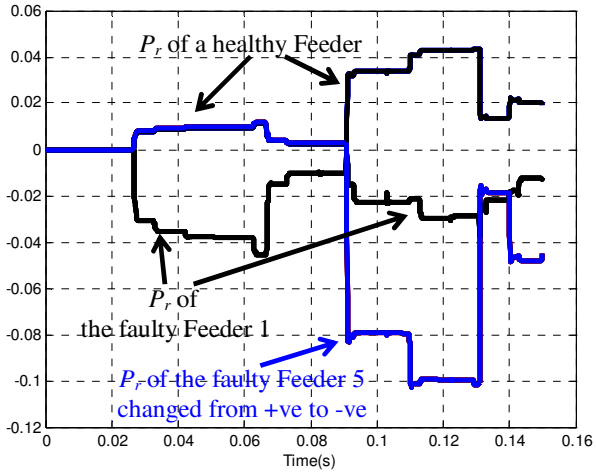

a. At node A.

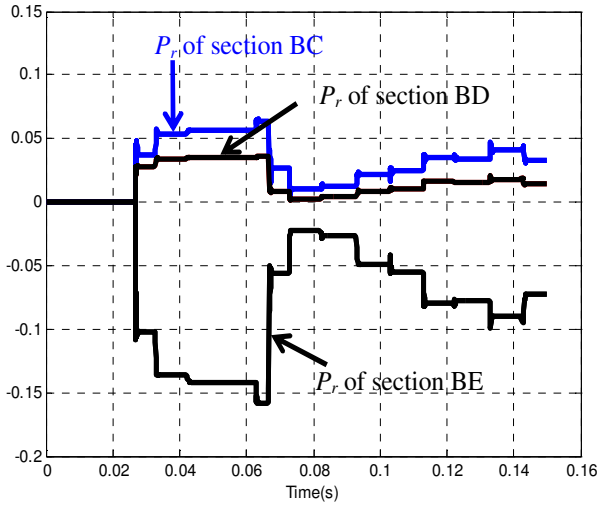

b- At node B.

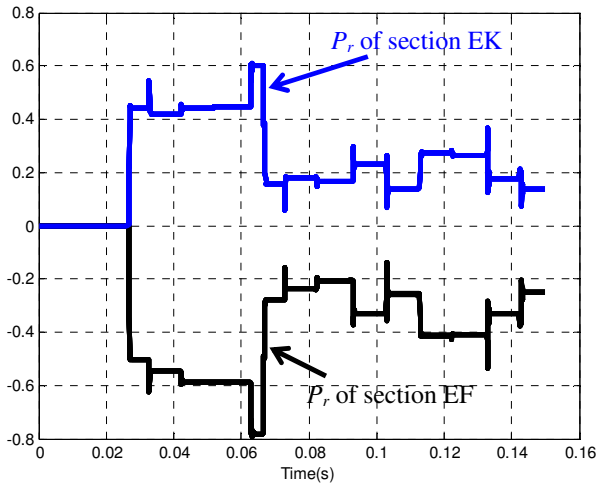

c- At node E.

Figure 5.20 The discriminator P_r behavior during a simultaneous fault case.

6- Conclusions and Future Work

6.1 Conclusions

A universal arc representation has been introduced using Modified Mayr (P-τ model) as an example, in which, the arc equations were solved in the TACS field of the EMTP program and represented in the power network by TACS controlled voltage source. The arc voltage and current signals have been measured from the power network into the TACS field using sensors type 90 and 91, respectively. They have been used as inputs to the dynamic arc equations. The model parameters have been computed exploiting the flexibility of FORTRAN expressions in the TACS field. SF6 breakers with experimentally defined arc parameters have been considered to perform a comparison between the proposed arc representation and the EMTP built-in model. The thermal limiting curve has been computed by the proposed and built-in models and compared with the measured characteristic. Such comparison has confirmed the accuracy of proposed arc representation. Also, the universality of proposed arc representation has been verified via carrying out different arc model examples of circuit breaker and transmission line arcing faults. The study results validated the proposed representation regarding accuracy and universality.

A model for high impedance arcing faults due to leaning trees in MV networks have been proposed and experimentally verified. The fault was represented in two series parts; an arc model and a high resistance. The arcing element has been dynamically simulated using thermal equations. The arc model parameters and resistance values were determined using the experimental results, where for representing short length and small current arcs, the parameters have been changed to fit the new application. The fault behavior has been simulated by the ATP/EMTP program, in which the arc model has been realized using the universal arc representation.

The electromagnetic transients due to the earth fault caused by tree leaning in MV networks were discussed where the fault model was incorporated in a 20 kV distribution network at different locations using ATP/EMTP program. The residual voltage and current associated with this disturbance have been measured considering different neutral earthing methods. The main found features of this fault type that can enhance its detection were the electromagnetic transients created by the periodic arc-reignitions.

Features of earth faults due to leaning trees have been extracted from phase currents using DWT. Due to the periodicity of arc reignitions, the initial transients have been localized not only at the fault occurrence instant but also during the fault period that enhanced the detection security. The absolute sum of the DWT detail d3 coefficient has been computed over one power cycle for each phase current of each feeder. The faulty phase had the highest absolute sum when it has been compared with the other healthy phases. Similarly, the absolute sum of the faulty feeder has been the highest when the comparison was carried out with respect to other feeders. Therefore, two Logic Functions have been suggested to determine the faulty phase and faulty feeder.

The study has been extended to extract the fault features from residual currents throughout the network. The DWT performance at different measuring nodes has been gathered at the base station using wireless sensors concept. Therefore, the DWT has been evaluated for a wide area of the network and the fault detection has been confirmed by numerous DWT extractors. In this case, the term of locating the faulty section has been changed to be based on ratios of the residual current amplitudes.

The other selectivity term of the faulty feeder has been introduced based on a novel technique by extracting and examining the power polarity. This power is mathematically processed by multiplying the DWT detail coefficients of the phase voltage and current for each feeder. Its polarity has discriminated the faulty feeder, in which, the polarity has been positive when the feeder was healthy and it has been negative when the feeder was faulty. Such feature has confirmed when considered with any phase. In order to reduce the computational burden of the technique, the extraction of the fault features was examined using the residual components instead of the phase components. The same methodology of computing power has been considered with taking into considerations the residual voltage and current detail coefficients where the proposed algorithm performance became better. This proposed algorithm performance has been evaluated using staged fault data. However, the fault feature was only localized at the fault instant because there was no associated arc and therefore the transients were not repeated. When the signals have been de-noised, the detection performance has been improved. Then, this proposed detection technique has been processed on the residual voltages and currents at different measuring nodes throughout the network using the distributed wireless sensors and more precise faulty section discriminator has been attained.

6.2 Future Work

The following points of interest will be extended in work to follow:

1- The high impedance fault modeling issue is required to be extended to cover other faults such as incipient faults, different fault objects and downed conductor over different soils. That is because this work only models high impedance faults due to leaning trees.
2- More scrutiny on the proposed algorithms using staged fault data of the earth faults due to leaning trees. That is because the performance of the proposed detection technique is examined using a limited staged fault cases. Extended staged faults are to be captured with actual fault scenario of leaning trees.
3- Testing probabilistic techniques after extracting the fault features using DWT which can contribute to more selectivity functions of the fault detection.

References

[1] J. Bickford and A. Heaton “Transients Overvoltages on Power Systems”, IEE Proceeding, Vol. 133, No. 4, pp. 201-225, May 1986.

[2] G. Andersson, P. Donalek, R. Farmer, N. Hatziargyriou, I. Kamwa, P. Kundur, N. Martins, J. Paserba, P. Pourbeik, J. Sanchez-Gasca, R. Schulz, A. Stankovic, C. Taylor and V. Vittal "Causes of the 2003 Major Grid Blackouts in North America and Europe and Recommended Means to Improve System Dynamic Performance" IEEE Transactions on Power delivery, vol. 20, no. 4, pp. 1922-1928, November 2005.

[3] Report of PSRC Working Group D15 “High Impedance Fault Detection Technology” March 1996.

[4] Electric Power Research Institute (EPRI), Inc. and EMTP Development Coordination Group (DCG), Electromagnetic transient programs (EMTP96) rule book, ver 2.0 released on August 1986, and updated ver 3.x on June 1999.

[5] V. Phaniraj and A. Phadke "Modelling of Circuit Breakers in the Electromagnetic Transients Program" *IEEE Transactions on Power Systems*, vol. 3, no. 2, pp. 799 – 805, May 1988.

[6] H. Darwish, M. Izzularab and N. Elkalashy “Implementation of Circuit Breaker Arc Model Using Electromagnetic Transient Program” *Middle-East Power Systems Conference*, *MEPCON*, Hellwan University, Egypt, pp. 809-814, December 2001.

[7] B. Aucoin and R. Jones “High Impedance Detection Implementation Issues” *IEEE Transactions on Power Delivery*, vol. 11, no. 1, pp. 139148-594, January 1996.

[8] N. Bhatt "August 14, 2003 U.S.-Canada Blackout" IEEE/PES General Meeting Denver, USA, June 2004.

[9] U.S-Canada Power System Outage Task Force. (2004) Final Report on the August 14, 2003 Blackout in the United Sates and Canada: Causes and Recommendations. [Online]. Available: http://www.nerc.com.

[10] S. Larsson and E. Ek "The Blackout in Southern Sweden and Eastern Denmark, September 23, 2003" IEEE/PES General Meeting, Denver, USA, June 2004.

[11] S. Corsi and C. Sabelli "General Blackout in Italy Sunday September 28th, 2003, h 03:28:00" IEEE/PES General Meeting, Denver, USA, June 2004.

[12] A. Berizzi, “The Italian 2003 blackout,” in Proc. IEEE/PES General Meeting, Denver, USA, June 2004.

[13] “Final Report of the Investigation Committee on the 28 September 2003 Blackout in Italy,” UCTE, 2004.

[14] S. Hänninen , M. Lehtonen, and T. Hakola “Earth Faults and Related Disturbances in Distribution Networks” *IEE Proceedings-Generation, Transmission and Distribution,* Vol. 149, No. 3, pp. 283 – 288, May 2002.

[15] S. Hänninen "Single Phase Earth Faults in High Impedance Ground Networks Characteristics, Indication and Location" Technical Research Centre of Finland (VTT), Espoo, Finland, 2001.

[16] A. Girgis and F. Ham "A Qualitative Study of Pitfalls in FFT" *IEEE Transactions on Aerospace and Electronic Systems*, vol. AES 16, no. 4, pp. 434-439, July 1980.

[17] C. Moo, Y. Chang and P. Mok "A Digital Scheme for Time-Varying Transient Harmonics" *IEEE Transactions on Power Delivery*, vol. 10, no. 2, pp. 588-594, April 1995.

[18] Y. Chang, Y. Hsieh and C. Moo "Truncation effects of FFT on estimation of dynamic harmonics in power system" International Conference on Power System Technology, PowerCon 2000, Australia, vol. 3, pp. 1155 – 1160, December 2000.

[19] I. Daubechies "Ten Lectures on Wavelets" Regional Conference Series in Applied Mathematics, the society for Industrial and Applied mathematics, second printing, 1992.

[20] C. Kim and R. Aggarwal "Wavelet Transforms in Power Systems. Part 1 General Introduction to the Wavelet Transforms" *Power Engineering Journal*, vol. 14, no. 2, pp. 81-87, April 2000.

[21] M. Solanki, Y. Song, S. Potts and A. Perks "Transient protection of transmission line using wavelet transform" *IEE 7th International Conference on Developments in Power System Protection*, pp. 299–302, 9-12 April 2001.

[22] H. Darwish, M. Farouk, A. Taalab, N. Mansour "Investigation of Real–Time Implementation of DSP-Based DWT for Power System Protection" *IEEE/PES Transmission and Distribution Conference and Exposition*, Dallas, Texas, USA, May 2006.

[23] T. Zheng and E. Makram "An Adaptive Arc Furnace Model" *IEEE Transactions on Power Delivery*, Vol. 15, No. 3, pp 931-939, July 2000.

[24] M. Aucoin, B. Russell and C. Benner "High Impedance Fault Detection for Industrial Power Systems" Conference Record of the 1989 IEEE Industry Applications Society Annual Meeting, October 1989.

[25] V. Terzija, N. Elkalashy, G. Preston, V. Stanojević, G. Štrbac "Detection of Arcing Faults: Modelling, Simulation, Testing and Algorithms Aspects" PowerTech 2007, Lausanne, Switzerland, July 2007.

[26] N. Elkalashy, H. Darwish, A. Taalab, and M. Izzularab, "An Adaptive Single Pole Autoreclosure Based on Zero Sequence Power" *Electric Power Systems Research*, Vol. 77, No. 5-6, pp. 438-446, April 2007.

[27] R. Aggarwal, A. Johns, Y. Song, R. Dunn, and D. Fitton "Neural-Network Based Adaptive Single-Pole Aotureclosure Technique for EHV Transmission Systems," *IEE Proceedings-Generation, Transmission and Distribution*, Vol. 141, No. 2, pp. 155-160, March 1994.

[28] H. Darwish, M. Izzularab, and N. Elkalashy "Enhanced Commutation Circuit Design of HVDC Circuit Breaker Using EMTP", IEEE/PES, Transmission and distribution, TD 2005/2006, pp 978 – 985, USA, 21-24 May 2006.

[29] H. Darwish, M. Izzularab, and N. Elkalashy, "Real-time testing of hvdc circuit breakers" the 14th International Conference on power System Protection, PSP2004, Bled, Slovenia, 2004.

[30] J. Blackburn *Protective Relaying. Principles and applications*, second edition, Marcel Dekker, Inc, New Yourk, 1998.

[31] C.K. Wong, C.W. Lam, K.C. Lei, C.S. Lei, and Y.D. Han "Novel Wavelet Approach to Current Differential Pilot Relay Protection," *IEEE Transactions on Power Delivery*, Vol. 18, No. 1, pp 20-25, January 2003.

[32] H. Darwish, A-M. Taalab, A. Osman, N. Mansour and O. Malik "Experimental Evaluation of DWT-Based Current Spike Comparator for Line Protection" IEEE/PES Power Systems Conference and Exposition, PSCE '06, pp. 1371 – 1379, 2006.

[33] H. Darwish, A-M. Taalab and E. Ahmed "Investigation of power differential concept for line protection" *IEEE Transactions on Power Delivery*, Vol. 20, No. 2, pp 617-621, April 2005.

[34] A-M. Taalab, H. Darwish and E. Ahmed "Performance of Power Differential Relay with Adaptive Setting for Line Protection" *IEEE Transactions on Power Delivery*, Vol. 22, No. 1, pp 50-58, January 2007.

[35] A. Pradhan, A. Routray and S. Gudipalli "Fault Direction Estimation in Radial Distribution System Using Phase Change in Sequence Current" *IEEE Transactions on Power Delivery*, Vol. 22, No. 4, October 2007.

[36] M. Lehtonen and T. Hakola "Neutral Earthing and Power System Protection. Earthing Solutions and Protective Relaying in Medium Voltage Distribution Networks", *ABB Transmit Oy*, FIN-65101 Vassa, Finland, 1996.

[37] G. Benner and B. Russell "Practical High-Impedance Fault Detection on Distribution Feeders" *IEEE Transactions on Industry Applications*, Vol. 33, No. 3, pp. 635-640, May/June 1997.

[38] A. Girgis, W. Chang and E. Makram "Analysis of high-impedance fault generated signals using a Kalman filtering approach", *IEEE Transactions on Power delivery*, Vol. 5, No. 5, pp. 1714-1724, October 1990.

[39] A. Mamishev, B. Russell and G. Benner "Analysis of High Impedance Faults Using Fractal Techniques", *IEEE Transactions on Power delivery*, Vol. 11, No. 1, pp. 435-440, February 1996.

[40] A. Sedighi, M. Haghifam, O. Malik and M. Ghassemian "High Impedance Fault Detection Based on Wavelet Transform and Statistical Pattern Recognition" *IEEE Transaction on Power delivery*, Vol. 20, No. 4, pp. 1414-2421, October 2005.

[41] M. Michalik, W. Rebizant, M. Lukowicz, S. Lee and S. Kang "High-impedance fault detection in distribution networks with use of wavelet-based algorithm" *IEEE Transactions on Power Delivery*, vol. 21, no. 4, pp. 1793 – 1802, October 2006.

[42] C. Kim, H. Kim, Y. Ko, S. Byun, K. Aggarwal and A. Johns "A novel fault-detection technique of high-impedance arcing faults in transmission lines using the wavelet transform" *IEEE Transactions on Power delivery*, Vol. 17, No. 4, pp. 921-929, October 2002.

[43] D. Wai and X. Yibin “A Novel Technique for High Impedance Fault Identification”, *IEEE Transactions on Power delivery*, Vol. 13, No. 3, pp. 738-744, July 1998.

[44] B. Russell and C. Benner "Arcing Fault Detection for Distribution Feeders: Security Assessment in Long Term Field Trials", *IEEE Transactions on Power delivery*, Vol. 10, No. 2, pp. 676-683, April 1995.

[45] D. Jeeringes and J. Linders “Unique Aspects of Distribution System Harmonics due to High Impedance Ground Faults”, *IEEE Transactions on Power delivery*, Vol. 5, No. 2, pp. 1086-1094, April 1990.

[46] T. Grima and J. Flatermeier "A New Generation of Materials for Medium Voltage Compensated Neutral Networks" *IEE 14th International Conference and Exhibition on Electricity Distribution*, *CIRED*, Birmingham, 2-5 June 1997.

[47] G. Druml, A. Kugi and O. Seifert "A New Directional Transient Relay for High Ohmic Earth Faults" *IEE 17th International Conference and Exhibition on Electricity Distribution*, *CIRED*, Bercelona, 12-15 May 2003.

[48] Y. Assef, P. Bastard and M. Meunier "Artificial Neural Networks for Single Phase Fault Detection in Resonant Grounded Power Distribution Systems" *IEEE Transmission and Distribution Conference*, Los Angeles, September 1996.

[49] A. Sultan, G. Swift and D. Fedirchuk “Detecting Arcing Downed-Wires Using Current Flicker and Half-Cycle Asymmetry” *IEEE Transactions on Power Delivery*, Vol. 9, No. 1, pp 461-467, January 1994.

[50] V. Leitloff, R. Feuillet and D. Griffel "Detection of Resistive Single-Phase Earth Faults in a Compensated Power-Distribution System" *European Transactions on Electrical Power System, ETEP*, Vol. 7, No. 1, pp. 65- 73, January 1997.

[51] S. Santoso, E. Powers, W. Grady and P. Hofmann “Power quality assessment via wavelet transform analysis” *IEEE Transactions on Power Delivery*, vol. 11, no. 2, pp. 924 – 930, April 1996.

[52] P. Dash, B. Panigrahi, D. Sahoo and G. Panda “Power quality disturbance data compression, detection, and classification using integrated spline wavelet and S-transform” *IEEE Transactions on Power Delivery*, vol. 18, no. 2, pp. 595 – 600, April 2003

[53] C. Lin and C. Wang “Adaptive wavelet networks for power-quality detection and discrimination in a power system” *IEEE Transactions on Power Delivery*, vol. 21, no. 3, pp. 1106 – 1113, July 2006.

[54] S. Santoso, W. Grady, E. Powers, J. Lamoree and S. Bhatt “Characterization of distribution power quality events with Fourier and wavelet transforms” *IEEE Transactions on Power Delivery*, vol. 15, no. 1, pp. 247 – 254, January 2000.

[55] L. Tao, M. Tsuji and E. Yamada “Wavelet approach to power quality monitoring” The 27th Annual Conference of the IEEE Industrial Electronics Society, IECON '01, pp. 670 – 675, 2001.

[56] C. Kim, S. Park, R. Aggarwal and A. Johns “A noise suppression method for improvement of power quality using wavelet transforms” IEEE Power Engineering Society Summer Meeting, pp. 414 – 419, July 1999.

[57] M. Florkowski “Wavelet based partial discharge image de-noising” 11th International Symposium on High Voltage Engineering, pp. 21 – 24, August 1999.

[58] G. Hashmi, M. Lehtonen, R. Jabbar and S. Qureshi “Wavelet-based De-noising of Partial Discharge Signals in MV Covered-Conductor Networks" Australasian Universities Power Engineering Conference, AUPEC2006, Victoria, Australia, December 2006.

[59] W. Xiaorong, G. Zongjun, S. Yong and Y. Zhang “Extraction of partial discharge pulse via wavelet shrinkage” 6th International Conference on Properties and Applications of Dielectric Materials, Volume 2, pp. 685 – 688, June 2000.

[60] H. Zhang,T. Blackburn, B. Phung and D. Sen; “A novel wavelet transform technique for on-line partial discharge measurements. 1. WT de-noising algorithm” *IEEE Transactions on Dielectrics and Electrical Insulation*, vol 14, no. 1, pp. February 2007

[61] M. Hu; X. Jiang; H. Xie; Z. Wang; “A new technique for extracting partial discharge signals in on-line monitoring with wavelet analysis” International Symposium on Electrical Insulating Materials, pp.677 – 680, September 1998.

[62] O. Youssef "Applications of fuzzy-logic-wavelet-based techniques for transformers inrush currents identification and power systems faults classification" IEEE PES Power Systems Conference and Exposition, pp. 553 – 559, October 2004.

[63] O. Youssef "A wavelet-based technique for discrimination between faults and magnetizing inrush currents in transformers" *IEEE Transactions on Power Delivery*, vol. 18, no. 1, pp. 170 – 176, January 2003.

[64] H. Mortazavi, H. Khorashadi-Zadeh "A new inrush restraint algorithm for transformer differential relays using wavelet transform" International Conference on Power System Technology, PowerCon2004, vol. 2, pp. 1705 – 1709, November 2004

[65] K. Bulter-Purry and M. Bagriyanik "Characterization of Transients in Transformers Using Discrete Wavelet Transforms" *IEEE Transactions on Power Systems*, vol. 18, no. 2, pp. 648-656, May 2003.

[66] J. Faiz, S . Lotfi-Fard "A novel wavelet-based algorithm for discrimination of internal faults from magnetizing inrush currents in power transformers" *IEEE Transactions on Power Systems*, vol. 21, no. 4, pp. 1989- 1996, October 2006.

[67] C. Aguilera, E. Orduna and G. Ratta " Fault detection, classification and faulted phase selection approach based on high-frequency voltage signals applied to a series-compensated line" *IEE Proceedings on Generation, Transmission and Distribution*, vol. 153, no. 4, pp. 469 – 475, July 2006.

[68] H. Darwish, A-M. Taalab, A. Osman, N. Mansour and O. Malik "Spectral Energy Differential Approach for Transmission Line Protection" IEEE/PES Power Systems Conference and Exposition, PSCE '06, pp. 1931 – 1937, 2006.

[69] A. Osman, O. Malik "Transmission line distance protection based on wavelet transform" *IEEE Transactions on Power Delivery*, vol. 19, no. 2, pp. 515 – 523, April 2004.

[70] S. Saleem and A. Sharaf "Ultra High Speed Protection of Series Compensated Transmission Lines using Wavelet Transforms" Canadian Conference on Electrical and Computer Engineering, pp. 1130 – 1134, May 2006.

[71] A. Osman, O. Malik "Protection of parallel transmission lines using wavelet transform" *IEEE Transactions on Power Delivery*, vol. 19, no. 1, pp. 49 – 55, January 2004.

[72] O. Youssef "Online Applications of Wavelet Transforms to Power System Relaying" *IEEE Transactions on Power Delivery*, vol. 18, no. 4, pp. 1158 – 1165, October 2003.

[73] H. Mokhtari and R. Aghatehrani "A new Wavelet-Based Method for Detection of High Impedance Faults" International Conference on Future Power Systems, November 2005.

[74] D. Wai, X. Yibin "A novel technique for high impedance fault identification" *IEEE Transactions on Power Delivery*, vol. 13, no. 3, pp. 738 – 744, July 1998.

[75] S. Huang, C. Hsieh "High-impedance fault detection utilizing a Morlet wavelet transform approach" *IEEE Transactions on Power Delivery*, vol. 14, no. 4, pp. 1401 – 1410, October 1999.

[76] K. Silva, B. Souza, N. Brito "Fault detection and classification in transmission lines based on wavelet transform and ANN" *IEEE Transactions on Power Delivery*, vol. 21, no. 4, pp. 2058- 2063, October 2006.

[77] Z. Huang, Y. Chen and Q. Gong "A protection and fault location scheme for EHV line with series capacitor based on travelling waves and wavelet analysis" International Conference on Power System Technology, PowerCon 2002, vol. 1, pp. 290 – 294, October 2002.

[78] A. Ametani "Power System Transient Analysis by EMTP" *Middle-East Power Systems Conference*, *MEPCON*, Hellwan University, Egypt, pp. 1-12, December 2001.

[79] I. Marti and L. Linares "Real-Time EMTP-Based Transients Simulation" *IEEE Transaction on Power Systems*, Vol. 9, No. 3, P. 1309-1317, August 1994.

[80] R. Lasseter, K. Fehrle and B. Lee *Electromagnetic Transient Program (EMTP)*, Workbook IV (TACS). El-4651, EPRI Research Project 2140-6, Palo Alto, CA 94303, June 1989.

[81] L. Prikler and H. Hoildalen *ATPDraw Users Manual*, SINTEF Energy Research AS, Norway, TR F5680, ISBN 82-594-2344-8, August 2002.

[82] E. Shade and K. Ragaller "Dielectric Recovery of an Axially Blown SF6 Arc after Current Zero: Part I – Experimental Investigations" *IEEE Transactions on Plasma Science*, Vol. PS-10, No. 3, P. 141-153, September 1982.

[83] K. Ragaller, W. Egli and K. Brand "Dielectric Recovery of an Axially Blown SF6 Arc after Current Zero: Part II – Theoretical Investigations" *IEEE Transactions on Plasma Science*, Vol. PS-10, No. 3, P. 154-162, September 1982.

[84] K. Brand, W. Egli, L. Niemeyer, K. Ragaller and E. Shade "Dielectric Recovery of an Axially Blown SF6 Arc after Current Zero: Part III– Comparison of Experimental and Theoretical" *IEEE Transactions on Plasma Science*, Vol. PS-10, No. 3, P. 162-172, September 1982.

[85] H. Schoetzau, H. Meili, E. Fischer, C. Strurzenegger and H. Graf "Dielectric Phase in an SF6 Breaker" *IEEE Transactions on Power Apparatus and System*, Vol. Pas-104, No. 7, P. 1897-1902, July/August 1985.

[86] T. Browne "A Study of AC Arc Behavior Near Current Zero by Means of Mathematical Models" *AIEE*, Vol. 67, P. 141-153, 1948.

[87] P. Scarpa, B. Dauby, J. Defise, W. Legros, M. Barrault, G. Bernard and S. Rowe "SF6 Auto-Expansion Circuit Breaker Design: Numerical and Experimental Investigations of Arc-Gas Interactions" *IEEE Transactions on Power Delivery*, Vol. 7, No. 1, P. 339-345, January 1992.

[88] A. Cassie "Theorie Nouvelle des Arcs de Rupture et de la Rigidité des Circuits" *Cigre Report 102*, pp. 588-608, 1939.

[89] O. Mayr "Beitrage zur Theorie des Statischen und des Dynamischen Lichthogens" *Archiv für Elektrotechnik*, Vol. Band 37, No. Heft 12, pp. 588-608, 1943.

[90] W. Hermann, U. Kogelschatz, L. Niemeyer, K. Ragaller and E. Schade "Investigation on the Physical Phenomena around Zero in HV Gas Blast Breakers" *IEEE Transactions on Power Apparatus and System*, Vol. PAS-95, No. 4, July/August 1976.

[91] K. Ragaller, A. Plessel, W. Herman and W. Egli "Calculation Methods for the ARC Quenching System of Gas Circuit Breaker" *CIGRE-13.03*, Paris, France, 1984.

[92] Cigre Working Group 13.01 "Applications of Black Box Modeling to Circuit Breakers" *Electra*, No. 149, August 1993.

[93] T. Brwone "Practical Modeling of the Circuit Breaker Arc as a Short Line Fault Interrupter" *IEEE Transactions on Power Apparatus and System*, Vol. PAS-97, No. 3, P. 838-845, May/June 1978.

[94] U. Habedank "Application of a New Arc Model for the Evaluation of Short-Circuit Breaking Tests" *IEEE Transactions on Power Delivery*, Vol. 8, No. 4, P. 1921-1925, October 1993.

[95] P. Schavemaker and L. Sluis "An Improved Mayr-Type Arc Model Based on Current-Zero Measurements" *IEEE Transactions on Power Delivery*, Vol. 15, No. 2, P. 580-584, April 2000.

[96] L. Frost "Dynamic Arc Analysis of Short Line Fault Tests for Accurate Circuit Breaker Performance Specification" *IEEE Transactions on Power Apparatus and System*, Vol. PAS-97, No. 2, P. 478-484, March/April 1978.

[97] U. Habedank and H. Knobloch "Zero-Crossing Measurements as a Tool in the Development of High-Voltage Circuit Breakers" *IEE Proceedings-Science Measurement and Technology,* Vol. 148, No. 6, November 2001

[98] M. Hrabovsky, V. Mastny and Z. Vostracky "Application of Mathematical Arc Model for Determination of Thermal Failure Limiting Characteristics" *CIGRE*, 1984.

[99] K. Cornick, Y. Ko and B. Pek "Power System Transients Caused by Arcing Faults" *IEE Proceedings*, Vol. 128, No. 1, pp. 18-27, January 1981.

[100] M. Kizilcay and T. Pniok "Digital Simulation of Fault Arcs in Power systems" *European Transactions on Electrical Power System, ETEP*, Vol. 4, No. 3, pp. 55-59, January/February 1991.

[101] M. Kizilcay and K. Koch "Numerical Fault Arc Simulation Based on Power Arc Tests" *European Transactions on Electric Power*, *ETEP*, vol. 4, no. 3, pp. 177-186, May/June 1994.

[102] A. Johns, R. Aggarwal and Y. Song "Improved Techniques for Modeling Fault Arcs on Faulted EHV Transmission Systems" *IEE Proceedings-Generation, Transmission and Distribution*, Vol. 141, No. 2, pp. 148-154, March 1994.

[103] J. Sousa, D. Santos and M. Barros "Fault Arc Modeling in EMTP" *International Power System Transient Conference*, *IPST'95*, Lisbon, pp. 475-480, September 1995.

[104] V. Terzija and H. Koglin "Long Arc in Free Air: Laboratory Testing, Modeling, Simulation and Model-Parameters Estimation" *IEE Proceedings-Generation, Transmission and Distribution*, Vol. 49, No. 3, pp. 319-325, May 2002.

[105] Y. Goda, M. Iwata, K. Ikeda and S. Tanaka "Arc Voltage Characteristics of high Current Fault Arcs in Long Gaps" *IEEE Transactions on Power Delivery,* Vol. 15, No. 2, pp. 791-795, April 2000.

[106] M. Kizilcay and P. Seta "Digital Simulation of Fault Arcs in Medium-Voltage Distribution Networks" *15th Power Systems Computation Conference*, PSCC, Liege, Belgium, 22-26 August 2005.

[107] *Wavelet Toolbox for MATLAB*, Math Works 2005.

[108] J. Haung, C. Shen, S. Phoong and H. Chen "Robust Measure of Image Focus in the Wavelet Domain" *International Symposium on Intelligent Signal Processing and Communication Systems, ISPACS*, Hong Kong, December 2006.

[109] M. Nordman and T. Korhonen "Design of a Concept and a Wireless ASIC Sensor for Locating Earth Faults in Unearthed Electrical Distribution Networks" *IEEE Transactions on Power delivery*, Vol. 21, No. 3, pp. 1074-1082, July 2006.

[110] R. Fernandes "Electrical Power Line and Substation Monitoring apparatus and systems" *European Patent Application* 0314849, May 1989.

[111] O. Vähämäki, K. Rautiainen and K. Kauhaniemi "Measurement of Quantities of Electric Line" *Patent Application* WO0171367, September 2001.

[112] M. Vieira, C. Coelho, D. da Silva and J. da Mata "Survey on Wireless Sensor Network Devices" *Emerging Technologies and Factory Automation*, ETFA'03, pp. 537–544, September 2003.

ISBN 978-951-22-9014-7
ISBN 978-951-22-9015-4 (PDF)
ISSN 1795-2239
ISSN 1795-4584 (PDF)